TECHNISCHE UNIVERSITÄT MÜNCHEN

Lehrstuhl für Mikrotechnik und Medizingerätetechnik

A novel glove monitoring system for quantifying neurological symptoms during deep-brain stimulation surgery

Houde Dai

Vollständiger Abdruck der von der Fakultät für Maschinenwesen der

Technischen Universität München zur Erlangung des akademischen Grades eines

Doktor-Ingenieurs (Dr.-Ing.)

genehmigten Dissertation.

Vorsitzender: Univ.-Prof. Dr. med. Dr.-Ing. habil. Erich Wintermantel

Prüfer der Dissertation:

1. Univ.-Prof. Dr.rer.nat. Tim C. Lüth

2. Univ.-Prof. Dr.-Ing. Veit St. Senner

Die Dissertation wurde am 22.10.2013 bei der Technischen Universität München eingereicht und durch die Fakultät für Maschinenwesen am 12.05.2014 angenommen.

Danksagung

I have gained a profound amount of knowledge during my four years of study and research at the Technische Universität München (TUM). Throughout these years, my research ability has continually improved.

Here, I first wish to express my sincere gratitude to Prof. Dr. rer. nat. Tim C. Lüth, for his constant support throughout my graduate studies at the Institute of Micro Technology and Medical Device Technology (MIMED, TUM). I also wish to express my sincere gratitude to the Chinese Scholarship Council (CSC) for their financial support of my studies in Germany.

Furthermore, I would like to thank Dr.-Ing. Lorenzo T. D'Angelo, for his patient instruction, constant encouragement, and friendly assistance in relation to my studies and research. I would like to thank Jakob Neuhäuser and Yan Zhao for their kind support, insightful research discussions, and invaluable suggestions for this thesis. I also wish to express my sincere gratitude to Jiaxi Shi for his kind suggestions regarding the structure of my dissertation.

I would also like to offer my thanks to Dr. Jan H. Mehrkens, from Ludwig-Maximilians-Universität München, for his expert suggestions in this study. I would also like to acknowledge the great amount of help provided in this study by my student Bernward Otten.

In particular, many thanks to Jordan Evans, Jeremiah Hendren, and the other TUM English Writing Center staff, for their proofreading of this thesis and their invaluable suggestions.

I would like to thank Mrs. Renate Heuser, Barbara Govetto, and Dr. Franz Irlinger for their kind work.

Also, I offer my thanks to my colleagues Dr. med. Karin Tonn, Dr.-Ing. Khalil Niazmand, Ian Somlai, Dr.-Ing. Axel Czabke, Cheng Fang, Joachim Kreutzer, and Samuel Reimer.

In addition, I would like to thank Professor Chao Hu, Dr. Wanan Yang, Zhenglong Chen, and Professor Guotai Jiang, who have always offered their help.

I would like to thank all the kind people at MIMED and TUM.

Finally, to my family, I would like to thank them for their eternal support and encouragement.

Houde Dai,Oct.,2013

Index

1. Introduction

1.1 Project Description

Parkinson's disease (PD) and essential tremor (ET) are the two common movement disorders, which denote degenerative and progressive disorder of the central nervous system (CNS). Tremor, bradykinesia, and rigidity are the three primary symptoms of PD (Elbe *et al.*, 2011). ET is a tremor of the hands when a patient is performing voluntary movements.

Deep-brain stimulation (DBS) is a crucial surgical procedure for PD, ET, and other neurological symptoms (Okun *et al.*, 2008). At present, DBS can only relieve the severe symptoms of PD, ET, and other nervous system disorders, and then improve the quality of patients' lives.

The precise mechanisms of PD and how DBS works remain uncertain at present (Dauer *et al.*, 2003). However, the stimulation in specific areas of the patient's brain by sending high frequency electrical impulses can alleviate symptoms or diminish the side effects of medications. Therefore, DBS is the most effective surgical procedure for patients with severe symptoms of PD, ET, dystonia, or dyskinesia when the patients are insensitive to drug medications.

The positioning target area of an electrode is first confirmed by the three-dimensional structure obtained from magnetic resonance imaging (MRI). During the positioning of the electrode in the brain by using microelectrode-guided mapping, the neurosurgeon may choose an optimal location based on the results of sensorimotor mapping or subjective methods, involving observation according to the clinical scales (Unified Parkinson's Disease Rating Scale, etc.) and the assessment of handwriting such as a drawing of an Archimedes spiral. This is usually accompanied by several small movements of the electrode in a target area. Although used under clinician observation, these largely subjective scales lack validation against the actual stimulating effect. Furthermore, the coarse resolution of the ratings is insufficient for assessing small changes in symptom severity. Finally, the extent of inter-clinician and inter-subject rating variability is unknown (Machado *et al.*, 2003).

There is no designated instrumental method for the accurate monitoring of the stimulating effect during DBS surgery as of yet. Nevertheless, neurosurgeons need to know the exact position and stimulating intensity of the deep-stimulation electrode to achieve the best effect.

The goal of the present project is to develop a portable assessment system to quantify the three primary symptoms of PD and ET during DBS surgery. These movement disorders and their changes should be monitored to obtain the optimal electrode target position and stimulation intensity during intraoperative stimulation. It is also supposed to support choosing the optimal stimulation settings of the DBS electrodes after DBS surgery.

In this study, a new concept for quantifying neurological symptoms during DBS surgery was developed, specifically concerning portability, wearability, and intraoperative application. In this concept, the current possibilities of inertial sensor technology and motion-tracking algorithms could be used to implement quantitative assessments of the primary neurological symptoms without disrupting existing DBS processes. User-friendly human-machine interfaces were designed to monitor the changes of symptoms.

1.2 Structure of the Thesis

The organization of this thesis is as follows.

Chapter 2 describes the motivation of this study, both for clinical and technical needs. The introduction of PD, ET, and DBS are presented in this chapter.

Chapter 3 reviews the intraoperative assessment approaches of neurological symptoms and the systems that can be used to quantitatively assess these neurological symptoms. Inertial sensors and sensor fusion methods for motion tracking are also introduced in this chapter.

Chapter 4 describes the parameters, goals, and expected advantages of the glove monitoring system. Its system concepts are presented in Chapter 5, which includes static and dynamic system descriptions. The quantification algorithms of neuromotor symptoms are based on statistical analyses, especially the estimation theory and its least squares methods.

For the prototypical realization in Chapter 6, designs with wireless communication interfaces are presented first. In the first step of this study, the glove monitoring system was divided into two separate systems: one for tremor and bradykinesia assessment and the other for rigidity assessment. Their prototypes were based on six-axis motion tracking sensors (gyroscope and accelerometer) and force sensors. According to the operations during clinical experiments and the suggestions of surgeons, a modified version with combined hardware and software was developed. As a result, a prototype that could assess all three symptoms was implemented.

Chapter 7 describes the verification of analytical methods, and clinical experiments. Comparative experiments between these two prototypes and an electromagnetic motion-tracking system were carried out. The prototype for tremor and bradykinesia assessment was tested with clinical experiments in the hospital.

Finally, conclusions and future work are given in Chapter 8.

2. Application Description

The information about PD, ET, and DBS surgery are presented in Chapter 2.1. The technical need to quantify neurological symptoms is introduced in Chapter 2.2.

This chapter shows that the quantification of neurological symptoms during DBS surgery plays a key role in the surgical treatment of PD or ET. It provides feedback to the stimulation settings of each DBS electrode. Thus the optimal location for the electrode implantation can be found.

2.1 Clinical Need

2.1.1 Parkinson's Disease and Essential Tremor

It was estimated that 1% of 70-year-olds suffer from PD (Chaudhuri *et al.*, 2011). About 10% of PD patients are younger than 50 years old. At present about four to six million people are PD patients. A series of studies indicated the overall prevalence of ET to be 0.4%–0.9% and the prevalence in 60-year-olds to be 4.6% (Louis & Ferreira, 2010). Due to demographic increase of the elderly population, movement disorders such as PD and ET will occur more frequently in the future.

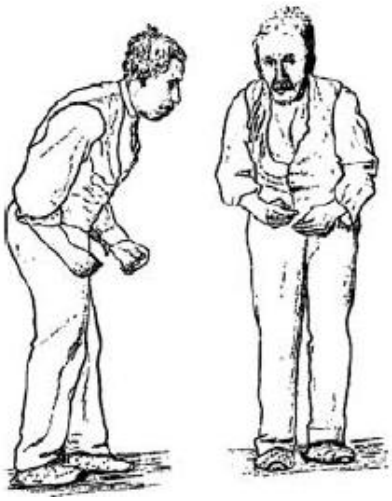

Figure 2-1: Symptoms of Parkinson's disease (Taken from Gowers, 1886). Parkinson's disease affects patients in many different ways with a variety of symptoms. These symptoms can be classified as motor symptoms, neuropsychiatric symptoms, and autonomic dysfunction.

PD occurs mainly in a patient's hands, feet, and head. As shown in Figure 2-1, tremor (rhythmic back and forth motion), bradykinesia (slowness of motion), rigidity (resistance to movement), poor balance, and parkinsonian gait are the five motor symptoms of PD (Jankovic, 2013). Poor balance and parkinsonian gait, however, are hard to assess during DBS surgery. Tremor is a central symptom of PD, and is generally judged according to hand tremor with a particular frequency (3.5–7.5 Hz) and amplitude (speed and range) (Salarian *et al.*, 2004). Bradykinesia is a feature of basal ganglia disorders. It involves difficulties with planning, beginning, and executing movement; and with performing sequential and simultaneous tasks. Rigidity means increased muscle tone, which is defined as a resistance to a passive movement.

An ET can be difficult to distinguish from a parkinsonian tremor. However, ET generally presents itself with a higher frequency (4–12 Hz) and occurs only when the affected muscle is in an active state. Physical or mental stress will also make ET worse. Therefore, rest tremor is usually not part of the ET. In addition, the target areas of an electrode for ET and parkinsonian tremor are different. The assessment method for both ET and parkinsonian tremor, however, can be almost the same (Fekete *et al.*, 2010).

Problem: Reduce the Severity of Symptoms

The mechanism responsible for PD and ET is not clear now. The primary goal in PD and ET treatment strategies is to maintain a patient's independence and quality of life, and at the same time minimize potential complications of treatment. The challenge of the PD and ET treatment strategies is to reduce the severity of symptoms.

At first, PD patients are treated with Levodopa medications. However, drug efficacy decreases in later stages, together with the period of drug medication. For the patients with severe symptoms of PD or ET, who are insensitive to medications, DBS is the most effective treatment (Kringlbach *et al.*, 2007).

2.1.2 Deep-Brain Stimulation Surgery

DBS was approved by the Food and Drug Administration (FDA) as a surgical treatment for ET in 1997 and for PD in 2002. DBS can only ease some symptoms of a patient with PD or other neurological disorders. Medications for the patient are needed even after DBS surgery (Bittar *et al.*, 2005). More than 80 000 DBS surgeries had been performed worldwide up until 2011 (Oluigbo *et al*., 2012).

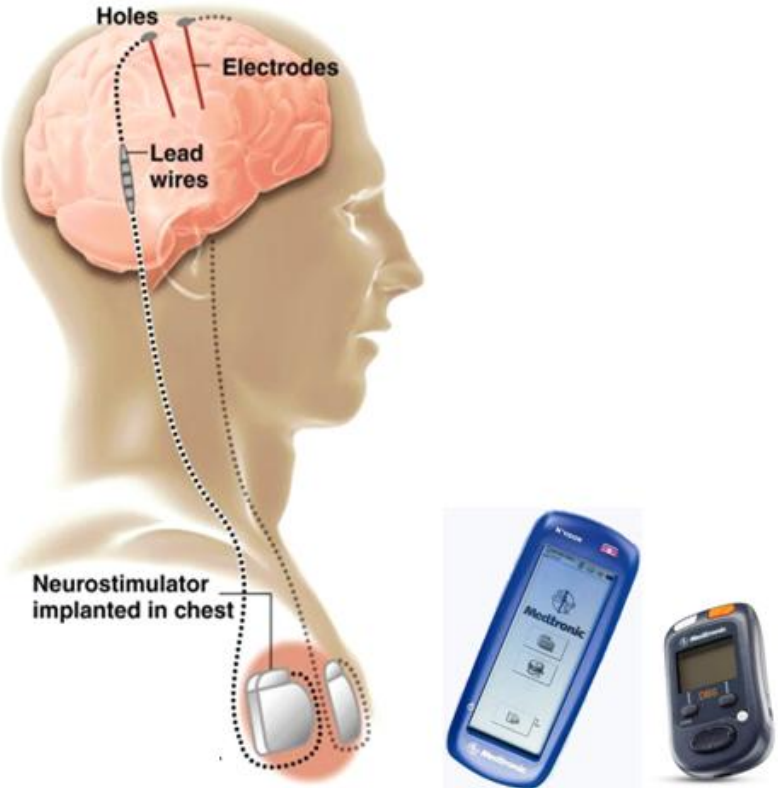

Figure 2-2: DBS system (© Medtronic, 2009). Left: DBS system diagram; middle: DBS clinician programmer (size: 22cm × 10cm × 4cm); right: DBS patient programmer (size: 9.4cm × 5.6cm × 2.8cm). Meditronic Inc. is the major manufacturer of DBS devices.

A deep-brain stimulation system includes neurostimulators (a surgically implanted, battery-operated medical device), electronic leads (also called electrodes, two thin, insulated wires for each side of the brain), and extensions. These components can be placed in either one or both sides of the brain. They are implanted inside the body and powered by batteries. DBS uses a neurostimulator, which is similar to a heart pacemaker and approximately the size of a stop-watch, to deliver electrical stimulation to targeted areas in the brain that control movement, thus blocking the abnormal nerve signals that cause motor symptoms. As Figure 2-2 shows, there are also two programmers which can be used by the surgeon or the patient outside the human body. The stimulating mode, intensity and frequency of the neurostimulators can be adjusted using the clinician programmer. The patient programmer can be used to turn the therapy on or off.

Current Application Flow of DBS Surgery

At first, a stereotactic head frame is placed on the patient's head to precisely target the brain structure. The neurosurgeon uses magnetic resonance imaging (MRI) or computed tomography (CT) scanning to identify and locate the exact area (coordinate) within the brain in which electrical nerve signals generate the PD or ET symptoms. A three-dimensional (3D) offline graphics program provides detailed information on the function of the area (Kringlbach *et al.*, 2007).

Then the patient enters the operating room and lies on a surgical bed in a reclined and comfortable position. The head frame is fixed to the table. In general, at least five members of the hospital staff are required in the operating room, including a surgeon, a nurse, an anesthesiologist, a technician, and an assistant, during DBS surgery. The installation of the components is under the condition of general anesthesia (Bittar *et al.*, 2005).

As Figure 2-2 shows, a surgeon has drilled two small holes in the patient's skull and has threaded two insulated wires, with electrodes attached at the top of the brain. Lead wires are run under the skin from the brain to the upper chest. The lead wires are attached to two neurostimulators that are surgically implanted in the chest and provide electricity to stimulate the brain. Two electrodes and neurostimulators on both sides are implanted one by one by using the same surgical procedure.

Each neurostimulator sends electrical pulses to one of the three active areas of the brain via the electrode to interfere with neural activity. There are a few target sites inside the brain for achieving differing results, and the most common sites are the subthalamic nucleus (STN) and the globus pallidus interna (GPi). In addition, the caudal zona incerta and the pallidofugal fibers medial to the STN are being assessed in some situations. Then a site will be chosen for each electrode based on the individual patient (Bittar *et al.*, 2010).

Challenge: Select an Optimal Electrode Position

An optimal electrode position is significant for the effect of surgery. The implantation of electrodes is performed only one side at a time. Before the surgery, the coordinates for the electrode target area inside the brain, which can be seen from Figure 2-3, are identified with the help of an optimum radiologic targeting (MRI-based) and a 3D offline graphics program.

The key point of the surgery is to define an optimal point for each electrode positioning.

For each electrode, 4 to 10 points inside the brain are tested during the surgery in order to evaluate the electrode's position and stimulation intensity. This is usually accompanied by

small movements in a small target area. After surgery, a neurologist also needs to adjust the stimulation amplitude of the stimulator which is implanted in the chest of the patient for the best treatment effect (Machado *et al.*, 2006).

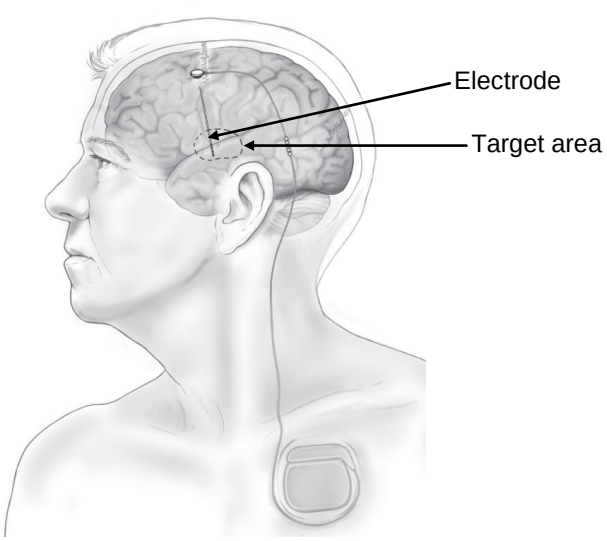

Figure 2-3: Electrode implantation (Based on Hotzheimer & Mayberg, 2012). The tips of the electrodes are implanted one by one within the targeted brain area.

During DBS surgery, it is important to monitor the patient's stimulation effects, based on his or her individualized response to the stimulation. The quantified severity values of symptoms can be used as feedback for the stimulating setting of the DBS electrode (Kern *et al.*, 2007).

After its optimal target is found, an electrode is permanently implanted. For the electrode with misplacement or in a suboptimal target, the positive effect of DBS cannot be reached or restricted. Some patients need to adjust the electrode through another DBS surgery.

Assignment: Monitor the Severity of the Neurological Symptoms

Some surgeons may use microelectrode recording (MER), which involves a small wire that monitors the activity of nerve cells in the target area, to more specifically identify the precise brain target that will be stimulated.

The current standard for evaluating motor symptoms associated with PD is the Unified Parkinson's Disease Rating Scale (UPDRS), a qualitative assessment that is completed by the subjective judgement of the surgeons. Essential Tremor Rating Assessment Scale (TETRAS) is the standard for evaluating the severity of ET. Motor symptoms are rated on a scale from 0 to 4 corresponding to normal, slight, mild, moderate, and severe (Tagliati *et al.*, 2007).

The Hoehn and Yahr scale, Schwab and England Activities of Daily Living Scale, and Webster Scale are also used for the assessment of PD. These subjective assessment ratings lead to problems when evaluating the effectiveness of therapies for PD or ET (Pahwa *et al.*, 2007).

At present, there is no designated instrumental method of monitoring the immediate motor effects of DBS procedure. Nevertheless, surgeons need to get feedback on the stimulating electrode in order to achieve optimal therapeutic efficacy. There is, therefore, a need to develop a monitoring system that is able to quantify tremor, bradykinesia, and rigidity in real-time during DBS surgery, instead of subjective assessment.

A DBS stimulator can be turned on and programmed in three to four weeks after implantation. The first programming session can take several hours in order to ensure the device is correctly functioning and that various stimulation parameters (voltage, frequency of the DBS stimulator, and electrodes mode) are optimally programmed.

Routine outpatient programming sessions at approximately one, two, and four months after DBS surgery are needed for the patient. Because the neurostimulator contains a battery, it must be surgically replaced every three to five years.

2.1.3 Special Concerns - Motor Fluctuations and Dyskinesia

About 50% of PD patients have motor fluctuations (MF) and dyskinesia after five years of levodopa medications. As Figure 2-4 shows, motor fluctuations indicate the effective period of certain doses is shorter all the time (this is known as "end-of-dose deterioration"). It also means the alterations between "ON", which is a state of good response to anti-parkinsonian medications, and "OFF", which is a state for patients experiencing pakinsonian symptoms. The symptoms of a PD patient may reappear unexpectedly and quickly. This switch sensation is described as "ON/OFF" syndrome. Levodopa-induced dyskinesia (LID) involves a series of hyperkinetic movements (involuntary, episodic, and irregular) such as athetosis, chorea, and dystonia (Hause *et al.*, 2000).

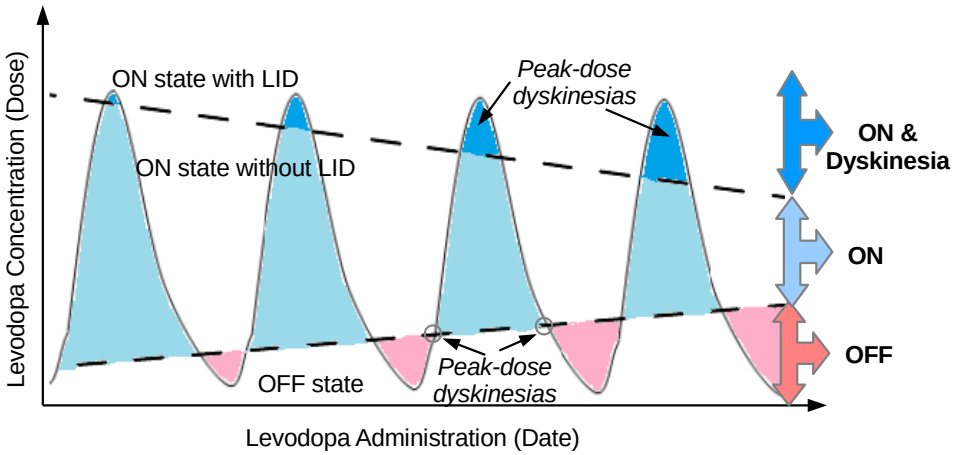

Figure 2-4: Motor fluctuations and dyskinesia. Levodopa's therapeutic window narrows overtime during ON state. As a result, the patient's response to Levodopa shortens over time.

Dyskinesia is one of the side effects of DBS surgery. Dyskinesia appears when the electrode stimulating voltage is too high. Thus, it is important to avoid such over-stimulation.

2.2 Technical Need

In 1872, Jean-Martin Charcot (1825–1893), the most celebrated clinical neurologist of the 19th century, developed a tremor recording device, as Figure 2-5 shows. This device provided a new approach to assess the symptom severity of movement disorders, other than visual observation and clinical maneuvers.

At present, several groups have used electromyography (EMG), computer tracking, digital tablets, infrared video cameras, and laser transducers to assess tremor and bradykinesia objectively. All these solutions have demonstrated limited usability in clinical settings due to deficiencies in wearability, fidelity, and flexibility (Pahwa & Kvons, 2007).

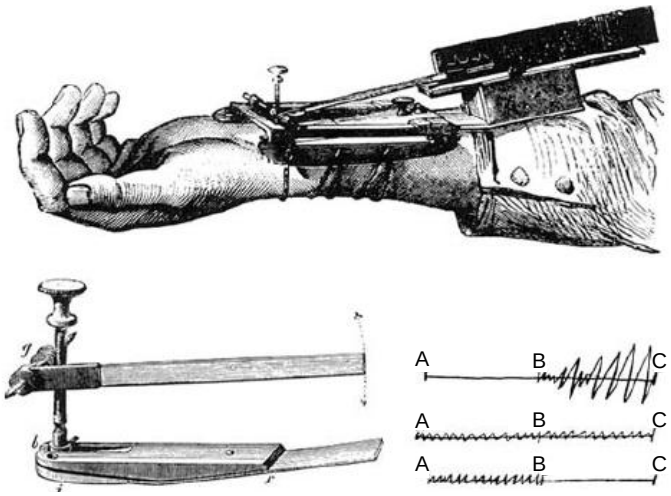

Figure 2-5: Charcot's early tremor recording device (lower left) and its recordings (lower right). Charcot used the sphygmograph to record tremors in the wrist. The resultant tremor recordings were conducted at rest (A–B) and during activity (B–C) of a patient with Parkinson's disease (Based on Pahwa & Kvons, 2007).

There has recently been growing interest in the application of body-fixed sensors (BFS) and in particular inertial sensors for long-term monitoring of PD symptoms. Micro-Electro-Mechanical Systems (MEMS) gyroscope and accelerometer are widely used for the motion tracking in tremor and bradykinesia assessments. With the development of new MEMS technology, the dimension of the sensor circuit board is smaller and the signal processing is easier to be carried out than before.

Other kinematic sensors and force sensor have been used to detect and quantify rigidity. These sensors were placed on the body, feet or arms of the patients and were not specifically designed for DBS (Patel *et al.*, 2008).

The assessment system of neurological symptoms for DBS surgery must strictly adhere to the requirements in the operation room. It is important to perform three assessment tasks in a portable and wearable system with small dimensions. This system should be safe and not restrict the patient's movement.

In addition, a user-friendly human-machine interface should be designed to support the surgeons to monitor the changes of symptoms.

3. State of the Art

The clinical assessment tasks of tremors, bradykinesia, and rigidity is first introduced in Chapter 3.1.

The intraoperative assessment of neurological symptoms is introduced in Chapter 3.2. At present there are only two intraoperative approaches to assess neurological symptoms: MER/EMG techniques and subjective assessment by the surgeons.

There are also some systems which are used to quantitatively assess neurological symptoms outside of the operating room. Some researchers and companies have tried to assess the severity of neurological symptoms and their changes (OFF and ON state).

The quantitative assessment methods of neurological symptoms in these systems are introduced in Chapter 3.3. In addition, these systems are classified into commercial systems and systems in research and development. Detailed information of the assessment systems is described in Chapter 3.4 and Chapter 3.5 respectively. However, most of them are for tremor and bradykinesia assessment. Rigidity assessment is available only in a few research projects.

MEMS inertial sensors and sensor fusion algorithms for motion tracking are introduced in Chapter 3.6.

Limitations of the existed technology (disadvantages of the state of the art) are described in Chapter 3.7.

3.1 Neurological Symptoms and Assessment Tasks

In clinical practice, tremor assessment tasks include rest tremor, postural tremor, and action tremor movements. Bradykinesia measurement tasks include finger tapping, hand grasping, and rapidly alternating movements. Passive elbow or wrist movements (repeatedly flexing and extending) are used for rigidity assessment.

A detailed instruction of the assessment tasks is described as follows.

3.1.1 Tremor Assessment

Symptom

Tremor syndromes (oscillatory movements) are classified into three primary types: rest tremor (RT), postural tremor, and action tremor. Rest tremor, which is the characteristic of parkinsonian tremor, happens when a body part is relaxed, for example, when lying in bed. Postural tremor, which is the characteristic of ET, occurs while a body part is maintaining a position against gravity. Action tremor happens when a voluntary contraction of a muscle, follows the condition, for example, holding a cup. In most situations, parkinsonian tremor manifests the combination of rest, postural, and action tremors (Deuschl *et al.*, 1998). ET occurs in postural tremor and action tremor.

Parkinsonian tremor is the central symptom of PD. It is prominent in PD, about 70% of PD cases. The tremor associated with PD has a characteristic appearance, and reduces with purposeful activity. Symptoms often start with an occasional tremor in one finger that spreads

over time to involve the whole arm. ET is present when the limb is at rest or held up in a stiff unsupported position, and usually disappears briefly during movement.

Assessment

As shown in Figure 3-1, when the rest tremor is assessed, the patient should sit quietly in a chair or lie down in bed with his or her hands and feet comfortably placed for several seconds with no other activity. The stable tremor amplitude gives the final score.

Figure 3-1: Tremor assessment tasks: a) rest tremor; b) postural tremor; c) action tremor. When lying in the bed during DBS surgery, the assessment tasks for the patient are the same to the general clinical exams (Based on Dai *et al.*, 2013a).

When testing postural tremor, an examiner instructs the patient to stretch his or her arms out with the palms facing down. The wrist should be straight and the fingers comfortably separated so that they do not touch each other. This posture is observed for ten seconds.

Action tremor of the hands is tested by the finger-to-nose maneuver or by holding a cup. With the arm starting from the outstretched position, the patient performs at least three finger-to-nose maneuvers with each hand reaching as far as possible to touch his/her nose or the examiner's finger. The finger-to-nose maneuver should be performed slowly enough so as not to hide any tremor that may occur with very fast arm movements. This is repeated with the other hand, with each one rated separately. The tremor may be present throughout the movement, and the highest stable tremor amplitude is rated.

The patient needs to completely relax during the rest tremor task because the tremor may be heightened by the mental load. The patient should outstretch two arms during a postural tremor task. Drinking, spoon, and spiral movements can be chosen as additional action tremor tasks.

3.1.2 Bradykinesia Assessment

Symptom

Bradykinesia often initially manifests as slowness in performing activities. It is the most characteristic feature of PD and is often associated with an impaired ability to adjust the body's position (Jankovic *et al.*, 2008).

Bradykinesia encompasses slowness, decreased movement amplitude, and dysrhythmia. It means the inability of generating maximum speed, power, or force. According to the modified bradykinesia rating scale (MBRS), the speed, amplitude, and rhythm of bradykinesia task represent the parameters of bradykinesia, hypokinesia, and dysrhythmia, respectively. Hypokinesia refers to a decreased amplitude or range of bodily movement. In addition, the difficulty in selecting or activating motor programs in the CNS may result in akinesia (inabil-

ity to initiate movement) in the patient's daily life. Akinesia (absence of movement) during bradykinesia task is the delay (action time) of the patient to start the assessment task after the instruction from the examiner.

Assessment

Bradykinesia measurement tasks include finger tapping, hand grasping, and rapid alternating movements (Heldman *et al.*, 2008).

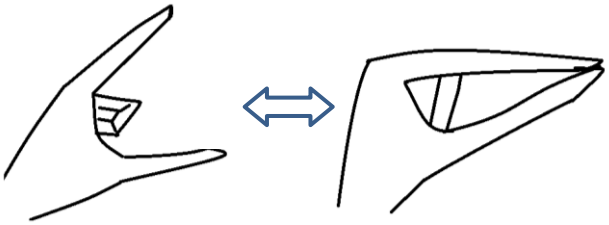

Figure 3-2: Finger tapping.

As shown in Figure 3-2, finger tapping is used to assess bradykinesia. The subject is instructed to tap his/her fingers in rapid succession as quickly and as widely as possible. After five seconds of practice, such open-close movement is performed for several seconds or several times. Speed, amplitude, halts, and any decline in amplitude are evaluated. At least two contact sensors on two fingers are used for the measurement of tapping duration. In order to measure the range of the finger tap actions, two gyroscopes and two accelerometers are also used when finger tapping is adopted.

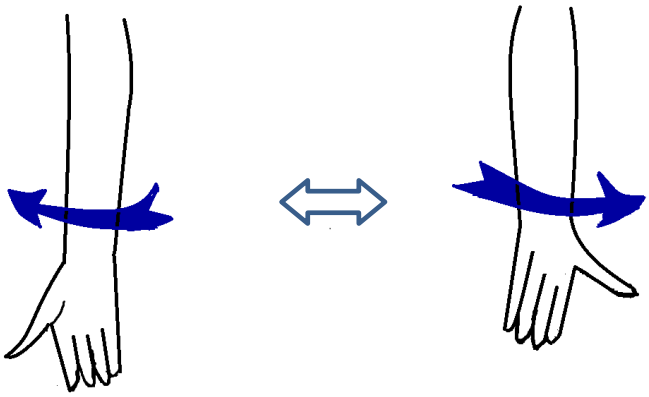

Figure 3-3: Supination-pronation movements of the hand.

As shown in Figure 3-3, supination-pronation movement is also used to assess bradykinesia. The patient is instructed to extend the arm out in front of his/her body with the palms facing down and then to turn the palm up and down alternately several times (or several seconds) as fast and as fully as possible.

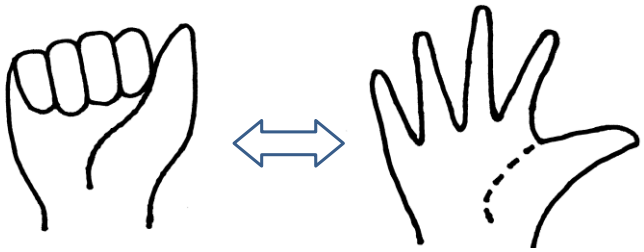

Figure 3-4: Whole-hand grasping (Based on Dai *et al.*, 2013a).

Whole-hand grasping is another movement used to assess bradykinesia. Figure 3-4 shows the bradykinesia task, when all the fingers are closing and opening repeatedly. A single closing and opening movement is regarded as a grasp cycle. The subject is required to grasp with the greatest possible range and frequency. A single assessment task lasts for 10 to 15 seconds.

For supination-pronation and whole-hand grasping movements, a triple-axis gyroscope is necessary to measure the angular displacement of the hand or finger. The gyroscope signals obtained from patients with mild bradykinesia have a consistent amplitude and frequency and appear sinusoidal. However, signals from patients with severe bradykinesia have much lower and inconsistent amplitude and frequency. Speed, amplitude, halts, hesitations, and any decline in amplitude are evaluated.

3.1.3 Rigidity Assessment

Symptom

Rigidity responds immediately upon PD treatment. It refers to a permanently elevated muscle contraction, independent of passive movement velocity. Patients with severe rigidity can hardly reach muscle relaxation and their voluntary movements are accompanied by an elevated contraction of antagonist muscles (Shapiro *et al.,* 2007).

Cogwheel rigidity, which means the muscles perform ratchet jerks when passive force bends the limb, always appears as an early sign of PD. It performs a cogwheel mechanism with the frequency range from 6 to 9 Hz and depends on the stretch velocity. This phenomenon seems to be the combination of rigidity and superimposed tremor, which has a higher frequency than parkinsonian tremor.

Assessment

Hand rigidity is more difficult to measure, and there is currently no standardized objective method for measuring rigidity. Quantification of the mechanical properties of a joint can be realized by passive joint movement, for example, flexion and extension of the joint by a clinician or a torque motor. Rigidity is commonly assessed in the upper limbs at the wrist or elbow.

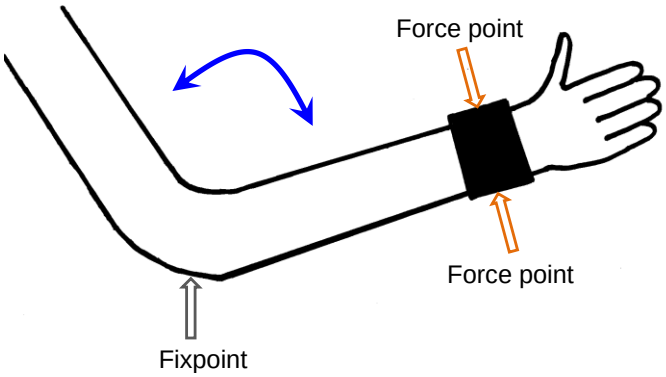

Figure 3-5: Elbow flexion-extension. An examiner holds the elbow of the patient for passive flexion-extension movement. The examiner first puts one hand on the fixpoint. At the same time, his/her other hand holds the patient's wrist, on both sides, to perform flexions and extensions of the patient's elbow.

As Figure 3-5 shows, passive flexion and extension of the elbow is used to assess rigidity. The examiner flexes and extends the elbow joint through the force at the wrist. In clinical practice, each test lasts for 10 to 30 seconds.

3.2 Intraoperative Assessment of Neurological Symptoms

Subjective Assessments

The assessment of rest tremor (RT), action tremor, and postural tremor in the clinic is currently mainly based on subjective methods and MER techniques according to clinical scales (UPDRS and TETRAS) (Elbe *et al.*, 2010).

When assessing bradykinesia during the DBS surgery, a neurologist asks the patient to perform rapid, repetitive, and alternating movements of the hand. The slowness level of the motion is scored according to the UPDRS. Based on experiences, the examiner classifies bradykinesia severity on a four-point scale from 0 to 4 (Salarian *et al.*, 2007).

In clinical practice, rigidity assessment is realized through passive movement of the subject's limb, which is controlled by a neurologist or another examiner. The level of instinctive resistance to the exerted movement is scored according to the UPDRS ratings. Based on experiences, the examiner classifies rigidity on a scale from 0 to 4, which is compared to a control group (Patrick *et al.*, 2001).

Quantitative Assessments: EMG and MER

At present, the Electromyography (EMG) method is used to measure tremor during DBS surgery in some hospitals. The EMG recording technique allows the detection and monitoring of electrical muscle activity following the attachment of surface electrodes to the surface of selected muscles (Rissanen *et al.*, 2007).

Figure 3-6: ISIS MER system (© inomed, 2012).

In addition, intraoperative microelectrode recording (MER) facilitates the surgeon in targeting the optimal placement of each electrode. The surgeon connects small microelectrodes into the intended target area and observes the pattern of neuronal activity to physiologically confirm the optimal stimulating position of the electrode. The small tips of the microelectrodes are placed close to the DBS electrode. They acquire the electrode activity (5–100 µA) of individual neurons at a very high frequency (300 Hz) (McClelland *et al.*, 2011).

Figure 3-6 shows the ISIS MER system with additional EMG function from inomed GmbH, Germany. It includes a monitor, operating panel, main isolation unit, computer, printer, loud-

speaker, ISIS headboxes, ISIS neurostimulator, keyboard, mouse, and a drawer for accessories.

a)

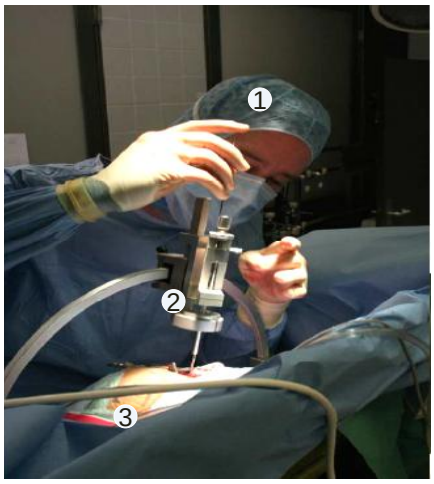

1) Surgeon

2) Sterotactic frame

3) Patient

b)

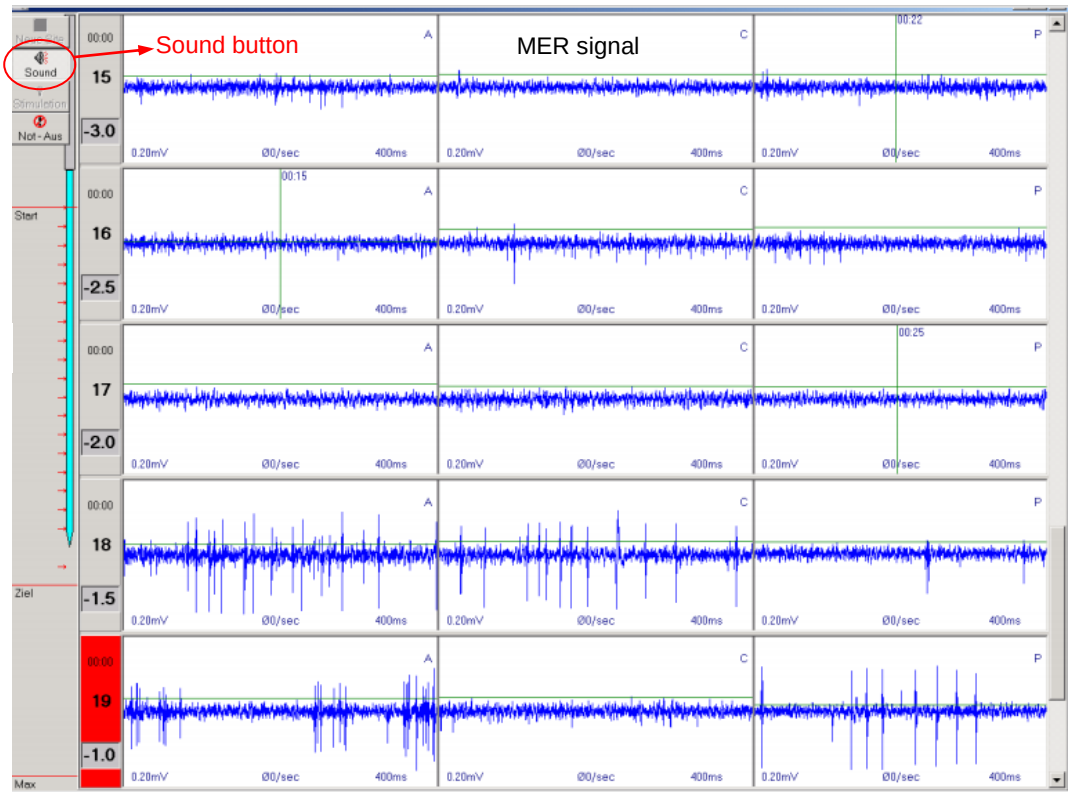

Figure 3-7: Electrode implantation and intra-operative MER recording during DBS surgery at the University Hospital of Munich (LMU) (© Mehrkens LMU, 2011). a) electrode implantation; b) MER graphical user interface.

Figure 3-7 shows the five-channel MER recording during a DBS surgery at the University Hospital of Munich (LMU, Germany). At the same time, there was an audio feedback of the relative neuronal activity.

Because there are differences between different patients' brains, the information obtained from MER provides a more accurate target as final DBS placement than the information from the MRI figures. Surgeons and technicians visualize and hear the neuronal activity from different points of the target area to identify specific structures based on the unique patterns of neuronal activity (Bittar *et al.*, 2005).

At the same time, the surgeon may move the patient's joints or ask the patient to perform physical examinations. The action of holding a cup or other objects by the patient is usually assessed to help detect hand tremor. Fast hand movement is adopted for bradykinesia assessment. Passive movement of the patient's joint is used for rigidity assessment. The surgeon assesses the symptom severity according to the clinical ratings based on experience.

The technician working with the MER or EMG equipment records the level of symptom severity when the electrode, after being implanted within the target brain area, is slowly moving within the brain. The surgeon can precisely map the target area (sensorimotor portion) in this way and the optimal location of the electrode is identified (Rissanen *et al.*, 2011).

Interventional MRI

Recently, an interventional MRI (or iMRI) with real-time imaging has appeared that has a higher target accuracy than the MER system during the surgical procedure, which as a result shortens the procedure time, even without a MER system (Ostrem *et al.*, 2013). However, as it is available in only a few hospitals, we do not discuss it in this study.

3.3 Quantitative Assessment of Neurological Symptoms

The summaries of quantitative assessment methods of tremor, bradykinesia, rigidity are listed from Table 3-1 to Table 3-3, respectively. The quantitative assessment method of dyskinesia is introduced in Chapter 3.3.4.

3.3.1 Tremor Quantification

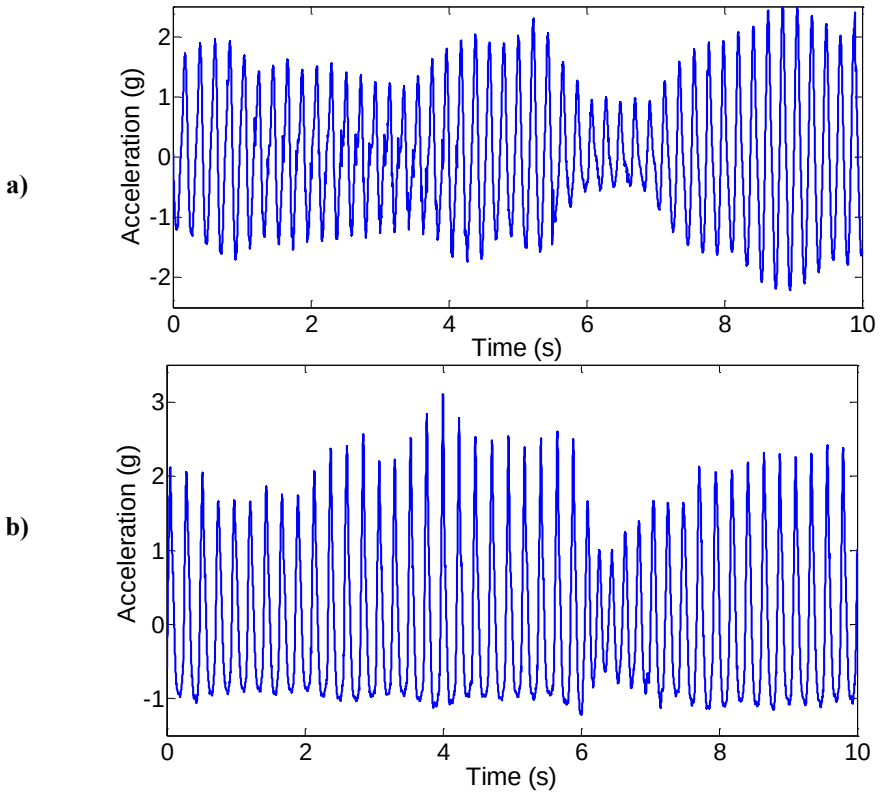

Figure 3-8: Representative segments of the normalized time series of tremor signals (Based on Timmer *et al.*, 2000a). a) parkinsonian tremor; b) essential tremor. These data were recorded from the main direction (up and down) of the tremors by the usage of a single axis piezoresistive accelerometer. These types of sensor data are usually sufficient for the analysis of ET but are insufficient for parkinsonian tremor because parkinsonian tremor is the movement of more than one dimension.

Tremor amplitude and frequency (3.5–7.5 Hz for parkinsonian tremor; 4–12 Hz for ET) are the important features (Elble *et al.,* 2011).

Tremor is the most apparent and well-known symptom of PD. According to the patient data from Prof. Dr. Jens Timmer at Freiburg University, representative segments of normalized time series of essential tremor and parkinsonian tremor are shown in Figure 3-8.

Timmer *et al.* revealed that both parkinsonian tremor and ET exhibit a 2-order nonlinear oscillation, which is not strictly periodic (Timmer *et al*., 2000).

Table 3-1: Summary of tremor assessment methods. *Peak power* represents the power estimation around the dominant frequency in the power spectrum of sensor signals; *RMS* refers to the root mean square value; and "–" denotes no exact information.

Company or author	**Tremor Assessment Systems**			
	Device or system	**Sensors**	**Sensors position**	**Amplitude parameter**
–	Examiner	Sight of the surgeon	–	UPDRS score
Inomed GmbH	ISIS MER	MER needle	Brain	Neuronal activity (voltage)
Giuffrida *et al.*, 2009	Kinesia	EMG, gyroscope, accelerometer	Finger	Peak power
Burkhard *et al.*, 2002	MOTUS	Gyroscope	Palm	Peak power
Narcisa *et al.*, 2011	CATSYS	Accelerometer	Hand	RMS of accelerations
Patel *et al.*, 2009	Shimmer	Gyroscope, compass	Body	Data range
Synnott *et al.*, 2012	WiiPD	Accelerometer, infrared	Hand	RMS of accelerations
Salarian *et al.*, 2007	ASUR	Gyroscope	Wrist	RMS of angular velocities
Spyers-Ashby & Stokes, 2000	FASTRK	Electromagnetic sensor	Hand	RMS of displacement

An overview of recent approaches in tremor assessment is given in Table 3-1. These sensor-based systems could access the alternate between therapy "OFF" and "ON" states during stimulation and medication. Most tremor assessment methods were based on the inertial sensors (gyroscope and accelerometer) and a computer-based system. Sensors were placed on the body, feet or arms of the patient.

More specifically, quantification of tremor has been achieved by numerical methods such as time-domain analysis, spectral analysis, time-frequency analysis, and nonlinear analysis.

According to the research by Elble *et al.* (2006), which enrolled 928 patients, hand tremor amplitude is logarithmically related to the 5-point clinical tremor ratings. According to the research by Giuffrida *et al.* (2009), for the rest and postural tremor in PD, the summation of logarithm peaks in both the power spectrums of accelerometer and gyroscope data has the highest correlation with UPDRS scores, while the coefficient of determination (r^2) was around 0.9. For the action tremor in PD, the root-mean-square (RMS) sum of both gyroscope

and accelerometer data has the highest correlation with UPDRS (r^2 = 0.69) (Mostile *et al.*, 2010).

3.3.2 Bradykinesia Quantification

Bradykinesia is quantified through finger tapping, whole-hand grasping, and supination-pronation movements of hands.

Several groups and companies have used computer tracking, digital tablets, infrared video cameras, or laser transducers in order to objectively assess parkinsonian bradykinesia.

An overview of recent approaches in bradykinesia assessment is given in Table 3-2.

Table 3-2: Summary of bradykinesia assessment methods. Here "–" denotes no exact information.

Company or author	Joint/ Task	Angle measurement	Parameters
–	Examiner	Sight of the surgeon	–
Inomed GmbH	ISIS MER	MER needle	Neuronal activity (voltage)
Niazmand *et al.*, 2011a	Fingers/ Finger taps	Accelerometer, touch sensors	Average and standard deviation of the duration
Salarian *et al.*, 2007	Wrist/ Postural move	Gyroscope	Speed, amplitude, rhythm
Heldman *et al.*, 2011	Hand/ Tap, grasp& pronation-supination	Accelerometer, gyroscope, EMG	Speed, amplitude, rhythm
Kim *et al.*, 2011a	Fingers/ Finger taps	Gyroscope	Root-mean-square, cycle
Su *et al.*, 2003	Hand/ Grasps	Electromagnetic sensors	Speed, frequency

Kim *et al.* (2011a), from Konkuk University, Korea, quantified parkinsonian bradykinesia during finger taps using a gyroscope. RMS velocity, RMS angle, and the estimated power around dominant frequency were correlated well with clinical finger tapping scores.

3.3.3 Rigidity Quantification

For the quantitative assessment of parkinsonian rigidity, there are no available devices on the market. According to research conducted by Patrick *et al.* (2001), expense, complexity, and time involved are the most common reasons for not introducing quantitative rigidity evaluation in clinical praxis.

Some research projects have tried to explore the relationship between biomechanical parameters and the UPDRS rigidity scale. In most research, an examiner or a motor drive flexes and extends a joint repeatedly, and then parameters from the applied torque are calculated. However, there are also researchers who calculate rigidity parameters from the electromyographic potentials during flexion-extension movement. Patrick's research indicated that the correlation of mechanical properties with the UPDRS scores is superior to the correlation of EMG with the UPDRS scores (correlation coefficient *r*: 0.60–0.86 compared to 0.37–0.79) (Sakoda *et al.*; Patrick *et al.,* 2001).

Table 3-3: Summary of rigidity assessment methods. Here "+" denotes the system performance in a certain aspect, the amount of "+" represents a better performance; and "–" denotes no exact information available.

Methods	Assessed joint	Inter-variability	Intra-variability	Parameter	Signal process	Size	Fixed frequency	Device or reference
Feeling	Elbow	+	++	Feeling of examiner	–	–	No	Examiner test
Electrical current	Brain	+++	+++	Neuronal activity	+	+	–	ISIS MER
Electrical current	Hand/ Foot	+++	+++	Muscle activity	+	+	–	EMG
EMG; torque-angle	Wrist	+++	+++	Work	++	+	Yes	Shapiro *et al.*, 2007
Torque-angle	Elbow	++	+++	Mechanical impedance	+++	+++	No	Patrick *et al.*, 2001
Torque-angle	Elbow	+++	+++	Viscoelastic values	++++	++	Yes	Park *et al.*, 2011
Force-angle	Elbow	++	+++	EMG, torque bias	++++	+++	No	Endo *et al.*, 2009
Torque-angle	Elbow	++	+++	Viscoelastic values	++++	++	No	Prochazka *et al.*, 1997

Some systems are designed to model the relationship between changing joint angles (degree) and measured torque (N·m), which includes non-neural torque and neural torque. Force or torque transducer, EMG, and position or angle sensors are used. Some approaches use kinematics to restrict the movement of the limbs, while others do not. An overview of recent approaches is given in Table 3-3.

A potentiometer is easy to use for angle estimation. However, a potentiometer requires the examiner to strap the patient's limbs to some kind of cinematic device.

3.3.4 Dyskinesia Quantification

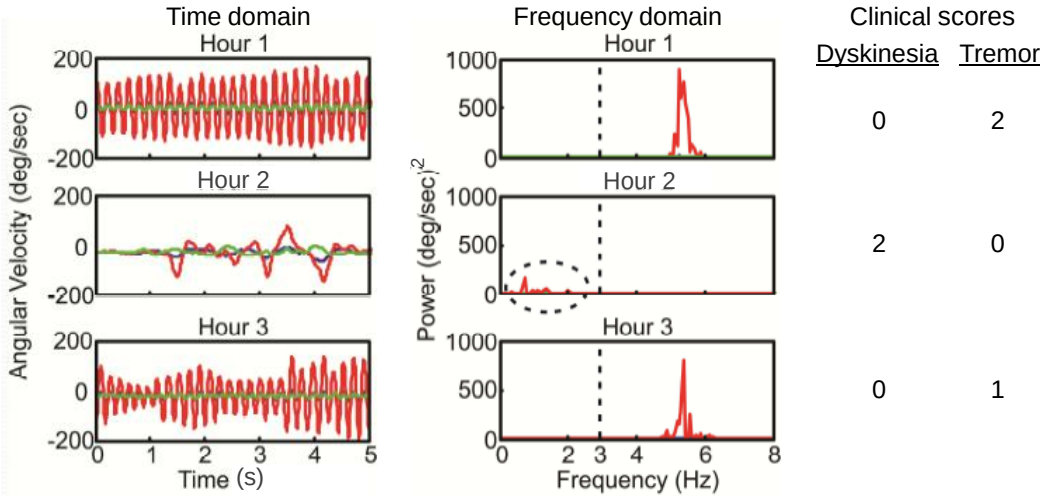

Figure 3-9: Signals of a triple-axis gyroscope and its power spectrums during an arms-extended task. This figure describes how the features change as a patient experienced one cycle of levodopa-induced dyskinesia. Tremor was apparent in hours 1 and 3, while the dyskinesia was experienced in hour 2 (Based on Mera *et al.*, 2013).

The research conducted by Burkhard *et al.* (1999) shows that the RMS of the power spectrum

of hand-attached gyroscope signals, from 0.25 to 3.25 Hz, during dyskinesia task correlated well with the five-point clinical ratings for dyskinesia severity.

As Figure 3-9 shows, Mera *et al.* (2012) revealed that the RMS of the frequency band, from 0 to 3Hz, from all the three gyroscope channels correlates well with the modified Abnormal Involuntary Rating Scale (m-AIMS). Two stationary motor tasks were performed during the arms-extended task: arms resting and arms extended. The dyskinesia severity was calculated based on the inertial sensor signal's range from 0 to 3 Hz. However, the algorithm could not be applied to voluntary motor tasks.

3.4 Commercial Systems for Quantification of Neurological Symptoms

Kinesia™ (CleveMed Inc., USA) is a compact, clinical device that is used to objectively quantify the motor symptoms of movement disorders such as PD and ET.

Figure 3-10: Kinesia™ (old version) for tremor and bradykinesia assessments (© CleveMed, U.S.A, 2010). On the left side of the figure, a subject performed the assessment task according to the video instruction. The right side of the figure shows the hardware of a Kinesia™ system.

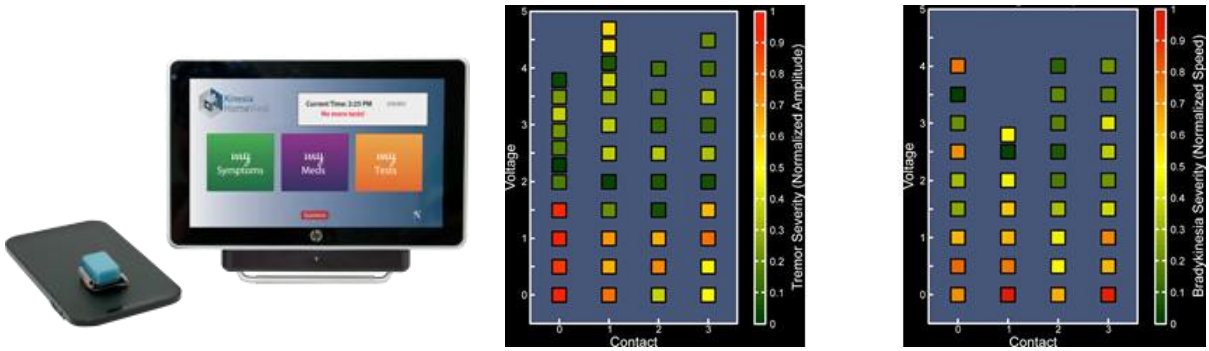

a) **b)** **c)**

Figure 3-11: Kinesia™ (new version) for tremor and bradykinesia assessments (© Great Lakes NeuroTechnologies, U.S.A, 2013). a) hardware and GUI; b) tremor tuning map for a patient during an outpatient programming session; c) bradykinesia tuning map for a patient during an outpatient programming session. The voltage is the stimulation intensity of the electrode. The color in the tuning maps means the severity of the symptoms from red (most severe) to green (no symptoms). CleveMed Inc. spun Great Lakes NeuroTechnologies Inc. in 2011, which focuses on the assessment of motor symptoms based on inertial sensors.

As shown in Figure 3-10, a *Kinesia*™ was worn on the finger and wrist of the patient while symptom information was wirelessly transmitted to a nearby computer for display, analysis, automated symptom severity scoring, report generation, and storage. Three orthogonal gyro-

scopes and three orthogonal accelerometers were placed on the finger, to capture motion with six degrees of freedom (DOF). This device can be used by PD patients to monitor the kinematics of motor symptoms such as tremor and bradykinesia. Several time- and frequency-based parameters are computed for each kinematic channel (axis) including peak power, frequency of the peak power, root mean square (RMS) of the angular velocity, and RMS of the angle. This device has been approved by the FDA (Giuffrida *et al.,* 2009). *KinetiSense,* an upgraded version of *Kinesia*™, is a small, lightweight, wireless device that integrates motion detection and EMG. Three orthogonal accelerometers and gyroscopes provide 3D motion tracking while two EMG channels record muscle activity.

As shown in Figure 3-11, Great Lakes NeuroTechnologies Inc. released the new generation of *Kinesia*™ in 2013, which can generate functional motor symptom response tuning maps. The wireless ring sensor communicates with the tablet computer via a Bluetooth interface. Tuning maps can be used to monitor the stimulation setting after DBS surgery for a particular symptom or averaged across multiple symptoms. Its scoring algorithms are clinically validated.

HandTutor™ (MediTouch Inc., Israel) is a state-of-the-art glove and software that enables intensive clinic- or home-based hand rehabilitation (quantitative assessment and customized training). As shown in Figure 3-12, it evaluates the extension/flexion of the fingers and wrist. It comprises six triple-axis accelerometers, five on the fingers and one on the wrist. The data recorded by the device include motion locus, spectrum, maximum velocity, and ROM (range of motion) (Carmeli *et al.,* 2009).

Figure 3-12: HandTutor™. Electro-optical sensors, bend sensors, and accelerometers are placed in the upper side of each finger. The training parameters of each finger are displayed in the GUI. It is power supplied by the USB interface of a computer (© MediTouch, 2010).

The *Motus Movement Monitor* (MOTUS Bioengineering Inc., USA) can be used to monitor the patient's responses for the electrode implantation during DBS surgery. As shown in Figure 3-13, only one gyroscope is used on the surface of the palm. The *Motus* system assists the neurologist in the selection process by providing quantification of movements, clearly documenting tremor characteristics, the extent of bradykinesia (via pronation/supination movements), and the prominent side of the disorder.

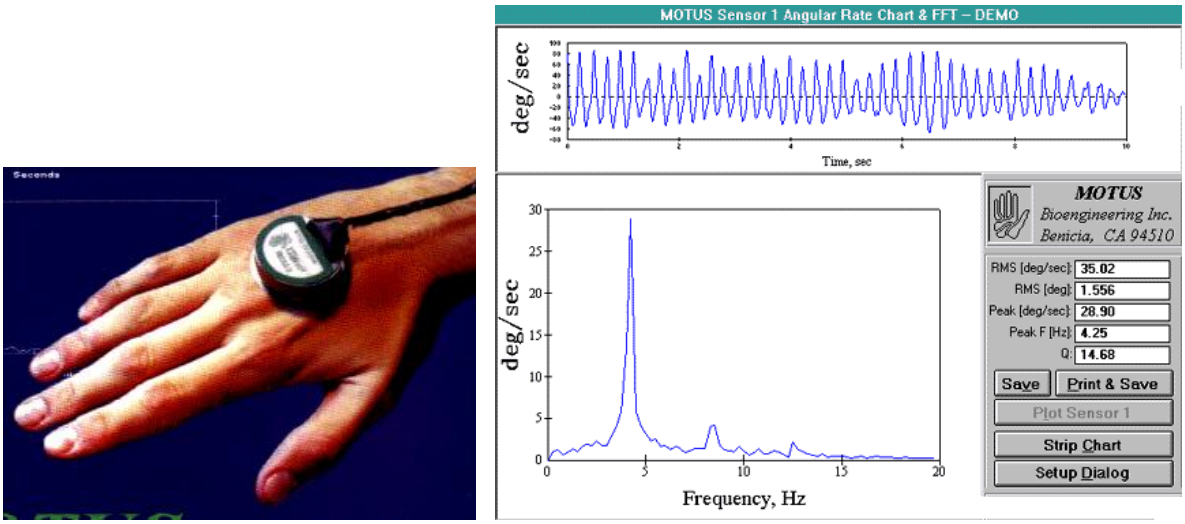

Figure 3-13: Motus Movement Monitor. The raw data, Fast Fourier Transform (FFT) chart and parameters are displayed in the GUI (© MOTUS, 2010).

In addition, glove-based hand motion tracking systems represent an appropriate method aimed at acquiring hand movement data. There are many products currently available on the market that can achieve these or similar goals. These include the *Cyberglove*, *P5 Glove*™, *5DT Dataglove*, *Acceleglove*, *Hand Mentor*, and *HandTutor*. They allow continuous tracking of hand joint angles and linear displacements.

3.5 Research Systems for Quantification of Neurological Symptoms

Su *et al*. (2003) of the University of East Anglia, UK, developed a three-dimensional motion recording system (data-gloves) for PD assessment. As shown in Figure 3-14 (a), this system uses 11 electromagnetic sensors on the hand. Time traces, frequency analysis, and speed analysis of these time traces are the key parameters. Tremor parameters, the rigidity of the wrist during rolling movements, the dexterity of finger pinching, and hand-gripping movements are recorded. As shown in Figure 3-14 (b), they later used EMG together with the previous motion system to obtain better results (Su *et al.*, 2003, 2007).

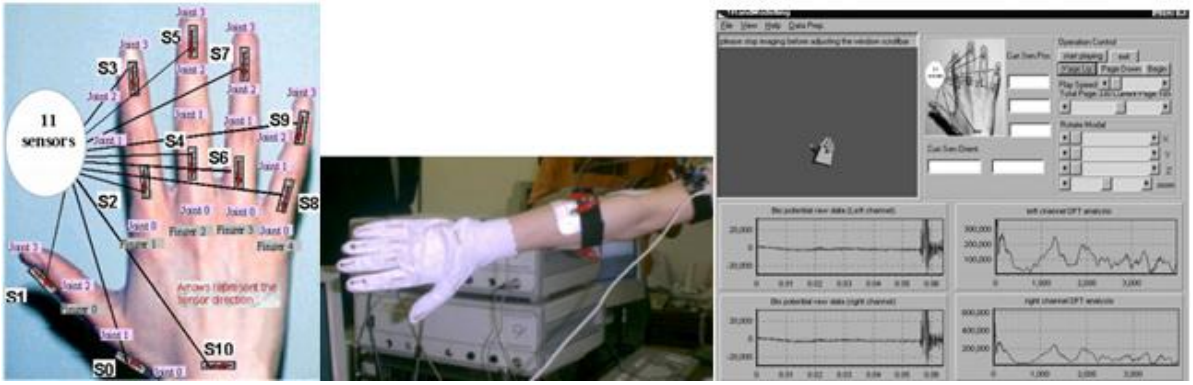

a) **b)** **c)**

Figure 3-14: 3D motion recording system. a) sensor layout; b) simultaneous recording system; c) user graphical interface of the simultaneous data recording (Taken from Su *et al.*, 2007).

Arash of the EPFL[1], Switzerland, designed a new measurement system consisting of five in-

[1] Ecole Polytechnique Fédérale de Lausanne

dependent, lightweight, autonomous sensing units, which were based on gyroscopes that can continuously record body movements during daily life. An accurate algorithm based on spectral estimation was proposed to detect and quantify tremor during the daily activities of PD patients with a resolution down to three seconds using gyroscopes attached to the forearms. This system, which is shown in Figure 3-15, also successfully detected ON and OFF periods in PD patients under ambulatory conditions (Arash *et al*., 2006).

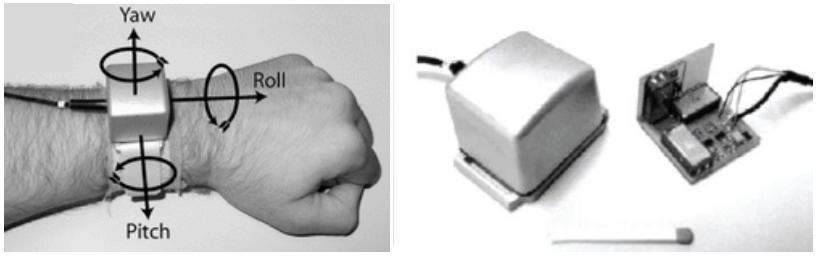

a) **b)**

Figure 3-15: Ambulatory system for quantification of tremor and bradykinesia. a) the sensitive axes of the 3D gyroscope; b) a closer photo of the module (Taken from Salarian *et al.*, 2006).

Bamberg from MIT (Massachusetts Institute of Technology), USA, built a shoe-integrated sensor system for wireless gait analysis. She used gyroscopes, accelerometers, and force sensors for the calculation of gait parameters. Detailed information on the gait cycle was obtained. Her PhD thesis described the signal processing methods of gyroscopes and accelerometers in great detail (Bamberg *et al.*, 2008).

Funded by EU Framework 7, and coordinated by Prof. José Luis Pons of the Bioengineering Group, CSIC (Spanish National Research Council), Spain, the tremor project team is developing an ambulatory brain-computer-interface-driven tremor suppression system based on functional electrical stimulation. This system will be used to detect and monitor tremor through a multimodal brain-computer-interface (BCI). The proposed BCI method will combine CNS signals (Electroencephalography, EEG) and peripheral nervous system signals (Electromyography, EMG) data with biomechanical data (inertial sensors) in a sensor fusion approach. It will model and track both tremor and voluntary motions (Ibánez *et al.*, 2010).

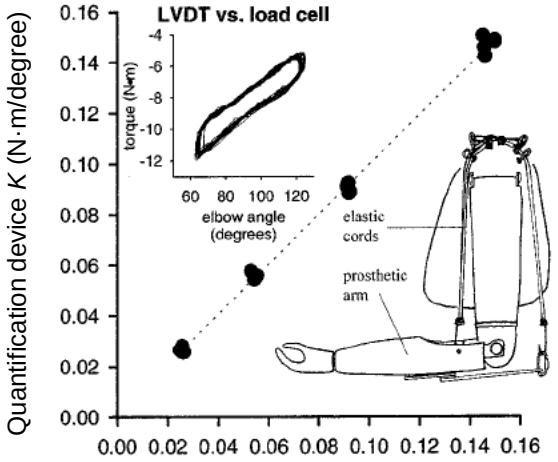

Figure 3-16: Validation of elastic stiffness (*K*) calculations using a model arm. The quantification device was tested on a prosthetic limb to which combinations of elastic cords were attached to produce different levels of constant stiffness. An examiner flexes and extends the subject's joint. A gyroscope in the arm was used to measure the elbow angular displacement, while a differential force transducer attached to the wrist was used to monitor the amount of force employed (Based on Patrick *et al.*, 2001).

Patrick *et al*. (2001), from the University of Alberta, Canada, have developed a stiffness quantification device. As shown in Figure 3-16, the device is based on two air-filled pads held distal to the joint and a gyroscope mounted on one of the force pads. Both pads are connected to a differential force transducer. Measurements of mechanical impedance (the magnitude of the vectorial sum of elastic stiffness and viscous stiffness) corresponded well with the clinical ratings of parkinsonian rigidity.

Other researchers have designed mechanical devices to simultaneously measure the torque and angular position of the elbow or wrist joint during flexion-extension movement (Shapiro *et al.*, 2007).

Sepehri *et al*. (2007), from the Islamic Azad University-Mashhad Branch, Iran, presented a test rig to measure the range of motion, and viscous and elastic components of elbow stiffness. As Figure 3-17 shows, the subject's elbow joint was fixed in the mechanical test rig. A balanced strain gage force transducer and a 10 KΩ potentiometer were used to measure attached force and angular displacement, respectively. Their results revealed that the elastic and viscous components of mechanical impedance measured with the device correlated well with the UPDRS ratings.

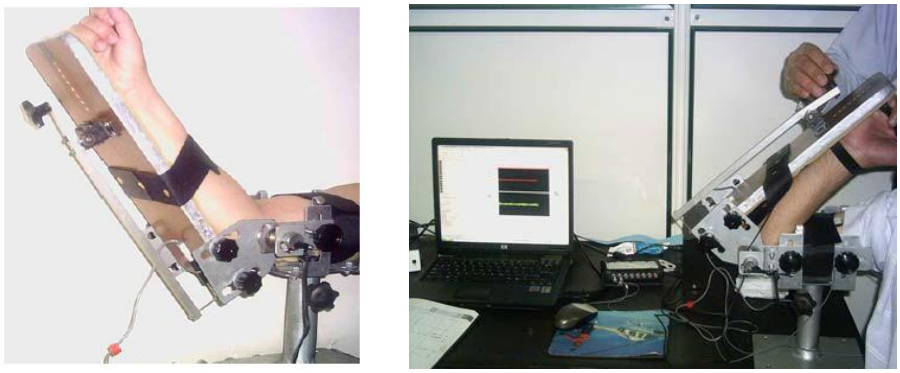

Figure 3-17: Mechanical rig test system and its operation (Taken from Sepehri *et al.*, 2007). The elbow movement was driven by an examiner.

As Figure 3-18 shows, Park *et al*. (2011), from the Korea University, analyzed the wrist's viscoelastic properties in PD patients. Their study suggested the mean viscosity during both flexion and extension correlated best with the clinical rigidity score.

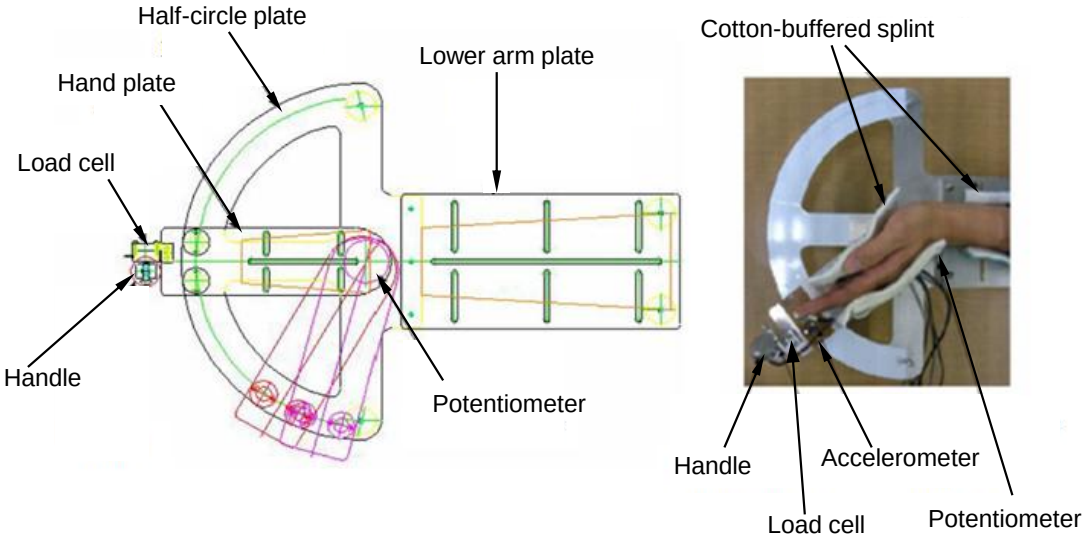

Figure 3-18: System structure and experimental setup for the analysis of the wrist joint's visco-elastic properties (Based on Park *et al.*, 2010). The wrist movement was controlled by a motor.

As shown in Figure 3-19, Niazmand *et al*. (2011a), from the TU Muenchen, Germany, presented a smart glove for quantitative evaluation of PD symptoms. Three primary symptoms could have been assessed. However, there was no correlation between the clinical rigidity severity and force sensor value. In addition, there was no discussion of tremor amplitude. The bradykinesia assessment task was finger taps.

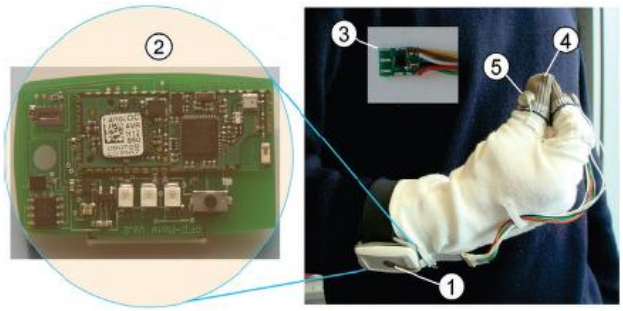

Figure 3-19: Smart glove for quantitative evaluation of PD symptoms (Taken from Niazmand *et al*., 2011a). 1) force sensor; 2) command module; 3) sensor board; 4) touch sensor (positive connector); 5) touch sensor (ground connector). The force sensor was attached to the surface of the command module.

Signal Processing Methods

In these products and research projects for the quantification of tremor or bradykinesia severity, a fast Fourier transform (FFT) or power spectral density (PSD) calculation in real-time is carried out. Fuzzy analysis, a machine-learning algorithm, and other algorithms are used for frequency and amplitude analysis. Regression analysis is used in most rigidity assessment systems.

3.6 Inertial Sensors and Sensor Fusion for Motion Tracking

3.6.1 Inertial Sensors and Inertial Measurement Unit

Some types of motion sensors have been commercially available for several decades in applications for ships, aircraft, and automobiles. However, these sensors' characteristics, such as dimension, power consumption, and price, have prevented their wide utilization in consumer electronic devices up until the past few years (Shaeffer, 2013).

Accelerometer (G-sensors), gyroscope, magnetic sensor (E-compass), and pressure sensors (barometers) are the four fundamental motion sensors for mobile device and other consumer electronics.

Accelerometers measure linear acceleration (dynamic acceleration) and tilt angle (static acceleration) with limited motion sensing functionality. Gyroscopes measure the angular velocity in one or more axes with high signal-to-noise ratio (SNR). Gyroscopes can accurately measure complex rotational motions in free space. Another difference between gyroscopes and accelerometers/compasses is that gyroscopes function fairly autonomously, other than depending on any external forces such as magnetic fields or gravity. Compasses detect only the heading of a triple-axis space based on the earth's magnetic field. Pressure sensors realize relative and absolute altitude by sensing the relationship analysis between atmospheric pressure and altitude.

Using a gyroscope or an accelerometer as the single source for angle calculation, also shows disadvantages (Patel *et al.,* 2008; Okuno *et al.*, 2009). The output of a gyroscope is read at

certain time intervals. Thus, the information between these periods is missed. In order to improve the accuracy of angular displacement, more gyroscope samples are needed, which takes more processing time. Due to the inaccuracy of each gyroscope reading, the angular displacement calculated will drift over time. The angle calculation with accelerometer data is based on gravity. The accelerometer will give an accurate reading of tilt angle in a static state. But accelerometers are slower to respond than gyroscopes and are prone to vibration or noise.

An accelerometer can be used to correct gyroscope drift errors and is more sensitive to non-rotation movement.

Another type of sensor commonly used to reduce drift is the magnetometer, which measures magnetic field strength in a given direction. The magnetometers measure the strength and direction of the local magnetic field, allowing the north direction to be found. The yaw angle is calculated from the magnetic field.

The silicon MEMS-based technology reduces the cost and package size of an inertial sensor. At present, most analog inertial sensors are replaced by digital inertial sensors, which means that there is no analog-to-digital converter (ADC) outside the sensor anymore. In addition, three axes sensors are combined in a single chip. Programmable filter and full-scale range setting are also available inside the chip. All these features give MEMS-based sensors better noise performance than before.

Motion processing with MEMS technology, which measures and intelligently processes the movements of subjects in three dimensional spaces, is the next major revolutionary technology that will drive innovation in mobile device design, human-machine interface design, and applications for navigation and control. Consumer-grade IMUs based on MEMS provide a simpler user interface for intuitionistic navigation and control of handheld mobile devices. Due to the advantages of IMUs, the operational complexities that have confused many owners of sophisticated consumer electronic devices can be resolved (Shaeffer, 2013).

Over the past 30 years, inertial sensors have been used in major automotive and industrial markets. With the development of mobile devices, especially the revolutionary iPhone and iPad from Apple Inc., U.S.A, motion MEMS sensors with low-cost, ultra-compact, low power consumption and multiple-axis sensing have been developed in last five years. ST, Invensense, Bosch, Freescale, and Kionix are the dominant motion MEMS manufacturers at present.

InvenSense claimed it was the first company to develop an integrated triple-axis MEMS gyroscope and six-axis motion-tracking device, with digital-output, for consumer electronics applications. In February 2011, Invensense Inc. launched MPU-6000, which integrates three accelerometers and three gyroscopes into a single package (4mm × 4mm × 0.9mm). In August 2011, nine-axis motion-fusion algorithms (together with a triple-axis compass outside connected) and an upgraded version (MPU6050) were presented.

3.6.2 Accelerometer-Magnetometer and Attitude Heading Reference System

A six-axis accelerometer-magnetometer unit, which contains a triple accelerometer and a triple magnetic sensor with about 0.6 mA of power, accurately determines heading and orientation. Some companies regard this type unit as a simulated IMU. However, this unit can only measure slow changes in a three dimensional space.

Gyroscopes and accelerometers are great, but they cannot provide precise and accurate calculations such as the absolute heading value. An attitude heading reference system (AHRS) consists of a triple-axis gyroscope, a triple-axis accelerometer and a triple-axis magnetometer (compass). The use of the compass, which provides a heading reading, offers enhanced angular position accuracy, and reduces gyroscope drift.

Raw output from multiple discrete sensors requires development and incorporation of a complex set of sensor fusion algorithms, calibration firmware, and performance testing prior to use (Paces & Popelka, 2012).

In August 2011, nine-axis motion-fusion algorithms (together with a triple-axis compass outside connected) and an upgraded version (MPU9050) of the Invensense MPU6050 were presented. After that, many manufacturers were forced to incorporate discrete motion sensor components to deliver nine-axis Motion Interface functionality.

Sensor fusion is not limited to a nine-DOF (degree of freedom) solution. For the requirement of indoor navigation, the 10-DOF or 10-ASF (Acclaim Skeleton File) solution includes a triple-axis accelerometer, triple-axis gyroscope, triple-axis magnetometer, and a single-axis barometer. Adding a barometer enables altitude detection, since pressure changes with altitude at a rate of about 10 Pa/m. At the moment, some mobile motion devices or some functions of other consumer electronics, such as iWatch, Google Glass, are based on nine-DOF or 10-DOF sensor fusion realization.

3.6.3 Sensor Fusion Algorithms

The primary feature of IMU and AHRS is the sensor fusion. For the rotation movement measurement with Euler angles, complex finite impulse response (FIR) or infinite impulse response (IIR) filters such as Kalman filters, Parks-McClellan filters, are widely used. The Direction Cosine Matrix (DCM) algorithm is used to calculate the orientation of a rigid subject, offering another way to construct a rotation matrix (Edwan *et al.*, 2011).

In addition, most inertial manufactures present unique on-board sensor fusion algorithms. For example, the inertial sensors from Invensens Inc. include an in-chip sensor fusion module named Digital Motion Processor™ (DMP™), which is capable of processing the complex nine-axis MotionFusion algorithms. ST Microelectronics Inc. presented sensor-fusion software named iNEMO Engine, which is based on dedicated filtering and prediction algorithms. DMP™ and iNEMO Engine combine different data from multiple sensors. These sensors can directly provide a series of outputs such as rotation, linear acceleration, gravity, and quaternion. The control of these sensors can be performed using an eight-bit microcontroller (MCU) and are independent of environmental conditions to achieve the best performance.

In addition, there are some inertial sensors embedded into a single chip with an MCU and other function modules such as a radio frequency (RF) module.

3.6.4 Discussion

The key difference between an IMU and an AHRS is that the AHRS provides accurate attitude and heading solutions (yaw angle) whereas the IMU only delivers the absolute attitude solution (pitch and roll angles). As hand tremor is mainly a rotational movement, an AHRS is good for measuring hand tremor. However, the magnetometer is susceptible to ferromagnetic material, and thus needs accurate soft and hard iron calibration. As the period of hand tremor

movement assessment is short, the drift of yaw is slow and can be removed with a threshold setting for gyroscope data. An IMU can also achieve good results when measuring hand tremor.

The accelerometer is good at measuring linear motion and the gyroscope is good at measuring rotational movement. When a gyroscope and an accelerometer are combined, a better result can be realized. The combination of small, low-cost but high performance triple-axis gyroscopes, which have recently become available, and the existing triple-axis MEMS accelerometers, enables the possibility of this six-axis measurement and control. Mobile devices have already embraced the novel features provided by the MEMS IMU, which combines a triple-axis gyroscope and a triple-axis accelerometer. The six-axis motion processing provides the mobile device's absolute position in a three dimensional space with greater accuracy, precision, and responsiveness.

3.7 Limitations of Existing Technology

The disadvantages of the state of the art are discussed in this section.

3.7.1 Real and Potentially Solvable Limitations

Subjective assessment by the surgeons and MER system are widely used to support symptom assessments during DBS surgery. The two intraoperative approaches for neurological symptom assessments show disadvantages as follows:

a) Subjective assessment by surgeons according to the five-point clinical ratings:

- The judgments of the surgeons are based on their experience and differ from each other.

UPDRS and TETRAS are discrete and subjective ratings. They require a neurologist to visually assess the patient based on experiences, and the neurologist cannot capture complex symptom variations that happen in response to the stimulations during DBS surgery. The symptom scores for the same patient may differ widely depending on the examiner (Jankovic *et al.*, 2007).

The coarse resolution of the ratings is insufficient for assessing small changes in tremor severity. Furthermore, the extent of inter-clinician and inter-subject rating variability is unknown (Machado *et al.*, 2003).

b) Micro-electrode recording (MER):

- It is an indirect motion tracking. The hair-thin microelectrodes are placed within the intended target to record brain cell activity. The surgeon needs to inspect and listen to the pattern of the cell activity. This physiological confirmation is also based on the experience of the surgeon (Winestone *et al.*, 2012).

- The MER signals are spike signals, which are not good for signal processing (Winestone *et al.*, 2012).

- Research shows that only about 67% of the cases initially planned with MER method were taken for the final target (Bour *et al.*, 2010).

> According to the research of Bour *et al*. (2010), the location of the best MER activity did not necessarily correlate with the position that produced the optimal clinical response to microelectrode testing intraoperatively.

EMG does not directly measure body movements and a large number of electrodes may be needed to investigate complex movements. Same with MER, the information collected on frequency is good, but that on the magnitude is less reliable. Contact resistance is also a significant variable. Furthermore, no information on displacement, velocity or power can be obtained. The EMG waveform of tremor is spiky and exhibits an impulse chain in the morphology. Impulse-like data are hard to analyze with Fourier spectral methods or other traditional amplitude methods. The measured amplitude is variable and thus the result is inaccurate (Saara *et al.*, 2007).

Devices other than the MER described above are used for general purposes, and are not specifically designed to be used as guiding tools during DBS surgery and do not meet the needs of the operating room. They have demonstrated limited usability in clinical settings due to deficiencies in wearability, fidelity, and flexibility. The severities of ET and parkinsonian symptoms, which are the effect of DBS therapy, require real-time and accurate assessment of major parameters according to the UPDRS. The severity changes of the primary symptoms are crucial when evaluating the effect of DBS. Easy manipulation and comfort are also important. The graphical user interfaces (GUI) of these systems are also unsuitable for the DBS monitoring.

Some of the glove-based systems, such as *Cyberglove*, are accurate but relatively costly ($10,000 per *Cyberglove*). Others are more affordable, for example, the *P5 Glove*™ (approximately $100 per glove) (Dipietro *et al*., 2008). Most use piezoresistive sensors, fiber optic sensors, and Hall-effect sensors, rather than inertial sensors. However, a major limitation of these systems is their limited portability caused by the presence of cloth support. The cloth support was believed to affect the measurement performance (Dipietro *et al*., 2008). The data obtained from these gloves have to be modified for further processing. In addition, the settings of the sensors are not easy to operate and calibrations are needed for new users. A new data glove with gyroscopes and accelerometers is more feasible.

For bradykinesia assessment, finger tapping, and pronation/supination movement are not easy to perform during DBS surgery. Rigidity is clinically defined as increased resistance to passive movement of a joint. For the joint movement, derived by a motor, has bigger dimensions and should be fixed on a table (Patrick *et al.*, 2001).

The displacement measurement for hand rigidity and hand grasping can be estimated through double integration of raw acceleration data over time. However, gravity vector and bias should be deducted from the raw acceleration. Then IMUs, which includes three-axis gyroscopes, should be utilized in this study.

3.7.2 Limitations That Cannot Be Solved at This Time with Reasonable Effort

The basic changes in the EMG and MER signals, which are caused by PD or ET, are an increased tonic background activity and an alternating pattern of signal bursts. During the EMG or MER analysis of the symptoms of PD and ET, special attention has been paid to the analysis of these bursts by measuring their counts, magnitudes, durations, and frequencies (Rissanen *et al.*, 2007). For the measurement of vigorous movement, an IMU provides good

results. However, for slight motion disorders, the difference between EMG and IMU requires further validation.

Tremor, bradykinesia, and limb rigidity are the characteristic features of PD. However, bradykinesia responds to DBS after a period of hours, whereas tremor and rigidity respond within seconds (Prodoehl *et al*., 2007). For the design of the assessment tasks, there is no concern about this situation yet.

The UPDRS is a subjective rating and the rigidity scores for the same patient may differ widely depending on the examiner. Because of the role of the patient's passive movement in assessing rigidity, the performance of the examiner also affects the assessment results through a rigidity assessment system without a motor (Patrick *et al.*, 2001).

Rigidity occurring in PD patients commonly has a "cogwheel" character, which is not represented by the UPDRS (Van Dillen *et al.*, 1988).

The extent of hand tremors in PD varies between patients. The ratio of rotational motion to linear motion is not fixed. An optimal ratio that fits all patients can only be obtained after a large number of clinical measurements have been taken (Timmer *et al.*, 1993).

The goal of DBS surgery is to obtain the best treatment strategy, because PD affects every patient differently. Tremors and other symptoms do not appear at the same time for every patient. The assessment results of a patient with the designed system also depend on the skill level or psychological factors of the patient. The significant individualized factors of the patient include the age, years of disease, level of functional impairment, concurrent medical issues, and sensitivity to medications (Spieker *et al.*, 1995). Therefore, it is important to consider various individualized factors of the patient when utilizing assessment results. These factors can be investigated only after long-term use of the glove monitoring system. Objective assessment methods which fit for all patients with PD or ET are needed in the assessment of their symptoms.

4. Glove Monitoring System

Because all the primary symptoms of PD and ET can be assessed on the hand, a glove monitoring system based on inertial sensors and force sensors is supposed to monitor the severities of tremor syndromes, bradykinesia, and rigidity during DBS surgery.

Chapter 4.1 introduces the task description of the glove monitoring system. Several assessment tasks for tremor syndromes, bradykinesia, and rigidity were chosen for the glove monitoring system according to the requirements of DBS surgery. The supposed parameters and their accuracy settings, together with the other requirements, are presented in this section too.

The expected advantages of the glove monitoring system are described in Chapter 4.2.

4.1 Task Description

Currently there is no system available for assessing all the primary PD symptoms. Therefore, it is important to realize three assessment tasks in one system. The goal of this project is to develop a measuring system to be used in DBS surgery, which quantifies the severity of hand tremors, bradykinesia, and rigidity.

4.1.1 Assessment Movements in This Study

According to the literature and the requirements of neurosurgeons, several assessment tasks should be chosen to assess the severity of the symptoms of PD and ET. All the assessment tasks are supposed to have the same duration (from five seconds to one minute). The surgeon instructs the patient to perform different tasks. The observers can view all the parameters and raw signals on the computer.

According to the MDS-UPDRS, tremor assessments include three tasks to test for the rest tremor, postural tremor, and action tremor.

According to the requirement of surgeons, whole-hand grasping was chosen as the bradykinesia assessment task because the patients can perform it easily during DBS surgery.

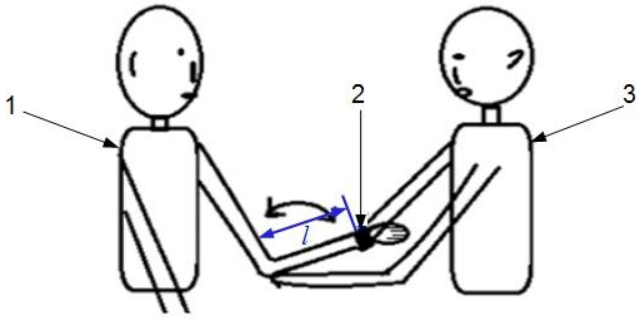

Figure 4-1: Rigidity assessment task. 1) subject; 2) rigidity cuff; 3) examiner. Here *l* is the arm length of the patient. The examiner flexes and stretches the elbow through the rigidity assessment cuff attached to the wrist. Several cycles are performed during the 10-second assessment task. The examiner should make sure the elbow position of the patient is stable (Based on Dai *et al.*, 2013b).

Passive flexion and extension of the elbow was used to assess rigidity. Figure 4-1 shows the rigidity cuff and rigidity quantification task in this project. The rigidity cuff is strapped to the

distal end of the patient's forearm. An examiner flexes and extends the patient's elbow joint through force at the point of the rigidity cuff on the wrist.

After discussion with the surgeons, the duration of a single task in this study was set at ten seconds. Each time two or more measurements for a single task should be repeatedly performed for better results.

4.1.2 System Objectives and Parameters

The parameters that should be obtained from both time- and frequency-domain signal processing methods and displayed in the GUI are listed as follows:

- Severity of hand tremors (frequency and amplitude of tremors).
- Severity of finger bradykinesia (mean and standard deviation values of angular displacements in hand grasps; dominant frequency in hand grasps).
- Severity of elbow rigidity (viscosity, elasticity, and the dominant frequency of elbow movement).

The angular displacements in the bradykinesia task represent peak-to-peak values of the hand grasping ranges during one time bradykinesia task.

In addition, the power spectral density of the signals from the gyroscope and accelerometer (from 0.25 Hz to 12 Hz), together with the raw data, needs to be displayed in real-time.

The severities of tremors, bradykinesia, and rigidity should be displayed at levels from 0 to 4 according to the UPDRS ratings. There is, however, no literature about the bradykinesia parameters of hand grasping movement and UPDRS scores. The severity of parkinsonian rigidity is very difficult to assess. Therefore, the severity scores of bradykinesia and rigidity according to the present parameters need to be further investigated.

Fluctuations in the motor performance (ON/OFF fluctuations) of PD patients can also be indicated by the changes in these parameters.

For DBS electrode positioning, only the tremor amplitude is required, because the tremor frequency has no relation to the symptom severity of parkinsonian tremor or ET. The tremor amplitudes, which are regressed from the peak powers of the IMU signals, can be gauged as the clinician ratings. However, the parameters of bradykinesia and rigidity cannot be normalized directly as UPDRS ratings at present.

Unlike for tremor, peak power during hand grasping is not correlated with the clinical UPDRS score. Instead, the mean value and standard deviation (SD) of hand grasping ranges ($\overline{|\varphi|}$ and $\sigma_{|\varphi|}$), where φ is the peak-to-peak values of the hand grasping cycles, can be used as the parameters of bradykinesia. However, the correlation between these two values and the UPDRS score needs further study (Post *et al*., 2005).

In the clinic, rigidity is assessed by a neurologist who moves the subject's limb, scoring the result according to the UPDRS ratings. However, rigidity scores for an individual patient may vary depending on the examiner. Such scales are susceptible to the problems of sensitivity and reliability. Mechanical impedance, which means the magnitude of the vector sum of elas-

tic stiffness and viscous stiffness, is nonlinearly related to UPDRS rigidity ratings (Charles, 2003).

4.1.3 Accuracy Settings of the Parameters

After the clinical measurements and experiments, the correlations between the measured parameters (dominant frequency and amplitude in each tremor task; dominant frequency, mean, and standard deviation values of grasping ranges in bradykinesia task; viscosity, elasticity, and frequency of elbow movement) and the UPDRS or TETRAS scores can be determined.

For calculating the accuracy settings in Table 4-1, the parameters obtained from the glove monitoring systems with the IMU and force sensors must be compared to the judgments of doctors according to the UPDRS ratings. The parameters should meet the accuracy setting as shown in Table 4-1. In Table 4-1, r^2 is the coefficient of determination and RMSE is the root-mean-square-error (RMSE).

Table 4-1: Parameters and their required accuracies. For the *RMSE* in rigidity parameter (mechanical impedance), there is no relative literature.

Task	**Parameter**	**Unit, [Range]**	**Required accuracy**		**Reference**
			r^2	RMSE	
Rest tremor	R_1	1, [0–4]	0.85	0.32	Giuffrida *et al.*, 2009
Postural tremor	R_2	1, [0–4]	0.88	0.32	Giuffrida *et al.*, 2009
Action tremor	R_3	1, [0–4]	0.60	0.45	Giuffrida *et al.*, 2009
Bradykinesia	$\overline{\lvert\boldsymbol{\varphi}\rvert}$	°, [0–360]	0.72	0.52	Heldman *et al.*, 2011
Bradykinesia	$\sigma_{\lvert\boldsymbol{\varphi}\rvert}$	°, [0–360]	0.62	0.65	Heldman *et al.*, 2011
Rigidity	Z	N/°, [0–50]	0.35	-	Patrick *et al.*, 2001

With patients and volunteers, the functionality and accuracy of the glove monitoring system should be tested and verified.

4.1.4 Requirements

General requirements of the glove monitoring system are listed as follows:

- Easy to perform for both the surgeons and patients (based on the intraoperative test tasks).
- Help the surgeons to quantify symptom severities during DBS surgery and as feedback to the electrode stimulation.
- Accurate and reliable: the parameters should meet the accuracy settings in Table 4-1.
- Quantify symptom severities according to the UPDRS or TETRAS ratings.
- Provide parameter-recording lists to compare symptom severities in all tested electrode positions.

- High security and low risk.
- Does not restrict the patient's movement (comfortable).
- Portable and with small dimensions.
- Meet the requirements of the operating room.

Some technical requirements are listed as follows:

- Accurate calibration plays a key role in the IMU measurements: the accuracy of the force measurement and the angular displacement measurement should be higher than 20% and 10% respectively.

- A large amount of clinical measurements is needed for the modification of algorithms, especially the coefficients of the regression models used in this project: 30 patients for each symptom should be measured with this glove monitoring system.

- The raw data from the sensors should be displayed to show the original hand movement. The raw data and measured parameters should also be stored in a file. A real-time PSD display of the inertial sensor signals over the entire frequency range (0.25–10 Hz) should be incorporated.

- The user graphical interface should be easy to use and intuitive, both for technicians and surgeons.

- A database with customized reporting functions and data management is required.

- The assessed parameters should be updated quickly when the assessed symptom changes. These parameters should be saved and displayed for contrast when the electrode is moved to different positions.

- To avoid radio frequency interference (RFI) in the operating room, a wired measurement device is required during DBS surgery. A wireless measurement device is presented only for the measurement outside the operation room.

4.2 Expected Advantages

The major advantages of this glove monitoring system are:

- **Objective assessment, thus easing the surgeons' workload.**

This project focuses on DBS, specifically integrating the overall measurement of finger and elbow movement. By incorporating a glove for measuring and displaying the parameters and waveforms on a computer, the system will be easy to use and relieve the surgeon. The PSD method in this project does not simply divide the time dimension into windows (3–5 seconds or longer), and a single data point can be used more than once. Thus the PSD chart is continuous with the sampling interval. The single-sided, scaled, auto-power spectrum of the time-domain signals will be displayed together with the raw signals. This feature will allow better detection of changes of the symptoms.

- **Three primary symptoms of PD and ET are implemented in a portable system.**

Unlike previous studies, the three primary symptoms are included in a system. In addition, this system meets the requirements of DBS surgery.

- **Electronics safety because the electronic parts have no contact with the patient's body.**

These sensors have no direct contact with the human body, thus this system is safer than EMG and MER.

- **MEMS IMU technology makes the system smaller but with a higher performance compared to previous motor assessment systems.**

With ever-smaller dimensions and higher performance, it is easy to detect motor disorders in PD and ET. The latest motion MEMS sensors make it is possible to realize motor disorders with small dimension and higher performance.

- **Higher resolution compared to the UPDRS or TETRAS ratings: 0.01.**

Each sub-scale of the UPDRS are from 0 to 4, where 0=normal, 1=slight, 2=mild, 3=moderate, and 4=severe. Most of the previous research only compared the outputs of their systems to this five-point rating scale (Elble *et al*., 2006). During DBS, a higher resolution for all parameters is needed.

Accelerometer data showed strong correlations with UPDRS rest tremor scores for both tremor duration and amplitude, especially when the hand tremor involved non-rotational movement. However, accelerometers measure linear acceleration and are influenced by gravity, whereas gyroscopes measure gravity-independent angular velocity. Tremor measured using gyroscopes correlated well with UPRDS scores, with higher sensitivity and specificity than previous studies that used accelerometers (Giuffrida *et al.*, 2009). By using a six-axis sensor motion fusion method, the measured parameters are more sensitive to hand movements in all directions.

After surgery, this glove monitoring system also can be used to track the progress of the patients and to provide feedback to physicians on the long-term results of surgery. When the patient returns for periodic readjustment of the neurostimulator, the glove monitoring system can be used to provide quantitative measurements of tremors and bradykinesia to assist in selecting the optimum parameters for electrode stimulation.

5. System Concept

Two designs using wireless communication interfaces are first introduced in Chapter 5.1. These designs could be used for a series of tremor and bradykinesia assessment tasks. All fingers were attached with sensors. These designs are not for applications outside of the operation room, other than for DBS surgery.

According to the requirements during DBS surgery, the static and dynamic system descriptions of the glove monitoring system are described in Chapter 5.2 and Chapter 5.3 respectively. The first step in designing the glove monitoring system includes two parts: one for tremor and bradykinesia assessment, the other for the rigidity assessment. In the end, a combined version based on the two separate systems is introduced.

5.1 Designs with Wireless Communication Interfaces

At the beginning of the study, there were two designs for PD assessment based on wireless communication, touch sensors, and inertial sensors (gyroscope and accelerometer). Several prototypes based on these designs have been carried out but they were not for the purpose of DBS. They could be used for the parameter settings of the neurostimulator after DBS surgery.

According to the literature, accelerometers and gyroscopes placed on each finger can collect enough information about parkinsonian tremors (Dipietro *et al*., 2008). A gyroscope is better for bradykinesia assessment. This suggests that a triple-axis accelerometer and a triple-axis gyroscope on each finger will provide sufficient information regarding the hand activity of patients with PD or ET. Compared to a gyroscope and an accelerometer on one finger, the use of six gyroscopes and six accelerometers on all fingers and the wrist would provide more information about hand movement. Thus, the quantification of tremors and bradykinesia would be more objective.

Figure 5-1 shows the diagram of the first tremor and bradykinesia assessment system with a wireless interface. In addition to inertial sensors, four touch sensors were attached to the fingers as well. The touch sensors were used for bradykinesia assessment (finger tapping task).

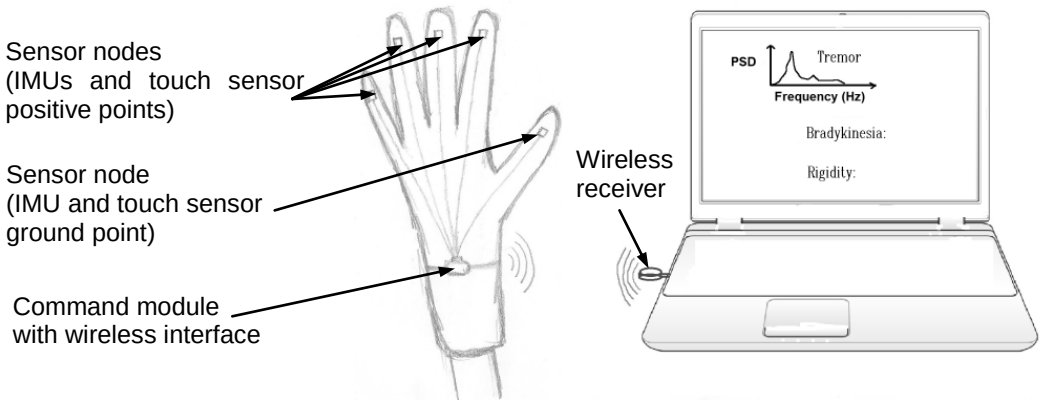

Figure 5-1: Components of the tremor and bradykinesia measuring system with wireless communications.

The mean tremor amplitude in all fingers, distance, and duration between two finger taps were calculated as the parameters of tremor and bradykinesia, respectively. As a result, from the measurement of the difference between finger motions, the obtained parameters could be more accurate.

After the analysis of these parameters, fewer sensors were adopted but with the same quality. For a simplified version of this design, the thumb and forefinger should be placed with the inertial sensors and touch sensors.

During DBS surgery, the glove monitoring system is wired to a computer, whereas after surgery a wireless system can be used. This system was for the assessment outside of the operation room and could not assess rigidity severity.

5.2 Static System Description

Figure 5-2 shows the original system diagram of the glove monitoring system. The glove monitoring system is based on MEMS IMUs, FSRs, and a medical textile glove. A sensor board with an IMU placed in the upper side of a finger is used to assess tremors and bradykinesia. The rigidity assessment part consists of a rigidity cuff, which was able to be attached to the wrist and includes two differential force sensor boxes and another IMU. The rigidity assessment cuff is designed to attain the model of a joint's movement state (angular displacement and velocity) and its measured torque (N•m), which includes non-neural torque and neural torque. The sensor data is acquired by a command module and sent to a computer via a USB cable. The sensor board, command module, and rigidity cuff can be integrated into a textile glove. Further signal processing is carried out on a computer using MATLAB, Visual Studio, or LabVIEW.

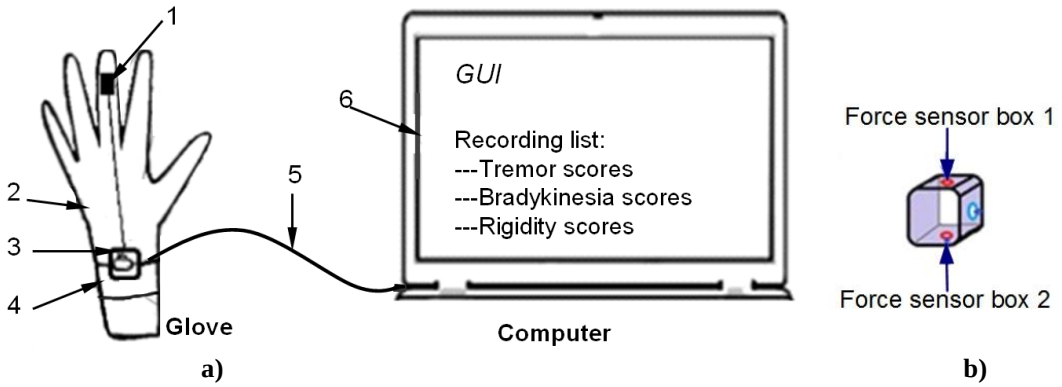

Figure 5-2: a) general system diagram of the glove monitoring system; b) rigidity assessment cuff. The components are: 1) sensor board (IMU); 2) textile glove; 3) command module; 4) rigidity assessment cuff; 5) USB cable; 6) graphical user interface (Based on Dai *et al.*, 2013a).

The computer communicates with the command module via a USB cable (Lorenzo, *et al.*, 2011). The wired communication, instead of wireless communication, has the advantage that this system even can be used in the operation room.

A 6-axis IMU module (combines a triple-axis gyroscope and a triple-axis accelerometer) on the upper side of the finger is connected to the command module using a Two-Wire Interface (TWI). The IMU module is used for tremor and bradykinesia assessments.

An IMU is attached to the wrist while two force sensor boxes are on both sides of the wrist. These sensors are used in the rigidity assessment. A medical textile glove incorporates the command module and the sensor board (IMU). A series of textile gloves are used to fix the command module and the sensor board to the user's hand.

The positions of all sensors are shown in Figure 5-3.

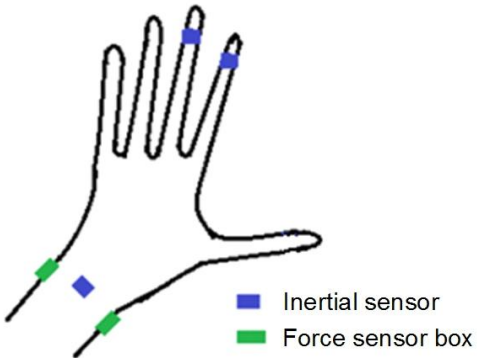

Figure 5-3: Positions of the sensors. For the position of the sensor board (IMU), only one finger from the index finger and middle finger was chosen according to tremor or bradykinesia tasks.

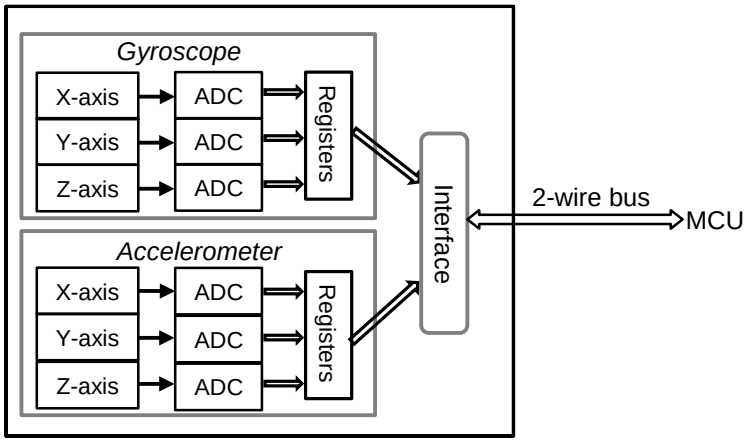

Figure 5-4: System diagram for an IMU chip. Two Wire Serial Interface (TWI) is compatible with the Philips's IIC protocol.

The system diagram of an IMU chip is shown in Figure 5-4. It includes a gyroscope and an accelerometer.

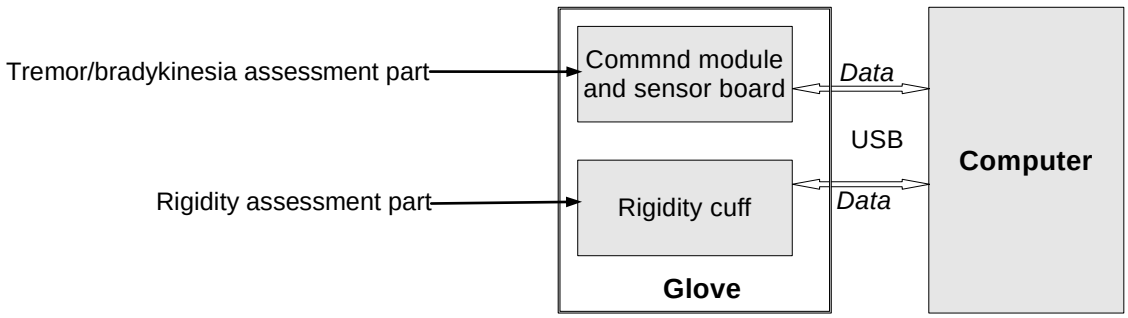

Figure 5-5: Two parts of the glove monitoring system.

At first, two separate parts were implemented as Figure 5-5 shows, because rigidity assessment is different from tremor and bradykinesia assessment. One part was the system for the tremor and bradykinesia assessment, while the other was for the rigidity assessment.

5.2.1 System for Tremors and Bradykinesia Assessment

Parkinsonian tremor is called "pill-rolling" tremor, as it is likened to rolling a pill between the thumb and index finger, because of this, the IMU was placed on the upper side of the index finger (Giuffrida *et al.,* 2009). For bradykinesia assessment, the inertial sensor in the middle finger has the best effect. All the data were transmitted to the computer in real-time via a seri-

al-to-USB communication interface. The system diagram of the tremor and bradykinesia quantification system is shown in Figure 5-6.

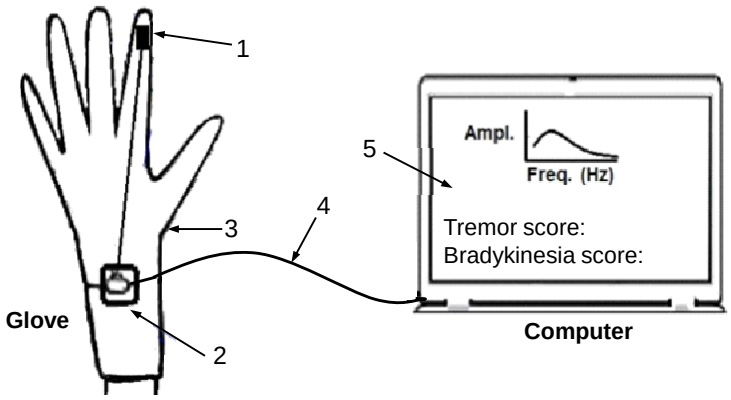

Figure 5-6: System diagram of the tremor and bradykinesia quantification system. 1) sensor board; 2) command module; 3) textile glove; 4) universal serial bus (USB) cable; 5) GUI.

5.2.2 System for Rigidity Assessment

The level of parkinsonian rigidity was able to be measured using an IMU and force sensors on the wrist. Figure 5-7 shows the system diagram of the rigidity assessment system. The rigidity cuff was connected to the computer via a USB cable.

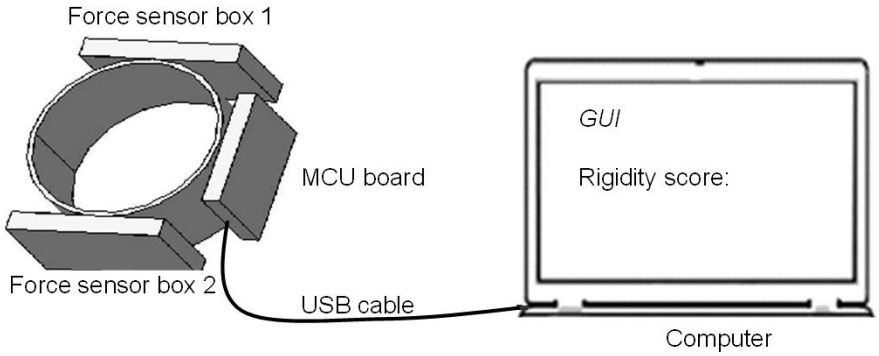

Figure 5-7: System diagram of the rigidity assessment system (Based on Dai *et al.*, 2013b).

Because the movement of the wrist and elbow has two directions: passive (PA) and contralateral active (CA), both sides of the wrist need a force sensor box.

Each force sensor box included four force sensitive resistors (FSR sensors or FSRs), which were in parallel connection to one output. The output connected one end to the power supply and the other to a pull-down resistor to the ground. The point between the fixed pull-down resistor and the force sensor box was connected to the analog input of a microcontroller. Compared to a single force sensor, the force sensor box had the benefits of higher measurement stability and a bigger contact patch for the examiner. Two force sensor boxes were connected to the command module. The IMU part (a triple-axis gyroscope and a triple-axis accelerometer) was also included in the command module. All the data were transmitted to the computer via a serial-to-USB communication interface.

Figure 5-8 shows the structure of a force sensor box. Four FSR sensors were located in the four bottom corners of the housing and were in contact with the rubber feet on its upper side. This structure has the advantage that the force sensor box provides almost the same value when an examiner presses on every point of the housing's upper side with the same force. The

viscosity and elasticity of the elbow, which are the major components of mechanical impedance, were calculated with the sensor data and displayed in the GUI (Post *et al.*, 2009).

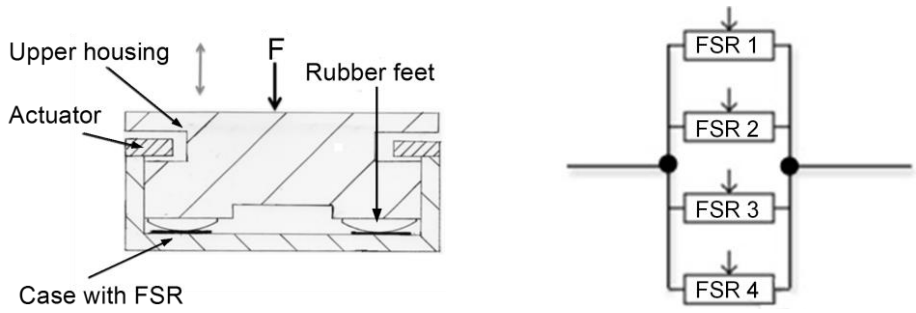

Figure 5-8: Structure of the force sensor box (Based on Dai *et al.*, 2013a). A force sensor box consisted of four FSRs in parallel configuration. These four FSRs were located on each corner of the box

Elastic stiffness depends on the torque and angular displacement of the elbow movement (Patrick *et al.*, 2001). If a joint shows viscous behavior, it means that the measured torque depends on movement velocity. In order to avoid modeling the viscous component, some research groups chose to either maintain a constant velocity by using motor actuated systems, or to advise examiners to impose the same movement on all subjects. This study does not utilize a motor part in order to keep the device portable nor does it change the clinical assessment course.

5.2.3 Combined Version

Because the rigidity assessment system was separated from the tremor and bradykinesia assessment system, a new concept with all three symptom assessments is presented. Figure 5-9 shows the system diagram of the combined glove monitoring system which can assess all primary symptoms. The circuit board and force sensors are embedded into a cuff which is produced by a 3D printer. There is only a microcontroller in the glove part. The textile glove is no longer necessary.

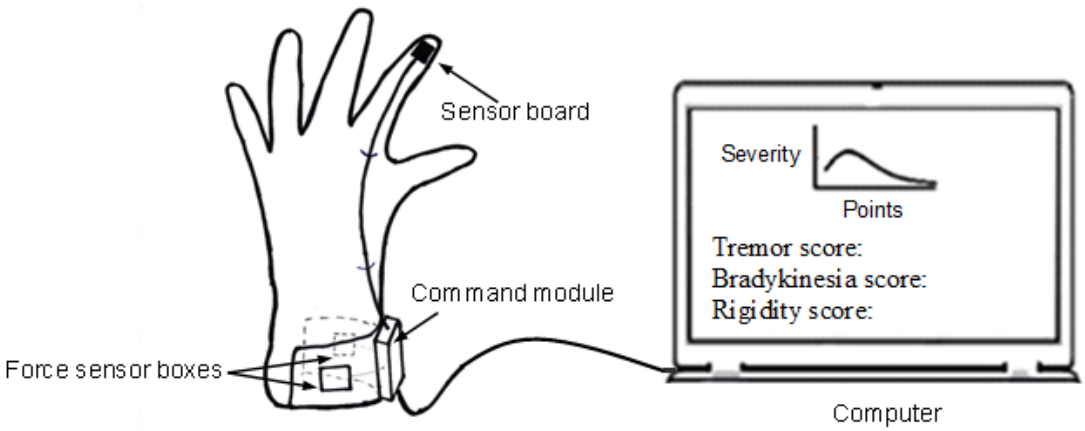

Figure 5-9: System diagram of the combined system. All the sensors are connected to a single microcontroller. The command module and force sensor boxes are embedded into a case.

Figure 5-10 shows the GUI diagram of the combined system. There are three major parts: recording lists in the upside of the GUI, start buttons for each task, and progress bars for each task.

The assessment tasks and algorithms of the separated systems and combined system are still the same.

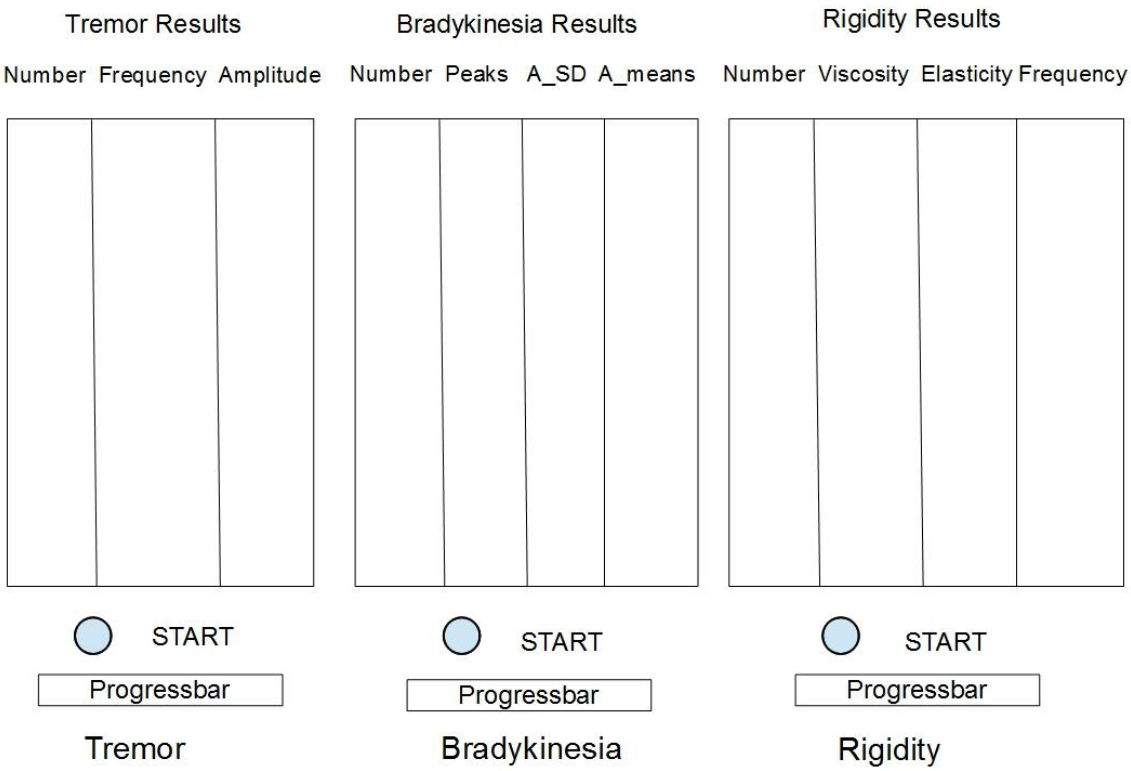

Figure 5-10: GUI diagram of the combined system. The start buttons, progress bars, and recording lists for each assessment task are listed in the GUI at the same time. Thus it is better for the surgeon to compare the parameters.

5.3 Dynamic System Description

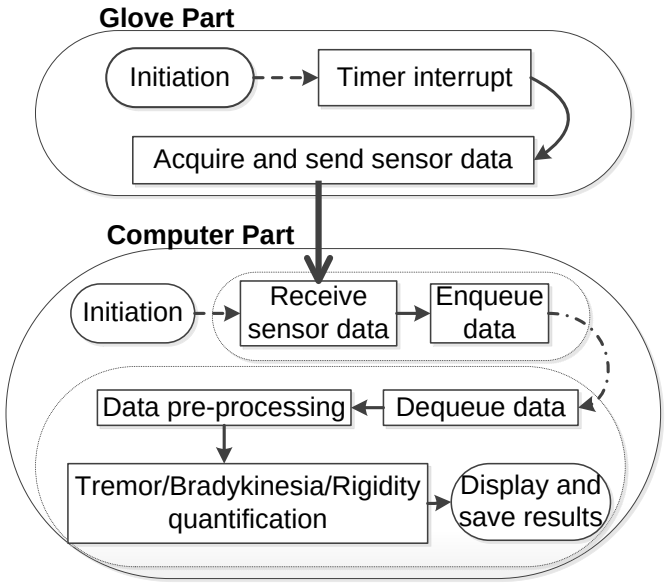

Figure 5-11: Flowchart of the signal processing in the glove monitoring system (Taken from Dai *et al.*, 2013a). The glove part was based on the sensors and command modules. The computer part was based on the program in the computer. The communication between them was the serial-to-USB port.

The flowchart of the signal processing methods in the glove monitoring system is shown in Figure 5-11. The system comprised of two major components: the glove part and the computer part. The sensor data were collected via a microcontroller. The microcontroller sent data to the computer at a defined time interval.

The sensor reading was taken by the microcontroller at timed intervals. Gyroscope and accelerometer data were simultaneously sampled in order to get high-quality position coordinate information. Low-pass filtering (LPF) was employed in all sensor outputs for the reason of anti-aliasing measures.

Inside the glove module, the sensor data were obtained and sent to the computer via a USB interface. Inside the computer, the received data were stored in a queue. The last cycle's data was de-queued for analysis at the same time. Three signal processing methods realized the three assessment tasks correspondingly. After each assessment task, the parameters according to the UPDRS score were listed in the recording list. The maximum and minimum values of the parameters were kept at the bottom of the recording list automatically.

Table 5-1 shows the quantitative models for the objective quantification of neuromotor symptoms. These models are based on estimation theory or other statistical analyses.

Table 5-1: Quantification algorithms of the neuromotor symptoms (PD and ET)

TASK	PARAMETERS AND METHODS
Tremors	Amplitude (Linear regression model)
Bradykinesia	Mean and standard deviation of grasp ranges (Statistic analysis)
Rigidity	Elasticity and viscosity (Least-squares parameter estimation)

For the rigidity task, viscous and elastic components should be calculated before the calculation of mechanical impedance.

The computer received the data for continuous signal processing, storage, and display. Data input and analysis took place in a multi-thread mode, with the use of a queue.

5.3.1 Processing Methods of Tremor Amplitude and Frequency

The algorithms used to quantify the severity of tremors are very important. Some researchers have proposed objective methods to detect and quantify the tremor severity.

According to the state of the art, Fourier-based spectral analysis, statistical measure (quadratic mean), and other computational methods such as neural network or fuzzy classifier are performed with the inertial sensor data for the tremor amplitude quantification (Burkhard *et al.*, 2002; Narcisa *et al.*, 2011; Patel *et al.*, 2009). However, spectral analysis is used for the majority of these studies.

In this study, signal processing involves IIR and FIR filters as well as other special algorithms such as PSD analysis. To detect tremors, the signals are then processed with auto power spectrum with a certain time length (3–10 seconds).

PSD Estimation

As Figure 5-12 shows, for PSD estimation, peak power means the power estimation around the dominant frequency in the power spectrum of sensor signals.

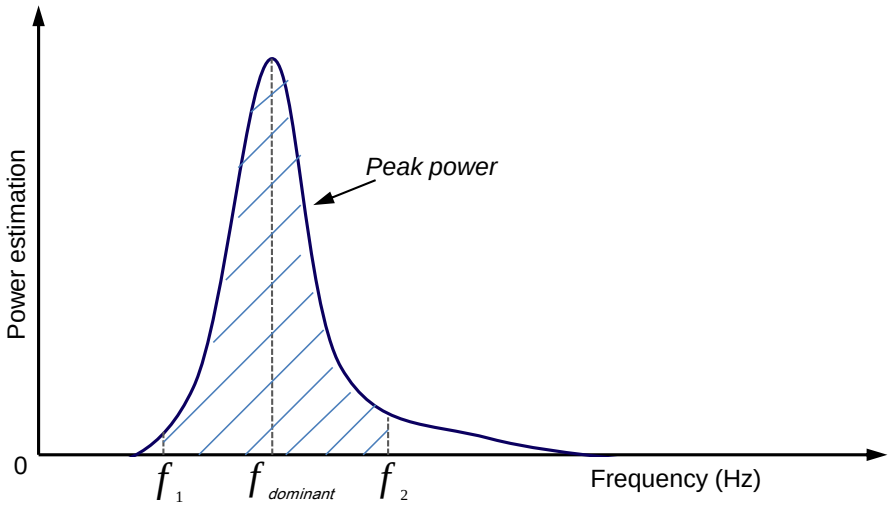

Figure 5-12: PSD estimation of ten-second inertial sensor signals. $f_{dominant}$ represents the dominant frequency of the signals.

Equation 5-1 shows the calculation of the peak power of inertial sensor signals:

$$Peak\ power = \int_{f_1}^{f_2} \frac{FFT^*(Signals) \times FFT(Signals)}{N^2} df\ , \tag{5-1}$$

where ***** denotes the complex conjugate and ***N*** is the number of sample points in the sensor signals.

The formula of the one-dimensional FFT in Equation 5-1 is described as

$$Y(k) = \sum_{n=0}^{N-1} X(n) \cdot e^{-j2\pi kn/N}, \quad \text{(n=0, 1, 2, …, } N\text{-1)}, \tag{5-2}$$

where X is the input sequence, N is the number of elements of X, and Y is the transform result.

The frequency resolution is $f_{sample\ rate}/N$, while $f_{sample\ rate}$ is the sampling frequency.

Then the power spectrum is converted into a single-side power spectrum. The power spectrum magnitude (peak power) has units of the input signal unit-RMS squared. The power estimation units of IMU signals are $(°/s)^2$ /Hz and g^2/Hz, respectively. Here g is equal to m/s^2.

Tremor Amplitude Estimation

For range (displacement) analysis, the angular velocity obtained from the gyroscope needs to be integrated over time only once, but the integration of the acceleration signals requires double integration. However, the sensor bias and drifts are integrated as well. Thus, the raw data from the inertial sensors are used for the tremor quantification.

According to the research conducted by Giuffrida *et al.* (2009), for the rest tremor and postural tremor in PD, the logarithm of the peak powers' summation of both power spectrums of accelerometer and gyroscope data had the highest correlation with UPDRS scores (coefficient of determination r^2=0.9). For the action tremor in PD, the RMS sum of both gyroscope and accelerometer data had the highest correlation with UPDRS (r^2=0.69) (Heldman *et al.*, 2011). In this system, the logarithm of the peak powers' summation of the IMU sensor signals is regarded as the tremor amplitude.

Given its oscillatory nature, tremors are well suited to spectral analysis, the most popular method for tremor quantification (Cameron *et al.*, 1997). The goal of PSD is to describe the

power distribution of a signal based on a finite set of data over the frequency domain.

Quadratic mean (RMS) interprets actual levels, while PSD results show frequencies that contribute the most to the tremor. Because the tremors are based on a dominant frequency, the advantages of PSD compared to a statistical measure (quadratic mean) are that it highlights the tremor signals from noise and other movement with analysis in the frequency dimension and the squared value of the signals. There are nonparametric methods, parametric methods, and subspace methods for PSD estimation. The nonparametric methods include periodogram, Welch's method, and the multitaper method (MTM). Parametric methods are used to estimate the output signal from a linear system driven by white noise. Subspace methods, which are also known as high-resolution methods, are used to generate frequency component estimations for the signal based on an eigenanalysis or eigendecomposition of the correlation matrix. The tremor signals will be tested with different types of methods for PSD estimation at a later time. In addition, for the offline tremor data analysis, PSD results should be used together with quadratic mean results to identify the overall features of tremors.

The flowchart of the signal processing for the tremor quantification in this study is shown in Figure 5-13. The sensor data are from the glove part, which is based on the sensor board and command module. In the computer part, the sensor data are band-pass filtered from 3 to 12 Hz (tremor band) before tremor amplitude quantification.

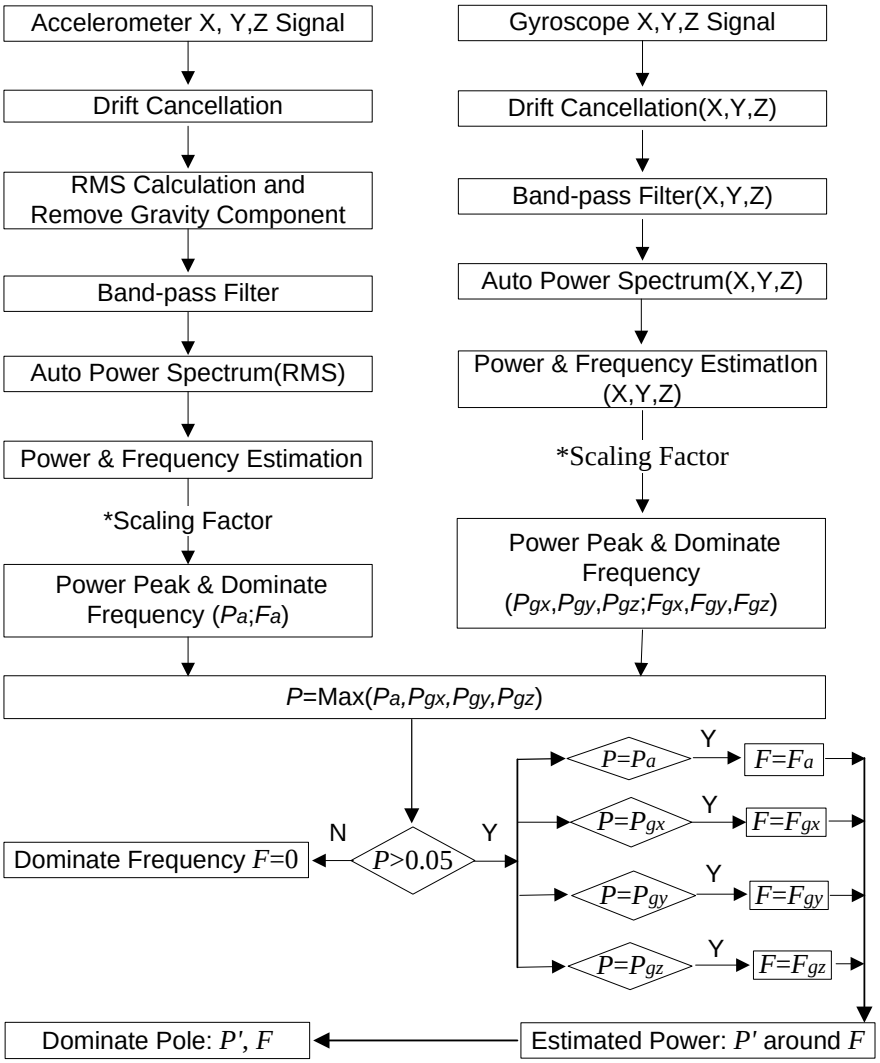

Figure 5-13: Signal processing for the tremor detection and quantification in a single finger (four channels).

Initially, the signals from the gyroscope and the accelerometer in a single finger are analyzed separately. The single-sided, scaled, and auto power spectra of the signal of each gyroscope axis and the combined values of all three axis outputs of the accelerometer, of which length is set to three seconds, are separately computed to get the four-channel power spectra in real-time. The dominant frequencies and the estimated peak powers of these frequencies are thus obtained. Then the estimated peak powers will be multiplied by scaling factors. The channel with the highest peak power is the dominant channel, and its dominant frequency is the dominant frequency (F) of all channels. Other channels are needed to perform PSD estimations again with the dominant frequency, and multiply the peak powers by the scaling factors again. The power estimations in all axes around the same dominant frequency (F) are calculated and sum up to $\boldsymbol{P'}$.

The power spectrum of every axis in a certain period (three seconds) is calculated continuously. The dominant frequency and peak power can be obtained as soon as the tremor occurs. When the dominant frequency is between 3.5 Hz and 7.5 Hz and the sum of peak powers is more than a threshold, the tremor is reported.

However, the signals in ten seconds are used for the PSD estimation at the end of the ten-second tremor assessment task. Then, the sum of peak powers, which is regarded as the tremor amplitude, and the dominant frequency can be displayed in the recoding list.

PSD estimation is the most popular method for tremor amplitude calculation, because the tremor is a rhythmic and involuntary movement based on a dominant frequency (Patel *et al*., 2009). Gyroscope and accelerometer react respectively to rotational and linear movements. Then a linear regression model is used to fit the clinical ratings (UPDRS tremor scores and TETRAS) and the peak powers from both the gyroscope and accelerometer signals.

The total output of a triple-axis accelerometer can be expressed as a_{xyz}:

$$a_{xyz} = \sqrt{a_x^2 + a_y^2 + a_z^2} \ . \tag{5-3}$$

a_{xyz} also includes gravitational acceleration, which equals 9.81 m/s^2 in vector product. Gravitational acceleration can be removed from the accelerometer outputs with high-pass filters. Then there is only one axis acceleration data for the following signal processing.

The dominant frequency can be calculated using PSD estimation. If the dominant frequencies in different axes are not the same, the valid dominant frequency in the axis with the highest peak power is defined as the dominant frequency of all axes. Then the total peak power in all four axes, which includes a_{xyz} and three-axis gyroscope signals, is the power of all axes' data around the valid dominant frequency with the PSD method. The peak power in all axes after normalization is regarded as the amplitude of tremor. Heldman *et al.* presented the discovery that the logarithm of the peak power in all triple-axis accelerations and three-axis angular velocities correlates well with the clinical scores of tremor (Burkhard *et al*., 2002).

Because the accelerometer and gyroscope are used to measure linear and rotational movement respectively, the accelerometer presents a higher correlation for some tremor tasks, while the gyroscope performs a higher correlation for other tremor tasks. Then a multiple linear regression model is used to fit the clinician ratings (UPDRS tremor scores) and the peak powers during each tremor task (Timmer *et al.*, 1997):

Then the linear regression model (Giuffrida, *et al.*, 2009) can be expressed as

$$R = R_0 + \ln (b_0 \cdot PA_{xyz} + c_x \cdot PG_x + c_y \cdot PG_y + c_z \cdot PG_z), \quad (5\text{-}4)$$

where R is the predicated tremor score; R_0, b_0, c_x, c_y, and c_z are the regression coefficients; PA_{xyz}, PGx, PG_y, and PG_z are the peak powers for the triple-axis accelerometer and triple-axis gyroscope, respectively. R_0 and the three scaling factors are different for the three tremors (rest, posture, and action).

For different tasks and different tremor types, these regression coefficients are different. The peak power in this study is the power estimation around the dominant frequency with ± 0.3 Hz length in the single sided power spectrum of ten-second sensor signals (Heldman *et al.*, 2011).

These three regression coefficients were obtained according to Stevens' power law in psychophysics (Luce & Krumhansl, 1988). Table 5-2 shows the initial coefficients and scaling factors for different tremor tasks.

Table 5-2: Coefficients and scaling factors of the tremor amplitude regression models

Tremor	**Coefficients**				
	R_0	b_0	c_x	c_y	c_z
Rest	0.8	10	0.001	0.001	0.001
Posture	0.6	5	0.0001	0.0001	0.0001
Action	0.3	2	2e–5	2e–5	2e–5

In the future, the parameters in Table 5-2 will be modified according to the results of measurements in patients with tremor.

The occurrence of tremor in a patient depends on many factors. Tremor can disappear sometimes even for a patient with severe tremor. Therefore, it is important to quantify tremor severity during the stable tremor state. The tremor state is classified into two types in this project: valid state and invalid state. The signals in invalid state will be discarded.

After a ten-second tremor assessment task, the tremor signals need to be checked. Valid state means the stable state in both the time domain and frequency domain. The judgments of valid state are listed as follows:

- In the frequency domain of ten-second signals, the proportion of peak power to the whole power estimation should be bigger than 85%.
- In the time domain, the standard deviation of ten-second angular velocity ranges (peak-to-peak values of all axes of the gyroscope) should be smaller than 30% of the mean gyroscope signal ranges.

5.3.2 Processing Methods of Bradykinesia Parameters

Hand grasping is easier to perform during DBS surgery. The signals of healthy people have a consistent amplitude and frequency, thus appearing sinusoidal. On the other hand, patients with severe bradykinesia have an inconsistent amplitude and frequency.

Signal processing for bradykinesia quantification is done by the computer. After receiving the sensor data from the microcontroller, the gyroscope signals are filtered firstly in real-time. The flowchart of bradykinesia detection and quantification using a gyroscope is shown in Figure 5-14.

As shown in Figure 5-14, the angular displacement during hand grasping can be calculated by numerical integration of the triple-axis angular velocities at the end of the middle finger. Then the mean value and standard deviation value ($\overline{|\varphi|}$ and $\sigma_{|\varphi|}$) of hand grasping ranges ($|\varphi|$) can be acquired by statistical methods. After a ten-second assessment, a second-order integration is performed with all the gyroscope signals. Then a peak-detection algorithm and statistical analysis are performed.

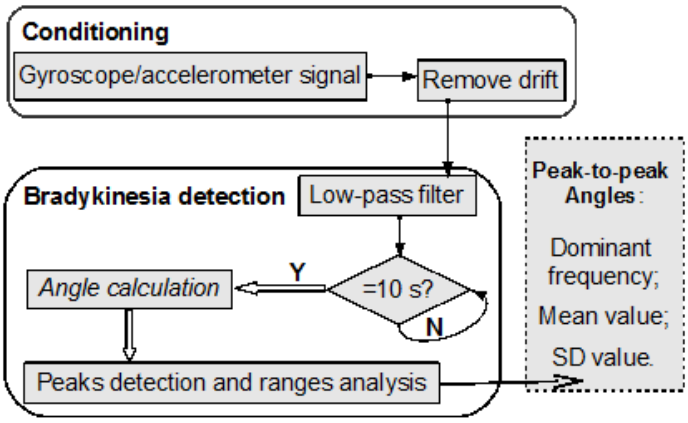

Figure 5-14: Flowchart of the signal processing for bradykinesia quantification in the computer (Based on Dai *et al.*, 2013a). Here peak-to-peak angles, which are calculated with a peak detection algorithm, mean the peak to peak values of all hand grasping cycles.

Figure 5-15 shows the peak-detection method during bradykinesia quantification.

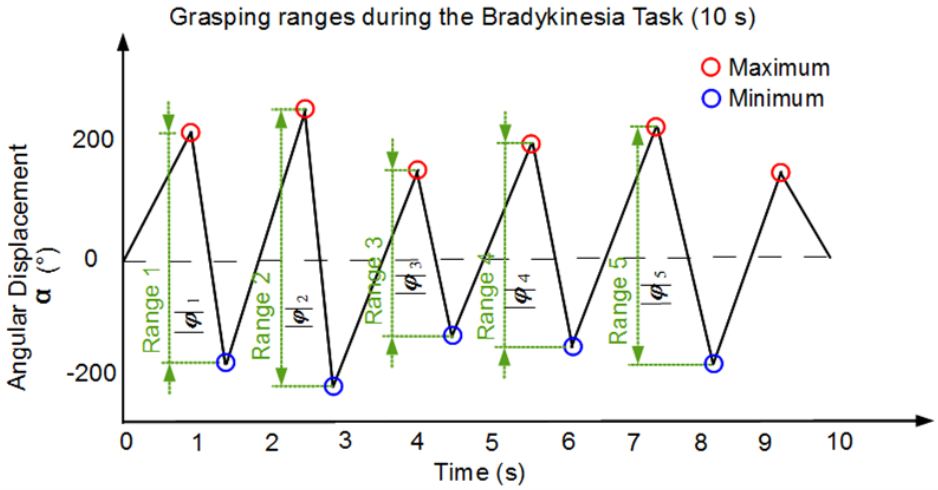

Figure 5-15: Peak detection for grasping ranges in a bradykinesia task. There are five hand grasping cycles in this figure. A peak-detection algorithm could be used to calculate peak to peak angle values (Ranges 1 to 5: $|\varphi|_1$ to $|\varphi|_5$). An angular displacement threshold, for example ±20° for both maximum and minimum, can be used to remove the unnecessary peak points.

The grasping ranges (α_{PP} or φ) are the three-dimensional peak-to-peak values during grasping cycles of a bradykinesia task. At first, the triple-axis grasping ranges are calculated sepa-

rately. The combined triple-axis grasping range ($|\boldsymbol{\varphi}|$) is the sum of the three-axis grasping ranges ($\boldsymbol{\varphi}$).

The number of peak to peak angle values during the ten-second assessment period is related to the dominant frequency of hand grasps. The mean value of peak to peak angle values (grasp ranges) represents the amplitude of bradykinesia. The standard deviation value of grasp ranges represents the change of amplitude during the grasping task.

The mean and standard deviation of hand grasping ranges are easy to calculate with statistical methods. The dominant frequency of hand grasps is calculated from the gyroscope signals using the FFT method.

The observed parameters are:

- Dominant frequency of hand grasping movement (*f*).
- Mean range in hand grasps ($\overline{|\boldsymbol{\varphi}|}$).
- Standard deviation value of hand grasp ranges ($\boldsymbol{\sigma}_{|\boldsymbol{\varphi}|}$).

These parameters are calculated based on the gyroscope signals from the middle finger. For a patient with mild bradykinesia, the signals obtained from the gyroscope should have a consistent amplitude and frequency and should appear sinusoidal. Conversely, the signals from a patient with severe bradykinesia should have a much lower and inconsistent amplitude and frequency. Thus the mean value and SD value of the hand grasping ranges and hand grasping frequency during a bradykinesia assessment task represent the bradykinesia severity (Zhang *et al*., 2011). The grasp cycles during a bradykinesia assessment task (ten seconds) are approximately equal to ten times the dominant frequency of the hand grasping movement (*f*).

Equation 5-5 and Equation 5-6 show the mathematical formulas used to determine $\overline{|\boldsymbol{\varphi}|}$ and $\boldsymbol{\sigma}_{|\boldsymbol{\varphi}|}$:

$$\overline{|\boldsymbol{\varphi}|} = (\sum_{i=1}^{N} |\boldsymbol{\varphi}|_i)/N, \tag{5-5}$$

$$\sigma_{|\boldsymbol{\varphi}|} = \sqrt{\frac{1}{N} \cdot \sum_{i=1}^{N} \left(|\boldsymbol{\varphi}|_i - \overline{|\boldsymbol{\varphi}|}\right)^2}, \tag{5-6}$$

where $|\boldsymbol{\varphi}|_i$ is the combined hand grasping range (peak-to-peak values) in a single grasp cycle, and *N* is the number of the hand grasping cycles in a ten-second bradykinesia task.

Grasping Angle Calculation

There are three methods for the hand grasping angular displacement (grasping range) calculation:

- Triple-axis tilt angle calculation based on the gravity accelerations from a triple-axis accelerometer.
- Triple-axis angular velocity integration calculation with the triple-axis gyroscope signals.

- Six-axis sensor fusion with the signals from a triple-axis gyroscope and triple-axis accelerometer.

Tilt calculation is a static measurement. The gravity is used as an input to determine the orientation of an object calculating the tilt degree.

For the angle calculation with the triple-axis gyroscope signals, first order approximation (trapezoidal method), Simpson's rule or bodes rule can be utilized.

For sensor fusion, the gyroscope is used as the primary source of orientation information. The accelerometer is used for roll-pitch drift correction.

It is not easy to separate the gravity components from the accelerometer data as the hand grasping is not static movement. A Kalman filter or the DCM algorithm is used to combine the data from the gyroscopes and accelerometers to produce an output that is better than that obtained from individual sensors. However, sensor fusion (DCM or Kalman filter algorithm) makes the program more complicated, because several parameters need to be set and there are several seconds of adaptive time before the stable state is reached in the program (Madgwick *et al*., 2011).

Second-order integration approximation (Simpson's method) is easy to perform, and the drift in ten seconds has a small effect on the angle calculation. Then the grasping range is calculated via triple-axis angular velocity integration and combination (National Instrument Inc., 2011). The single-axis angular displacement (α_i) in *i*-th sampled point is calculated according to Equation 5-7 (Simpson's method).

$$a_i = (dt/6) \cdot \sum_{j=1}^{i} \left(v_{j-1} + 4v_j + v_{j+1} \right), \tag{5-7}$$

where v_j is the angular velocity in *j*-th sampled point and *dt* is the sample interval (0.02 s for 50 Hz sampling rate).

Because there are three axes in the signals of hand grasps, the hand grasp angles should be calculated in three axes separately.

5.3.3 Processing Methods of Rigidity Parameters

At first, the IMU and force sensor boxes should be calibrated and verified.

Mechanical impedance is a mathematic model used to describe the dynamic features of the linear vitiation system. For a stable linear-vibratory system, its outputs (displacement, velocity, and acceleration), under a simple harmonic and alternating force are the harmonic movements with the same frequency. There is, however, a delay in phase. Mechanical impedance is a feature of frequency response. The system outputs depend on the features of the system such as inertia, velocity, stability, and stiffness.

The viscous and elastic components, which are the main components of the mechanical impedance, are modeled in this study (Charles, 2003).

Rigidity assessment is performed by the measurement of elbow angle movement and torque on the wrist (Patrick *et al.*, 2001). The outputs of two force sensor boxes and an IMU around the wrist area are:

$$\left[F_1, F_2, \mathbf{a}, \dot{\boldsymbol{\alpha}}\right], \tag{5-8}$$

where F_1 and F_2 are the outputs of force sensor box 1 and force sensor box 2, respectively; **a** and $\dot{\boldsymbol{\alpha}}$ are the acceleration and angular velocity of elbow movement, respectively. Their units are N, g, and rad/s, respectively.

The triple-axis elbow angles ($\boldsymbol{\alpha}$) during the rigidity task can be calculated from the IMU outputs ($\mathbf{a}$, $\dot{\boldsymbol{\alpha}}$) in real-time using the DCM algorithm (Madgwick *et al.*, 2011).

The calculation of elastic stiffness (*c*) and viscosity (*d*) is realized by using a least squares parameter estimation method (regression analysis) to solve Equation 5-9 with ten-second data (Patrick *et al.*, 2001).

The torque (*T*) in a rigidity assessment task can be expressed as:

$$T = (F_1 - F_2) \cdot l = c \cdot |\boldsymbol{\alpha}| + d \cdot |\dot{\boldsymbol{\alpha}}| + e, \tag{5-9}$$

where *l* is the length of the subject's arm, *c* is the elastic stiffness of the subject's elbow, *d* is the viscous stiffness (viscosity) of the subject's elbow, and *e* is the constant offset of the sensors. The arm length (*l*) must be determined before the measurement, and set in the system's user interface through keyboard entry.

With ten-second duration and 100 Hz sampling rate, a 1000-point data array with the format of Equation 5-8 is obtained during a single rigidity assessment task. Equation 5-9, which is the model of the elbow joint movement, can be written as:

$$d \cdot |\dot{\boldsymbol{\alpha}}| + c \cdot |\boldsymbol{\alpha}| + e = \boldsymbol{T}. \tag{5-10}$$

Therefore, Equation 5-10 can be written in vector form as:

$$\boldsymbol{A}\boldsymbol{p} = \boldsymbol{T}, \tag{5-11}$$

where the components of Equation 5-11 are:

$$\boldsymbol{A} = \left[|\dot{\boldsymbol{\alpha}}| \; |\boldsymbol{\alpha}| \; 1\right], \tag{5-12}$$

$$\boldsymbol{p} = [d \; c \; e]^T. \tag{5-13}$$

After the angular displacement calculation of the elbow's passive movement, the angular velocities and elbow angular displacements are combined in matrix $\boldsymbol{A}$. Angular velocity ($\dot{\boldsymbol{\alpha}}$) is the first column in matrix $\boldsymbol{A}$. On the condition that the elbow moves exactly in one direction, the three-dimensional angular displacement and angular velocity of elbow movements can be replaced with single-axis data points in the Equation 5-8. In addition, the combination of all sensors and axes needs further signal proceeding, such as fuzzy analysis, classification and regression trees, artificial neural networks, support vector machines, or other pattern recognition techniques.

Thus, a least squares estimation is obtained using the following equation:

$$\hat{\boldsymbol{p}} = (\boldsymbol{A}^T\boldsymbol{A})^{-1}\boldsymbol{A}^T\boldsymbol{T}. \tag{5-14}$$

Mechanical impedance is the feature of the parkinsonian rigidity, and is calculated as follows:

$$Z = c + d \cdot \omega = c + d \cdot 2\pi \cdot f, \tag{5-15}$$

where f is the frequency of hand movement and is obtained with a peak-detection algorithm from the angular displacement of elbow movement; and $d \cdot 2\pi \cdot f$ is the modified viscous stiffness.

In order to acquire the relation between mechanical impedance and the UPDRS ratings, the relation of elastic stiffness and viscosity with the rigidity severity should first be investigated.

Six-Axis Direction-Cosine-Method Algorithm

Direction cosine method is another way to construct a rotation matrix, other than Euler angles (Edwan *et al.*, 2011).

The six-axis DCM algorithm is based on a triple-axis gyroscope and a triple-axis accelerometer. The gyroscope is used as the primary source of orientation information. The accelerometer is used for roll-pitch drift correction because it has no drift over time. Only the gravity vector of the accelerometer is used for the drift detection.

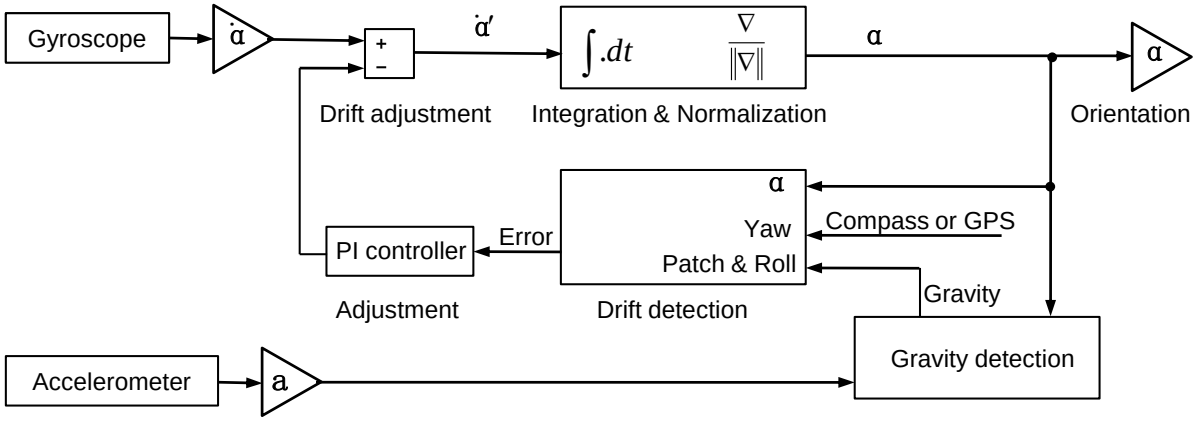

Figure 5-16: Block diagram of DCM algorithm. Here PI controller denotes a proportional-integral controller. For six-axis DCM algorithm, there is no yaw-axis input for the drift detection.

As shown in Figure 5-16, a proportional plus integral (PI) controller is used to control the drift adjustment. Each of the rotational drift correction vectors (roll and pitch) is multiplied by weights and fed to a PI feedback controller. Then the drift adjustments are added to the gyroscope vectors to produce corrected gyroscope vectors. The outputs of the algorithm are three-dimensional angles (orientation).

6. Prototypical Realization

At first, the realization of the nine-axis DCM algorithm is presented in Chapter 6.1. In addition, two tremor and bradykinesia assessment systems with wireless communication interfaces, which have already been implemented at the beginning of this study, are presented in Chapter 6.2. These systems could be used in patients' homes and in future versions.

After that, prototypical realizations of the tremor/bradykinesia assessment system and rigidity assessment system are presented. The materials, hardware configuration, and software description of these two systems are presented in Chapters 6.3, 6.4, and 6.5, respectively. As described in Chapter 6.6, inertial sensors and force sensor boxes of these systems were calibrated according to the sensor calibration procedures.

At last, the realization of the combined system, which can assess the three primary symptoms, is presented in Chapter 6.7.

6.1 Nine-Axis Direction-Cosine-Method Realization

As Figure 5-16 in Chapter 5.3.3 shows, signals of GPS (global positioning system) or a triple-axis compass can be used to reduce yaw drift. Such a multi-sensor fusion method, which includes the signal processing of a triple-axis compass, a triple-axis gyroscope, and a triple-axis accelerometer, is a nine-axis DCM algorithm.

The nine-axis DCM algorithm can be realized in an eight-bit MCU of small size. A prototype based on the nine-axis DCM algorithm and an eight-bit MCU has been implemented.

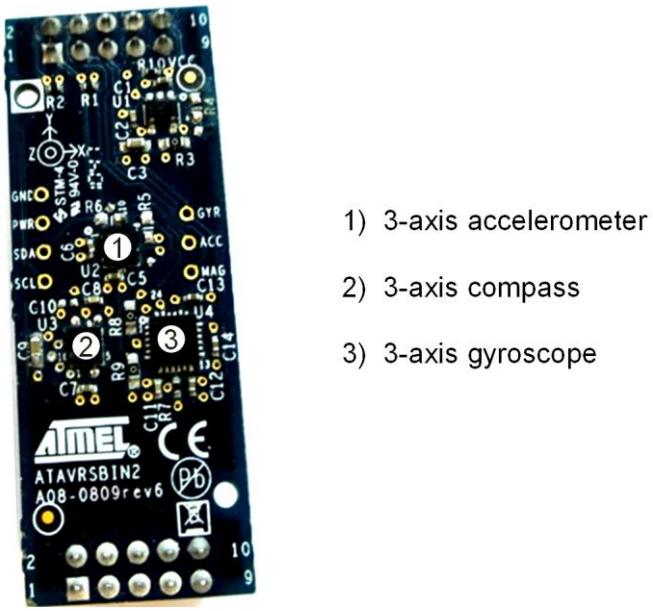

Figure 6-1: Atmel Inertial Two Sensor Board (AVRSBIN2) from Atmel Inc., USA (© Atmel, 2011).

As shown in Figure 6-1, an Atmel Inertial Two Sensor Board (AVRSBIN2), which delivered a full nine-DOF inertial sensor platform, was used to supply the sensor fusion algorithm. This circuit board combined an accelerometer (KXTF9, Kionix Inc., USA), a compass (HMC5883L, Honeywell Inc., USA), and a gyroscope (IMU-3000, InvenSense Inc., USA). Another circuit board, which included a microcontroller (ATMEGA644, Atmel Inc., USA) and other electronic components, was used to run DCM algorithm.

The sampling rates of both the gyroscope and accelerometer were 50 Hz, while the sampling rate of the compass was 10 Hz. The gyroscope measured rapid movement, while the accelerometer and compass removed the drift in the gyroscope signal.

The three-axis angles, which were the results of sensor fusion using the DCM method, were sent to a computer in 50 Hz. As shown in Figure 6-2, a 3D demo displayed the rotational movement of the sensor board (AVRSBIN2). This demo program was modified based on the program of Julio *et al.* (2009).

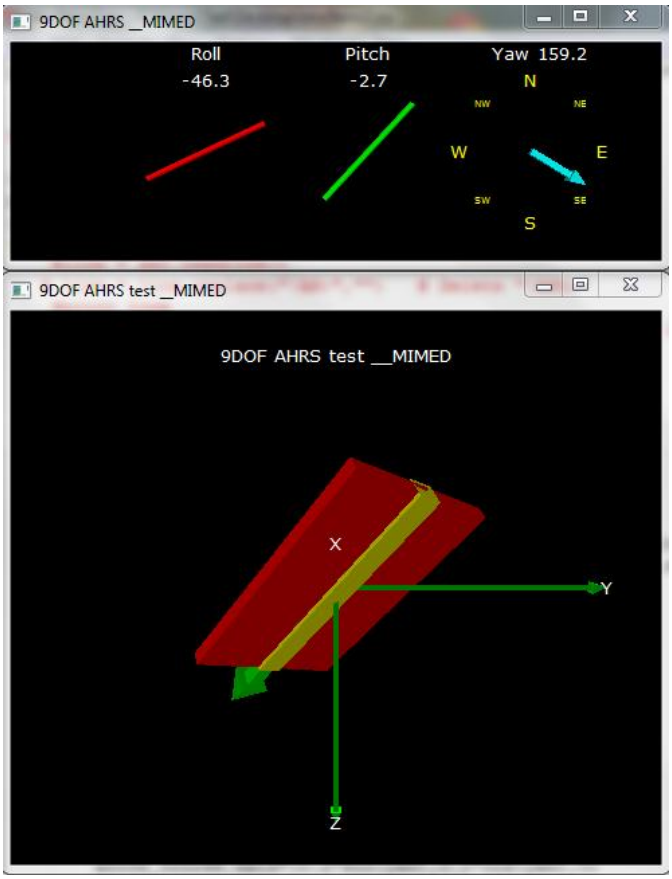

Figure 6-2: Nine-DOF AHRS demo based on Python 2.6.4. Python is a simple but powerful open-source programming language.

6.2 Prototypes with Wireless Communication Interfaces

Two prototypes with wireless communication for tremor/bradykinesia assessment are presented in this section. A prototype was for the motion tracking of the wrist and all fingers, while the other for the motion tracking of a single finger.

At first a glove-based system with several accelerometers and gyroscopes was used to measure the hand's motion. As shown in Figure 6-3, the desired hardware included sensors, a rechargeable battery, and a microcontroller. These electronic components were embedded in a small case in the same fashion as a wrist blood pressure monitor. The case incorporated connectors to the sensor module. The sensors were able to be attached and removed from the fingers without difficulty.

The IMU3000 gyroscope by Invensense Inc., with the dimensions of 4mm × 4mm × 0.9mm, and the SMB380 accelerometer (3mm × 3mm × 0.9mm) by BOSCH, and the MMA8452Q accelerometer (3mm × 3mm × 1mm) by Freescale were chosen for use in this design.

These inertial sensors were placed on the upside of a washable conductive textile (Textronics Inc.). Five of these conductive textiles were able to be attached on each finger of a hand. The conductive textile on the thumb was connected to the power supply (level "1"), while the conductive textiles on other fingers were connected to the circuit ground respectively via a resistor (level "0"). The communication between the microcontroller (ATMeaga644) and sensors was achieved with a two-wire serial interface (TWI) multiplexer (PCA9546A, TI, USA).

Two NanoLOC AVR Modules (microcontroller and 2.4 GHz radio transceiver, Nanotron Technologies GmbH, Germany) were used for the communication between the microcontroller and the computer. All the electronic components in the wrist were embedded into the cuff of a wrist blood pressure monitor and powered by a lithium-ion battery (3.7 V, 1400 mAh). The NanoLOC AVR Module included an Atmel AVR microcontroller, which managed the sensors and sent the data to a computer via wireless communication. Another NanoLOC AVR Module, which was plugged into a computer, received the data and sent it to the computer via RS232 to USB transmission.

a) **b)** **c)** **d)**

Figure 6-3: Components of the measurement system with wireless communication. a) NanoLocAVR Module (35mm × 14mm × 3mm); b) lithium-ion battery; c) touch sensor based on a washable conductive textile; d) the cuff from a blood pressure monitor (Beurer BC19, Beurer GmbH, Germany). A NanoLocAVR module, lithium-ion battery, and other additional components were placed inside the cuff of this blood pressure monitor.

Figure 6-4 shows the hand motion measurement system and the sensor module which can measure the movements in all fingers and the wrist.

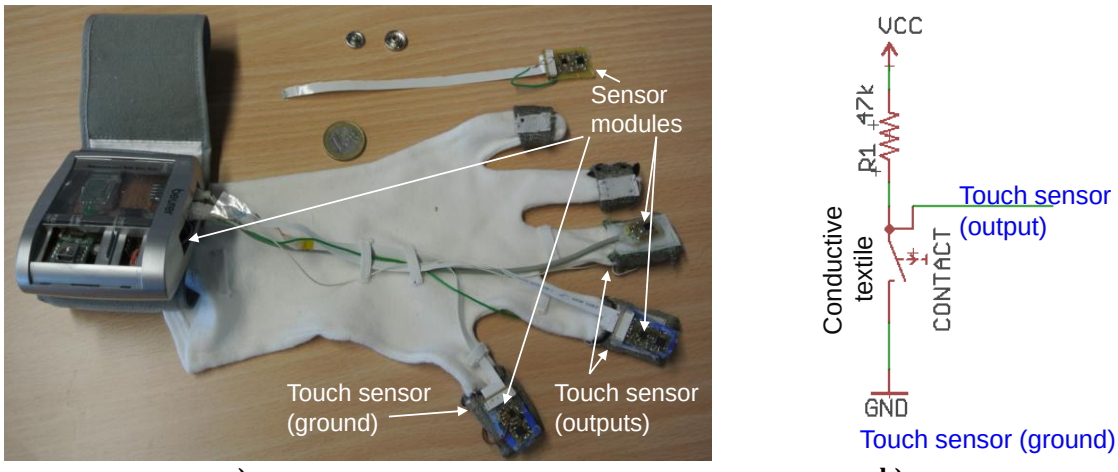

a) **b)**

Figure 6-4: Hand motion measurement system with sensor modules (inertial sensors) and touch sensors. a) hand motion tracking system; b) schematic of a touch sensor. Each touch sensor's output was connected to a digital input pin of the microcontroller. The sensor module can be attached to the fingers and connected to the command module

Figure 6-5 shows a prototype with the wireless communication interface. Rest, postural, and action tremor tasks, together with the finger taps task, can be assessed by this system. One disadvantage of this system is that it cannot be used in an operating room.

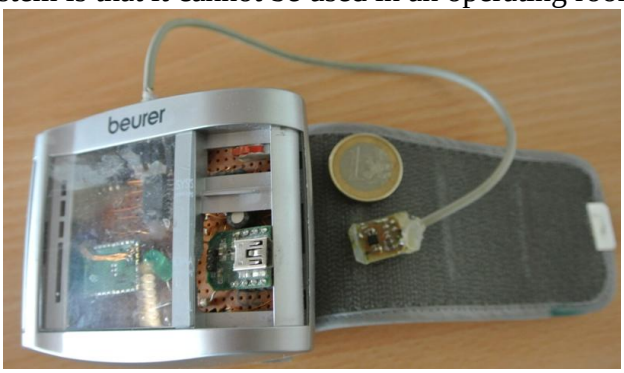

Figure 6-5: Wireless tremor and bradykinesia assessment monitor with a single sensor module. Its case was also based on a blood pressure monitor (Beurer BC19, Beurer GmbH).

6.2.3 Graphical User Interfaces

Figure 6-6 describes the GUI of the hand motion measurement system for tremor and bradykinesia assessments with four sensor modules, which were located on the wrist and three fingers. This system could be used for bradykinesia and tremor assessments.

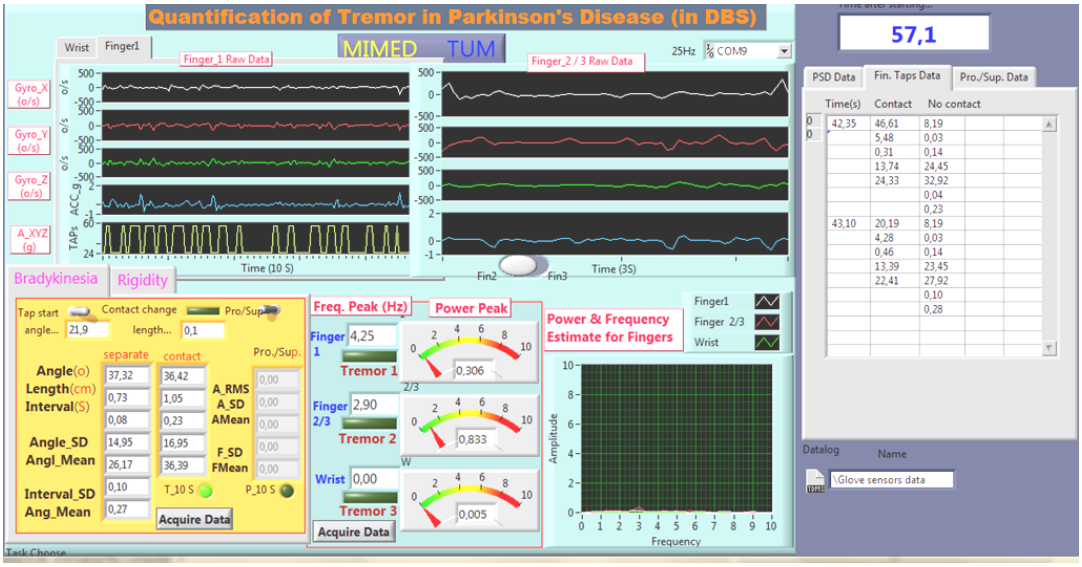

Figure 6-6: GUI of the hand motion tracking system (for finger tapping task). Finger 1 in this figure means the index finger. This GUI corresponds to hardware in Figure 6-4.

The raw data from each axis of the gyroscope and the combined value of all three axes' outputs of the accelerometer, together with the touch sensor signals, were displayed in waveform mode.

The dominant frequencies and the estimated powers of two fingers' movements were computed and displayed directly. The auto power spectrum of each finger movement was displayed at all times. When the dominant frequency and its estimated power met the definition (frequency range and amplitude threshold), the tremor indicator would light up. The display was refreshed at 0.05 second intervals.

To save the dominant frequency and power values, the key labeled "Acquire Data" was pressed.

Finger tapping and supination-pronation movements were used to assess bradykinesia based on the hand motion measurement system. The change in angles and the time taken for the two fingers to come into contact and separate were displayed in real-time. The raw data of all sensors were stored in the computer in real-time.

Figure 6-7 represents the GUI of playback mode for this measurement system. The stored raw data were able to be opened and replayed with this user interface.

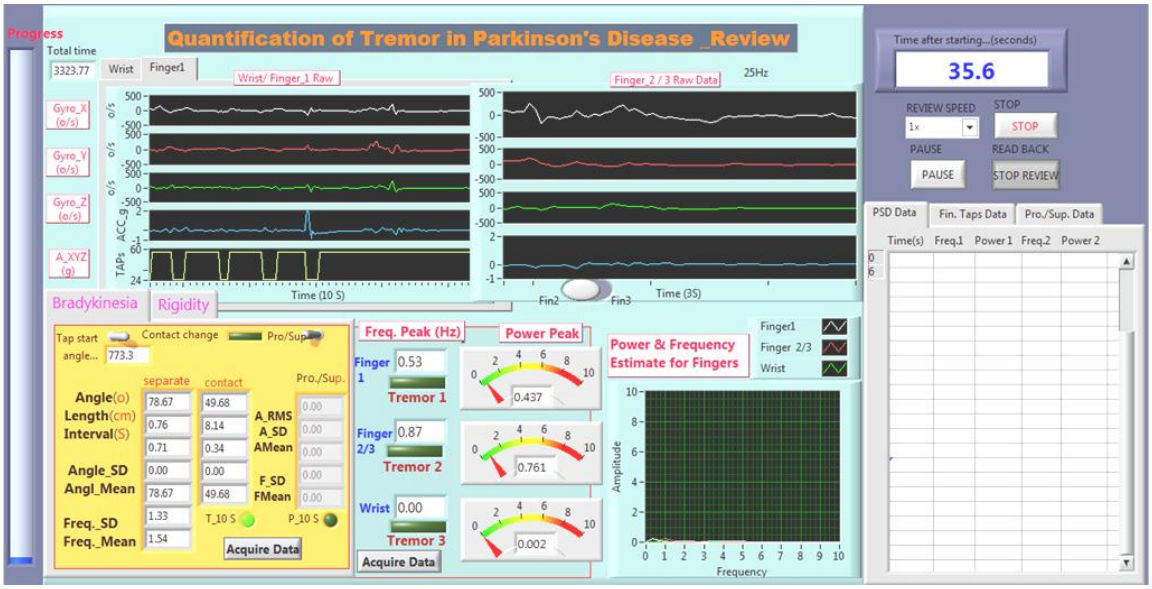

Figure 6-7: Review of the stored sensor signals in a tremor or bradykinesia assessment task of the hand motion tracking system (playback mode). This GUI corresponds to the hardware (Figure 6-4) and software (Figure 6-6).

Figure 6-8 and Figure 6-9 show the GUIs of the prototype in Figure 6-5, which only had a sensor board and a wireless communication interface. These GUIs were based on LabVIEW 2010 Evaluation Version (National Instruments Corp, USA) and Visual C# 2010 (Microsoft Inc., USA) respectively.

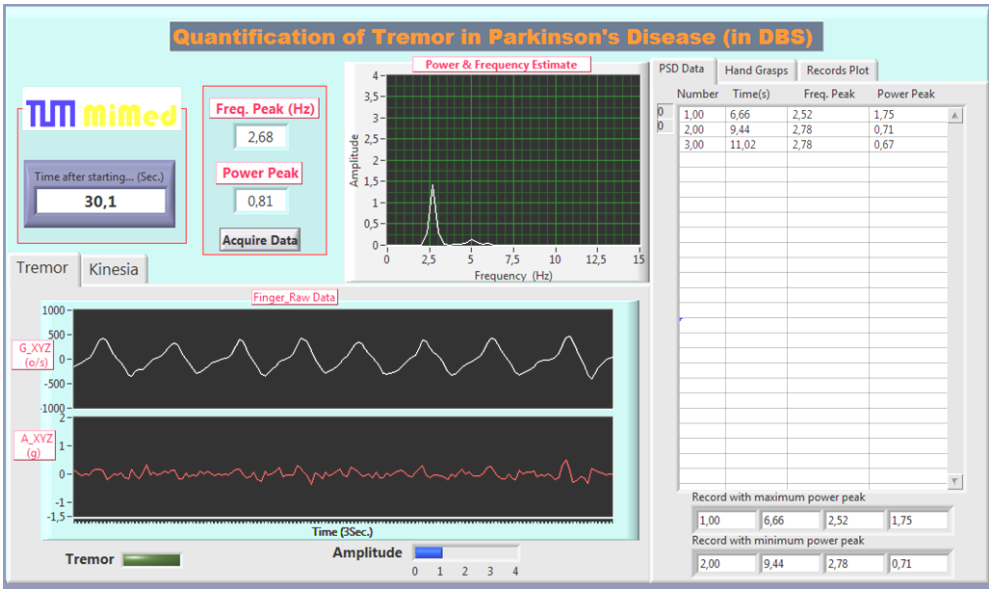

Figure 6-8: LabVIEW-based GUI of the wireless tremor and bradykinesia assessment monitor with a sensor board. This GUI corresponds to the wireless tremor and bradykinesia assessment system in Figure 6-5.

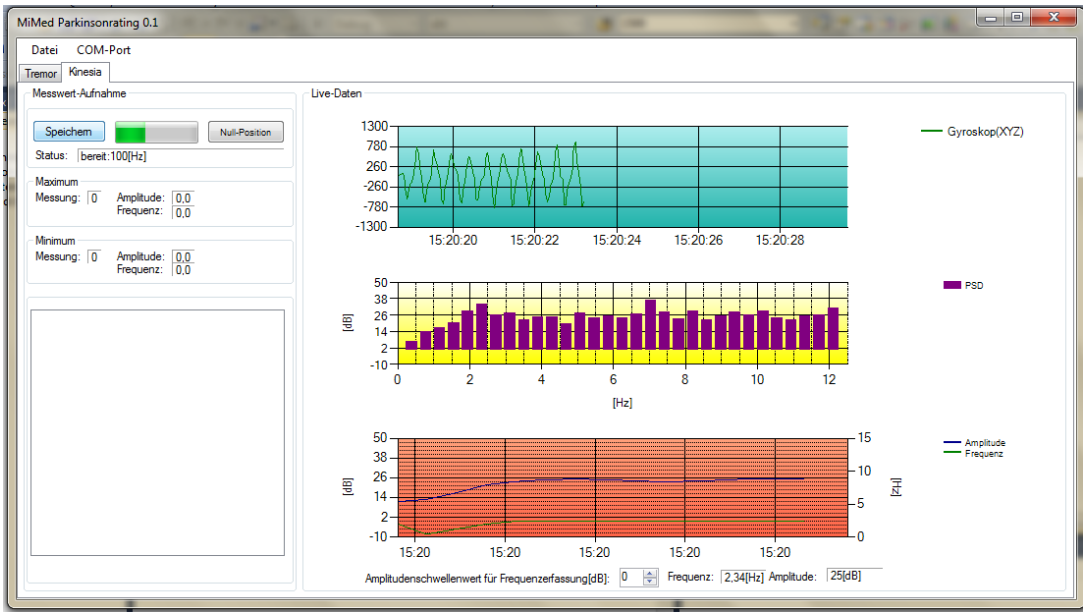

Figure 6-9: Visual C#-based GUI of the wireless tremor and bradykinesia assessment monitor with a single inertial sensor module. This GUI also corresponds to the wireless tremor and bradykinesia assessment system in Figure 6-5 (© TUM-MIMED, 2013).

As can be seen from Figure 6-8 and Figure 6-9, the built-in graphical user interface components, such as buttons and graphs, make LabVIEW more intuitive for displaying signals and results. It is also easy to modify the LabVIEW program. Thus, the realization of a test version using LabVIEW has some advantages. The program, which is based on Visual C#, is more readable and is better to be embedded in a commercial system considering its lower price.

6.3 Materials

6.3.1 Selection of Sensors

The first step in implementing the glove monitoring systems was to select the appropriate sensors.

Sensor Specifications

According to the literature (Giuffrida, *et al.*, 2009; Heldman, *et al.*, 2011a; Patrick, *et al.*, 2001), the full-ranges of sensors in the neurological symptom assessments are listed as follows:

- Angular velocity: ± 2000 º/s (degrees per second or dps) in three dimensions.
- Acceleration: ± 4 g in three dimensions; here g is the gravitational acceleration (1g = 9.8 m/s^2).
- Attached force on both sides of the wrist: 0–80 N; here N is Newton (1 Newton =101.97 grams).

MEMS IMUs and FSR sensors were chosen in this project for their small dimensions and low-cost compared to other types of sensors.

Figure 6-10 shows the inertial sensors involved in this study.

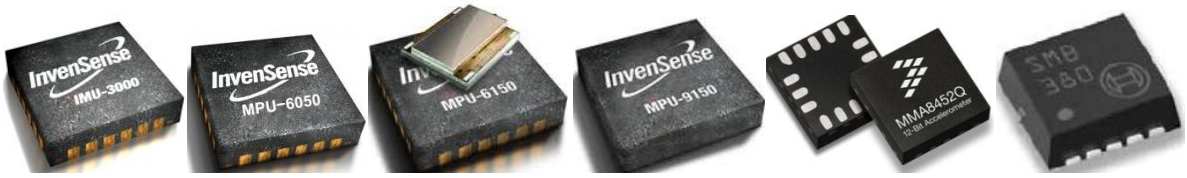

Figure 6-10: Inertial sensors used in this study (IMU3000 /MPU6050 /MPU6150 /MPU9150 /MMA8452Q /SMB380) (© Invensense, 2013; © Freescale, 2012; © Bosch, 2010).

The Standardized Sensor Performance Parameter Definitions for MEMS sensors, which was organized by Intel, Qualcomm, and the MEMS Industry Group (MIG), was not released until May 2013. Therefore, not all of the primary parameters of inertial sensors were available in the datasheets.

The primary features of available inertial sensors and IMUs are listed in Table 6-1. These parameters were taken from the relative datasheets. These sensors are from manufactures such as Invensense, Bosch, ST, Kionix, and ADI, respectively.

Table 6-1: Comparative specifications of inertial sensors. Here "⁄" means no embedded sensor fusion; "–" means no available information; *Gyro.* refers to a 3-axis gyroscope and *Acc.* denotes a 3-axis accelerometer.

Sensor	**Embedded sensor fusion**	**Package**	**Current (mA) [Gyro.; Acc.] (total)**	**RMS Noise [Acc.; Gyro.]**	**Resolution (bits) [Gyro.; Acc.]**	**Release date**
IMU3000	Digital Motion Processor	4×4×0.9 mm; QFN	6.1	0.1°/s rms, 0.01°/s/√Hz	16	05/2010
SMB380	⁄	3×3×0.9 mm; QFN	0.2	500 μg/√Hz	10	09/2007
MPU6050	Digital Motion Processor	4×4×0.9 mm; QFN	3.6; 0.5; (3.9)	400μg/√Hz; 0.05°/s rms	16;16	11/2010
MPU6150	Digital Motion Processor	4×4×0.9 mm; QFN	3.6; 0.5; (3.9)	400μg/√Hz; 0.2°/s rms	16;16	11/2010
LSM330	iNEMO	3×3.5× 1mm; LGA	6.1; 0.25	–	16; 16	07/2012
BMI055	⁄	3×4.5×0.95 mm; LGA	(5.15)	150μg/√Hz; 0.014°/s/√Hz	16; 12	09/2012
KXG02	⁄	4×4×0.9mm; LGA	3.75; (4.0)	150 μg/√Hz	16; 16	01/2012
ADIS16367	⁄	23×23×23 mm; ML-24-2	49	0.5mg//√Hz; 0.044°/s/√Hz	12; 12	01/2010

An IMU works by detecting both the current rate of acceleration (using a 3-axis accelerometer) and the changes in rotational attributes (using a triple-axis gyroscope). At the beginning

of this study, a triple-axis MEMS gyroscope and a triple-axis MEMS accelerometer were used to constitute an IMU. After the availability of single-chip IMUs, MPU6150 and MPU6050 were chosen in this project for the following reasons:

- Their pin-out and package (QFN) are compatible with the IMU3000, which we had used before the availability of IMU chips. MPU 6000 and MPU6150 were first available on the market as single-chip IMUs.
- A chip with QFN package is better to solder than the chip with LGA package in laboratory conditions.
- Their outputs are digital, obtained via a TWI/ SPI (serial peripheral interface) interface by the MCU.

MPU6150 is actually a lower cost version of the MPU-6050 and is focused on television remote control and gaming applications. MPU-6050 (or MPU-9150) has better performance with regard to bias offset, drift rate, and noise levels.

Figure 6-11 shows the system structures of MPU6150 and MPU9150, which has an additional compass layer.

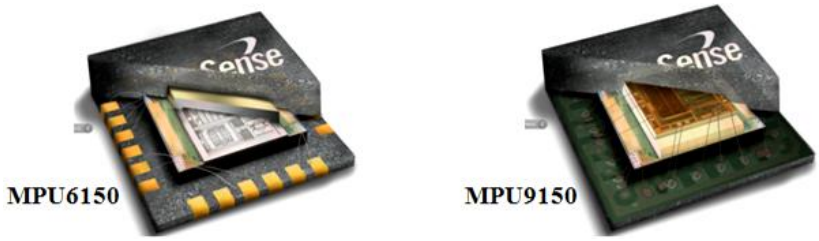

Figure 6-11: Structure of the multi-sensor integration (© Invensense, 2013). Six-axis MPU6150 has a die of two layers, while the nine-axis MPU9150 has a three-layer die.

Figure 6-12 shows the system diagram of MPU6150, which is same as MPU6050.

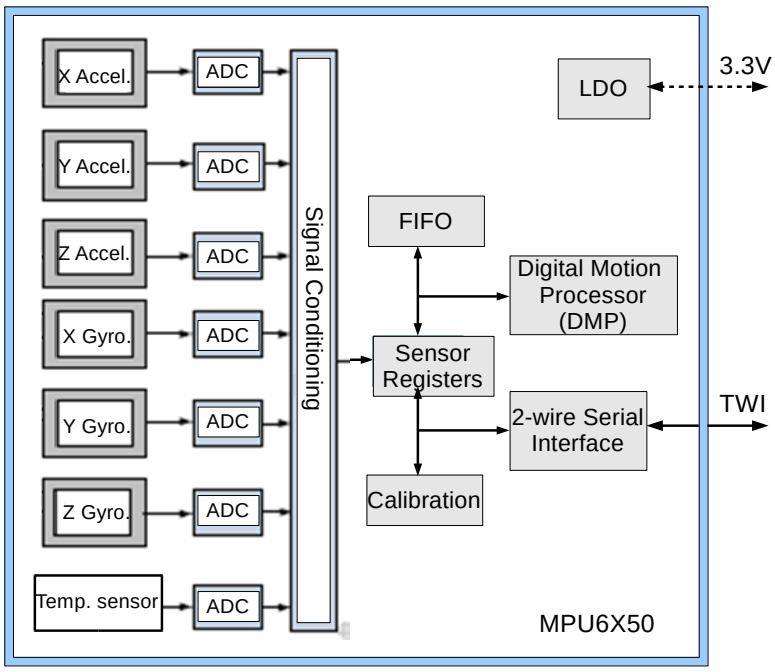

Figure 6-12: Block diagram of MPU6150/MPU6150.

A gyroscope has much higher power consumption than an accelerometer or a compass in working state, more specifically, 3.6 mA for a triple-axis gyroscope compared to 0.2 mA for a three-axis accelerometer inside the Invensense MPU6050 or MPU6050.

Figure 6-13 shows the axis orientations of MPU6050 and MPU6150.

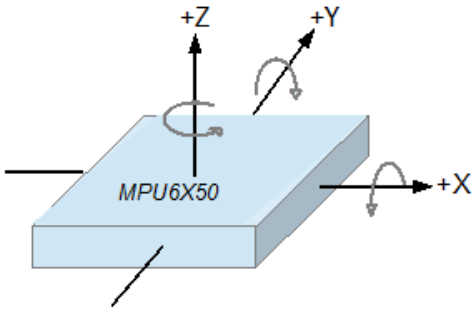

Figure 6-13: Axis orientations of MPU6150 and MPU6050. The benefit of this structure is that the axes of the accelerometer and gyroscope are the same. Thus the adjustment of axes before sensor fusion is not needed.

The main part of a force sensing resistor (FSR) is a conductive polymer, which detects physical pressure or force applied in the upside. FSRs are simple to use due to a low cost and small thickness. The disadvantages are their low precision (from 5% to 25%) and possible damage by continuously being attached with pressure (for several hours). The major manufacturers of FSRs are Interlink Electronics Inc., Tekscan (Flexifore sensors), and IEE International Electronics & Engineering Inc., etc. The information regarding the FSRs, which are suitable for this project, is listed as Table 6-2.

Table 6-2: Comparative information of FSRs. Here "–" means no available information. For the FSR402, the best force range is from 0 to 20 N, but it can be extended to 100 N when applying force evenly over the active area (0.125 cm^2) of its surface area.

Sensor	Range (N)	Repeatability	Linearity (Error)	Hysteresis	Response time	Active area	Current density
FSR402	0–20N*	+/- 2%	–	+10%	3 ms	Ø12.7 mm	< 1 mA
FSR149NS	0–100N	± 3%	–	20%	2–3 ms	Ø6 mm	< 1 mA/cm^2
FSR152	0–100N	± 3%	–	20%	2–10 ms	Ø15.2 mm	< 1 mA/cm^2
A401	0–110N	±2.5%	±3%	4.5 %	5µs (5 ms)	Ø25.4 mm	< 2.5 mA

These sensors are robust polymer thick film (PTF) sensors that exhibit a decrease in resistance to an increase in force applied to the surface of the sensors. They are with analog outputs. The output of an FSR should be connected to the ADC pin of a microcontroller.

One disadvantage of the FSRs is that they can provide only single-axis analog output, but the elbow movement during the rigidity assessment task is a three-dimensional motion. MEMS three-axis force sensors have appeared with digital interface but as of yet there is not a fully-developed product available for our project. For example, a capacitive three-axis force sensor (WEF-3A) from Wacoh Inc., Japan, is very small (Ø: 10mm, H: 7mm) and has a built in 32-bit ADC, but the operating current is 200 mA. In the future, MEMS three-axis force sensors can be used in this project.

Figure 6-14 shows the structure of a round FSR. Figure 6-15 shows the photo of FSR149NS and FSR 402 short.

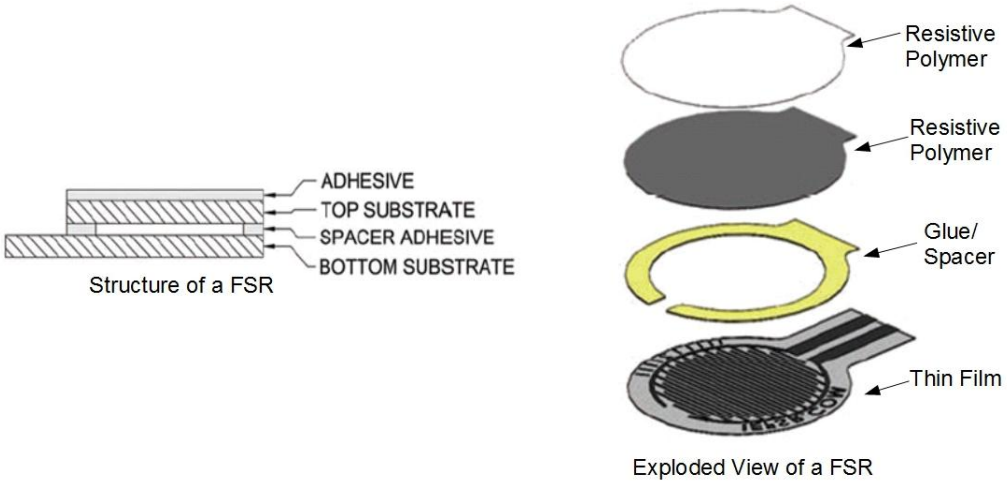

Figure 6-14: Structure of a round FSR (© Interlink, 2012).

Figure 6-15: FSR149NS and FSR 402 short.

6.3.2 Additional Components

As Figure 6-16 shows, a series of TG® medical gloves (L&R GmbH, Germany) can be worn by different patients. These gloves have the advantage of being washable, hard-wearing comfortable, and have high durability. They are also CE marked and sterilizable. In addition, they meet the sterilization standards in DIN EN ISO 11135, 11137, and 17665.

Figure 6-16: Medical gloves made by Lohmann & Rauscher TG, with four different sizes.

The microcontroller selected for the tremor/bradykinesia assessment system was an ATMega1284P, while the microcontroller selected for the rigidity assessment system was an ATMega328. Both these chips were manufactured by Atmel Inc., USA.

The missing sampling data have a very bad effect on the PSD results (Spieker *et al.*, 1995). The bit rate (or call baud rate) for the serial communication was set to 115200 bps (bits per second) or higher. The crystal oscillator frequency is better at 7.3728 MHz, 11.0592 MHz, 18.432 MHz or 22.118 MHz. Thus, the bit error rate of serial communication between the MCU and command module is about zero.

The speed grades of both the ATMega1284P and ATMega328 are:

- 0 – 10 MHz @ 2.7 – 5.5V.
- 0 – 20 MHz @ 4.5 – 5.5V.

The crystal oscillator frequencies of the two prototypes for the tremor/bradykinesia assessment and the rigidity assessment were higher than 10 MHz. Therefore, their power supplies were chosen to be +5 VDC.

FT232R (Future Technology Devices Inc., UK) is a USB to serial UART (universal asynchronous receiver/transmitter) interface which was to be used here.

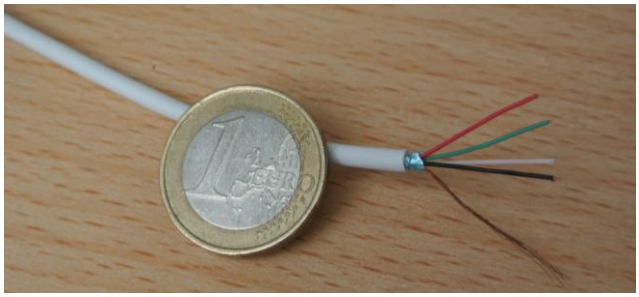

Figure 6-17: Alarm control cable LiYY 4 × 0.14 mm².

As Figure 6-17 shows, a shielded four-pin cable was used to connect the sensor board to the command module.

6.4 Physical Implementation

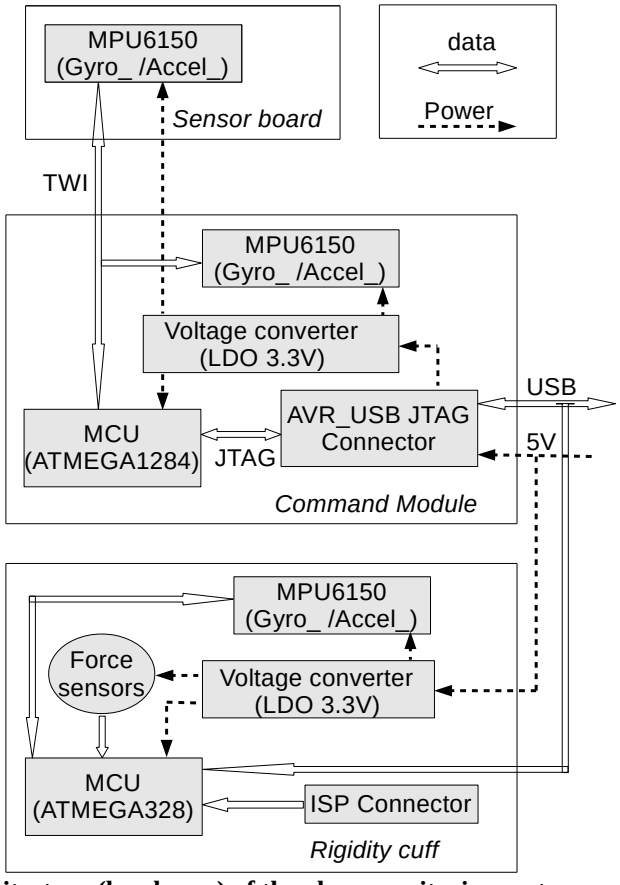

Figure 6-18: Internal architecture (hardware) of the glove monitoring system.

Figure 6-18 shows the hardware diagram of the glove monitoring system, which included two parts. The command module was for the tremor and bradykinesia assessment, while the rigidity cuff was for the rigidity assessment.

6.4.1 Prototype for Testing

At first, the command module was supposed to be integrated into the textile glove. As shown in Figure 6-19, the command module was fixed in the glove with a durable elastic fabric Velcro strap. A USB 2.0 type A to Mini-B five-pin cable was used to connect the command module to a computer.

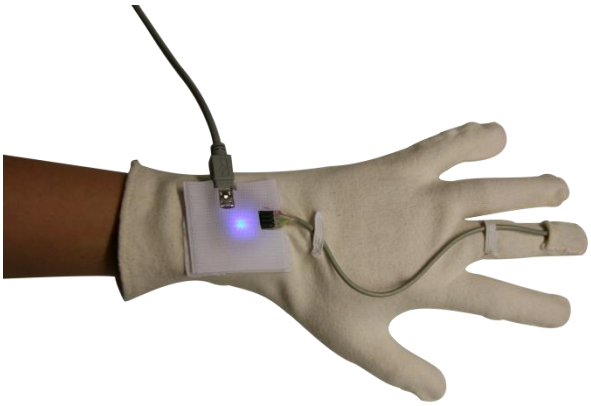

Figure 6-19: Photo of the textile-integrated command module and mini USB connector.

One disadvantage of this design was that the circuit part of the command module could come into contact with the human body. Another disadvantage of the design was that the USB connection was not stable.

Thus the command module was placed in a case for reasons of safety. According to the experiments by Lorenzo *et al.*, a USB JTAG cable (Lorenzo *et al.*, 2011) was chosen for its better connection stability.

6.4.2 Tremor/Bradykinesia Assessment System

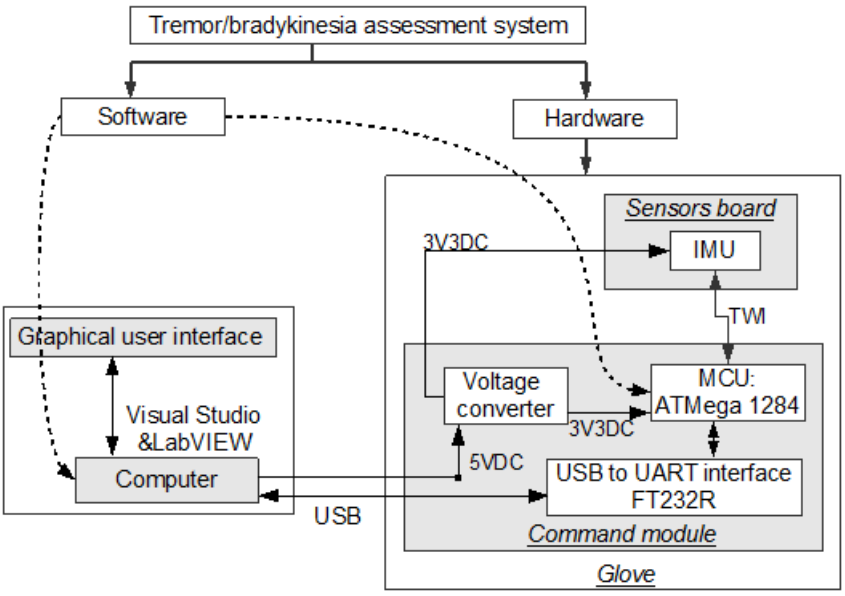

Figure 6-20: Internal architecture of the tremor/bradykinesia assessment system.

As Figure 6-20 shows, the command module and the sensor board were used for finger motion data acquisition and communication with a computer. The command module acquired sensor data and sent it to the computer. An IMU (MPU6150) was located on the sensor board.

The implementation of the sensor board is shown in Figure 6-21 and Figure 6-22. The sensor board (IMU) required a +3.3 V power supply and a TWI bus. Then a four-pin cable connected the sensor board with the command module.

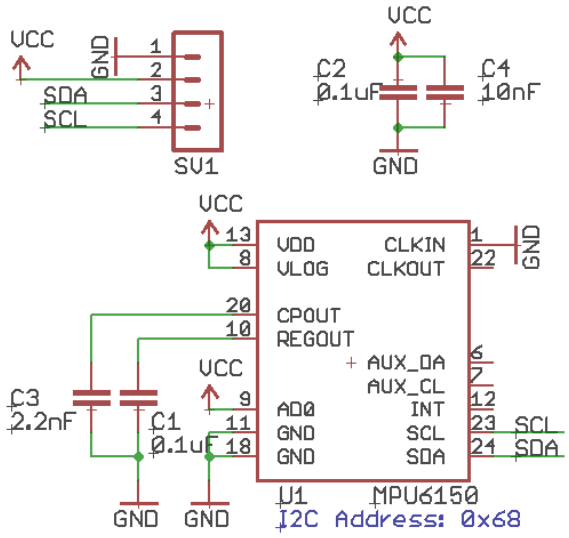

Figure 6-21: Schematic of the sensor board.

Figure 6-22: Photo of the sensor board (dimensions: 14mm × 11mm × 2mm).

As Figure 6-22 shows, the sensor board was put into a liquid insulation can (PLASTI DIP LIQUID TAPE, Plasti Dip® GmbH, Germany) for insulation protection. The board was inside the can for one minute and then taken out to cool for three hours.

Figure 6-23 shows the circuit board and the housing of the command module. Three screws were placed in the top side of the housing. The implementation of the command module is shown in Figure 6-24 (a).

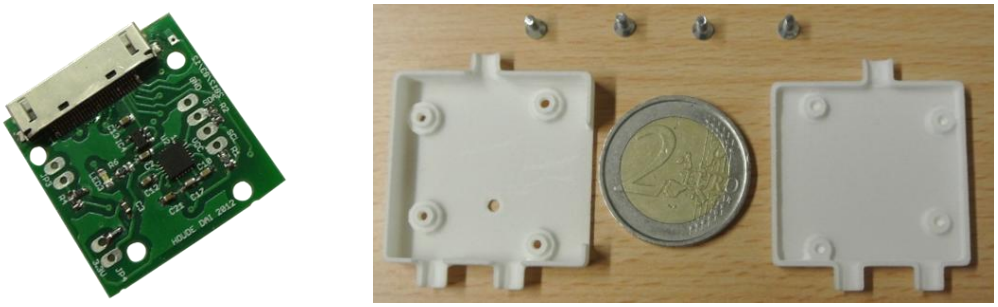

a) **b)**

Figure 6-23: Photos of the circuit board and housing of the command module. a) command board; b) housing with four screws (M2 × 6mm). There was also a prototype with only three screws.

Figure 6-24 shows the command module with the sensor board and a USB JTAG cable. The USB JTAG cable, which includes a serial-to-USB chip (FT232R, Future Inc., UK), was connected to a female 30-pin connector.

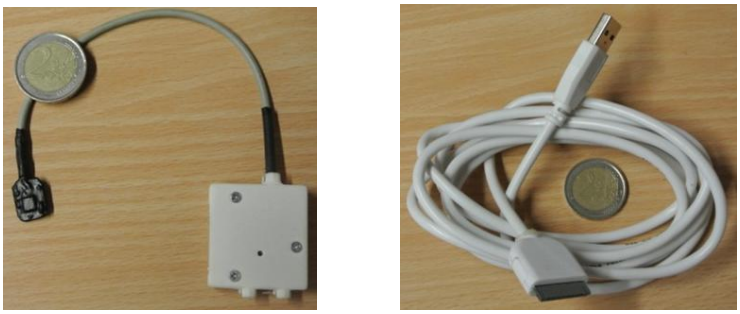

a) b)

Figure 6-24: Photos of the command module and USB JTAG cable. a) photo of the command board with the sensor board; b) USB JTAG cable for the communication between the command module and a computer.

There were five connectors on the circuit board of the command module. A female 30-pin connector was used to connect the command module to a computer via a JTAG USB cable. The JTAG interface of the microcontroller was connected to this connector for programming. A four-pin connector was used for the connection with the sensor board. Two connectors were available for the force sensor boxes but were not used in this version. The USB port of the computer provided the power supply (+5 V) for the command module. The voltage was regulated from 5.0 V to 3.3 V with a low dropout linear regulator (XC6204B332MRN, Torex Inc., Japan).

The IMU in the sensor board was connected to the microprocessor (ATMega 1284P, Atmel Inc., USA) via the TWI interface. The microprocessor sampled sensor data at 100 Hz or 50 Hz. A green light-emitting diode (LED) also indicated the state of sensor readings at 100 Hz or 50 Hz.

The final implementation of the tremor/bradykinesia assessment system is shown in Figure 6-25.

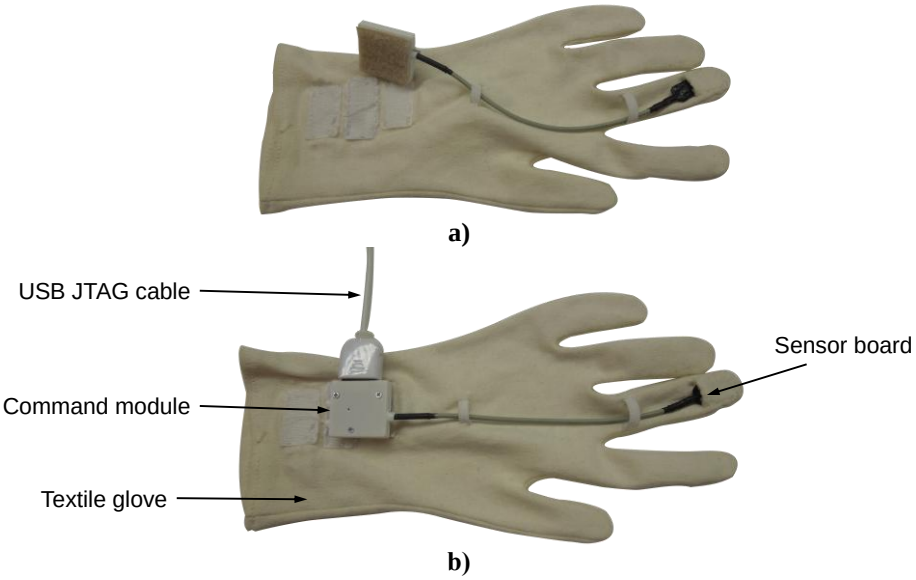

Figure 6-25: Overview of the prototype for tremor/bradykinesia assessment. The command module was 34mm × 32mm × 7mm. The command module and sensor board both had indirect contact with the human body.

The operation of the wired system for tremor/bradykinesia is shown in Figure 6-26.

Figure 6-26: Tremor/bradykinesia assessment system.

6.4.3 Rigidity Assessment System

The rigidity assessment system was implemented before the availability of single-chip IMUs such as MPU6150/6050. Therefore, two inertial sensors were adopted. A triple-accelerometer (MMA8452Q, Freescale Inc., USA) worked with a triple-gyroscope (IMU3000, Invensense Inc., USA).

Two differential force sensor boxes were used to measure the attached force on the wrist. Each force sensor box was built from four FSRs (FSR-149NS, IEE Inc., Luxembourg), which were connected in parallel. Each force sensor box had only one output, with a type of voltage divider.

Figure 6-27 shows the realization of a force sensor box. The output of the force sensor box (V_{out}) was directly connected to the ADC input of a microcontroller (ATMega 328p, Atmel Inc., USA).

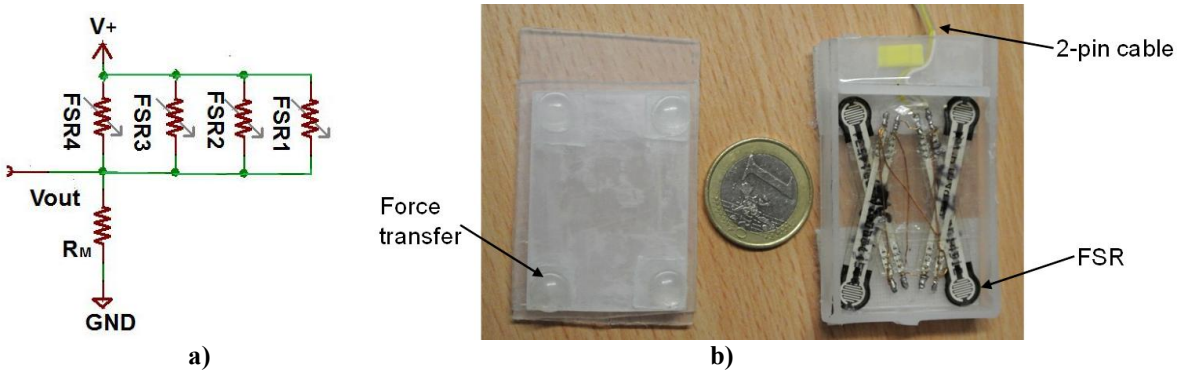

Figure 6-27: Implementation of a force sensor box. a) schematic of the force sensors; b) photo of the force sensor box (Based on Dai *et al.*, 2013a).

A plastic case was used to place the force sensor boxes and can be pressed by an examiner during rigidity assessment. The rigidity cuff consisted of a plastic housing, a Velcro textile band, and a microprocessor board.

Figure 6-28 shows the Velcro textile band. Through a combination of hard Velcro and soft Velcro, the two force sensor boxes and the microcontroller board were fixed on the wrist. The microcontroller board and the housing of the two force sensor boxes were all attached on the

outside of the band. The textile band had the advantage of being able to fit the different arm diameters of each patient.

Figure 6-28: Photo of the Velcro textile band (© TUM-MIMED, 2012).

Because the power supply of the microcontroller (5 V) differed from that of the inertial sensors, a dual bi-directional TWI bus voltage-level translator (PCA9306, TI Inc., USA) was used. Figure 6-29 shows the schematic diagram of the voltage-level translation circuit.

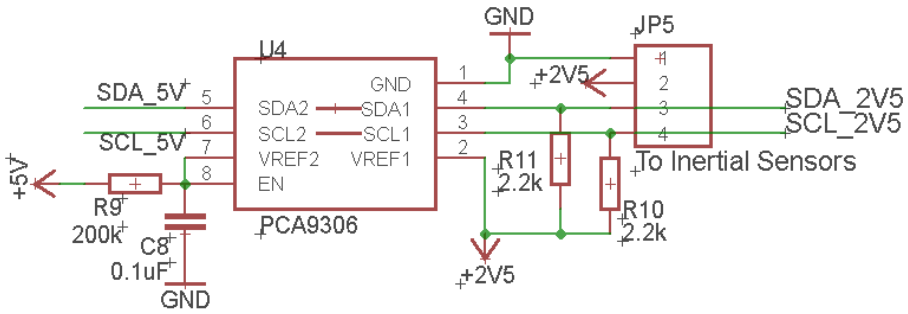

Figure 6-29: Schematic of the dual bi-directional TWI bus voltage-level translator.

Figure 6-30 shows the circuit board of the rigidity cuff. The implementation of the command module is shown in Figure 6-31. All the sensor data were sampled at 100 Hz by the microprocessor.

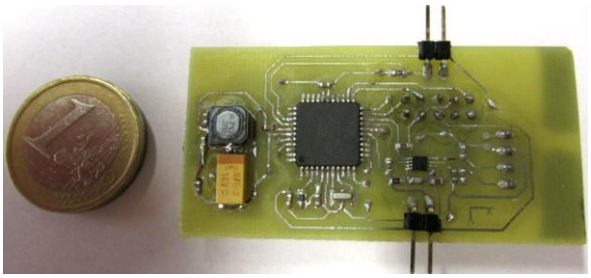

Figure 6-30: Photo of the microcontroller board in the rigidity cuff.

Figure 6-31: Overview of the prototype for rigidity assessment (Based on Dai *et al.*, 2013b).

The prototypes of both the tremor/bradykinesia and rigidity assessment system are shown in Figure 6-32.

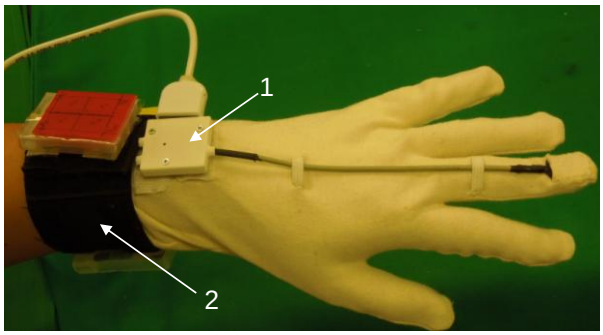

Figure 6-32: Prototypes of the glove monitoring system. 1) command module (tremor/bradykinesia assessment part); 2) rigidity cuff (rigidity assessment part). The command module and sensors did not have direct contact with the human body (Taken from Dai *et al.*, 2013a).

6.5 Graphical User Interface Implementation

The data transmission, signal processing, and GUI of the tremor/bradykinesia assessment system were carried out on a computer using LabVIEW 2010 Evaluation Version (National Instruments Corp., USA). Figure 6-33 shows the GUI of the bradykinesia and tremor assessment system.

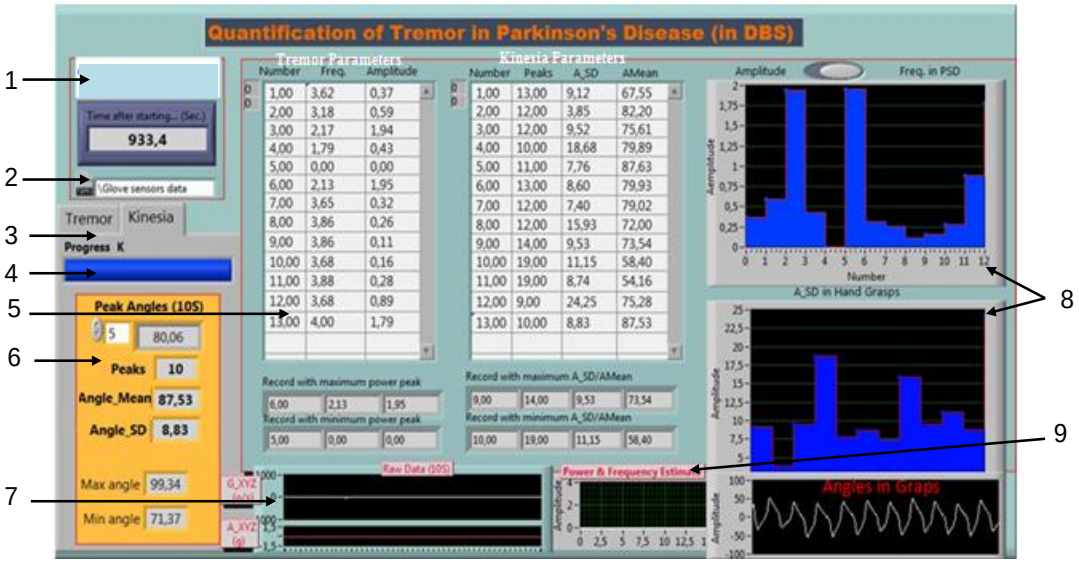

Figure 6-33: GUI of the tremor/bradykinesia assessment system. 1) serial interface setting; 2) raw data path configuration; 3) start button; 4) progress bar; 5) results recording list; 6) real time result area; 7) sensor raw data; 8) results recording chart; 9) PSD chart.

The GUI included the task start buttons, progress bars, recording lists, and the storage location setting of raw data.

To start the tremor assessment, the task button in the GUI must be set to "Tremor" and the examiner needs to press the start button. During tremor assessment, the raw data and the PSD figure of three-second signals were displayed at the bottom. At the end of the tremor task, the actual assessed results, which included dominant frequency and tremor amplitude during the ten-second assessment task, were displayed in the result area of tremor assessments.

To start bradykinesia assessment, the task button in the GUI must be set to "Kinesia". During bradykinesia assessment, the raw data and the PSD figure as well as the angular displacement were displayed at the bottom. At the end of the bradykinesia task, the actual assessed results,

which included dominant frequency, mean and standard deviation of the grasping ranges, were displayed in the result area of bradykinesia.

After each tremor or bradykinesia assessment task, the corresponding assessment result item, which consists of the assessment number and relative parameters, was added to the results recoding list automatically. The result items with the biggest and smallest amplitudes were displayed at the bottom of the results recoding list. All the raw sensor data were stored in the computer for offline analysis.

Data communication and the GUI of the rigidity assessment system were realized with Visual C# 2010 (Microsoft Inc., USA). This program invokes MATLAB 2012b (MathWorks Inc., USA) to perform signal processing. Figure 6-34 shows the GUI of the rigidity assessment system.

Because the patient's forearm length could not be measured directly with the above sensors, the examiner should record the subject's forearm length in the input box of the GUI.

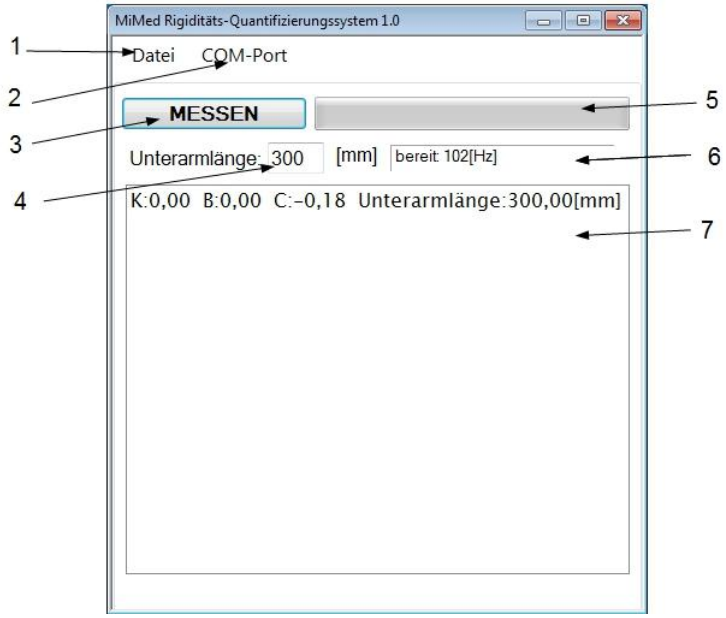

Figure 6-34: GUI of the rigidity assessment system (Baed on Dai *et al.*, 2013b). 1) raw data path configuration; 2) serial interface setting; 3) start button; 4) input box for the patient's forearm length; 5) progress bar; 6) communication status; 7) results.

6.6 Calibration of Inertial Sensors and Force Sensor Boxes

The calibration methods for inertial sensors are first introduced in Chapter 6.6.1. The sensors in the rigidity cuff were first calibrated. However, the calibration of the tremor/bradykinesia assessment system depends on each IMU on the sensor boards. There are several sensor boards available. Each IMU should be calibrated respectively.

6.6.1 Analysis of Inertial Sensors

The key issue in the performance of a motion tracking system is its accuracy. Although present inertial sensors are smart sensors (factory calibration and run-time calibration firmware are embedded into the sensors); bias, noise, scaling factor error, and the cross-axis misalignment compensation matrix still require consideration. Some initial calibration procedures for individual gyroscopes and accelerometers are needed.

Gyroscope Calibration

The single axis output (angular velocity $\omega_o(t)$) of a gyroscope in time *t* is expressed as follows:

$$\omega_o(t) = (1 + a)\omega(t) + b\ , \tag{6-1}$$

where $\omega(t)$ is the true angular velocity, a and b are the scaling and biasing of the output, respectively. The output bias error (offset) is related to its special structure, temperature change, magnetic field, and other noises. Linear acceleration can also result in bias in a gyroscope. In general, this bias error results in big drifts after an integration time.

Thus the first-order triple-axis gyroscope compensation equation is shown as follows:

$$\begin{bmatrix}\omega_x\\ \omega_y\\ \omega_z\end{bmatrix} = \boldsymbol{M}\begin{bmatrix}S_{gx} & 0 & 0\\ 0 & S_{gy} & 0\\ 0 & 0 & S_{gz}\end{bmatrix}\begin{bmatrix}\omega_{ox} - b'_{gx}\\ \omega_{oy} - b'_{gy}\\ \omega_{oz} - b'_{gz}\end{bmatrix}, \tag{6-2}$$

where S_{gx}, S_{gy}, and S_{gz} are the scaling factors in three axes; b'_{gx}, b'_{gy}, and b'_{gz} are the offsets in three axes; and $\boldsymbol{M}$ is the 3×3 cross-axis misalignment compensation matrix.

In this study, the offsets are calculated with the mean gyroscope outputs in a static state in ten seconds. The calculation function is described as follows:

$$\begin{pmatrix}b'_{gx}\\ b'_{gy}\\ b'_{gz}\end{pmatrix} = \frac{1}{N}\cdot\begin{pmatrix}\sum_1^N \omega_{ox}\\ \sum_1^N \omega_{oy}\\ \sum_1^N \omega_{oz}\end{pmatrix}, \tag{6-3}$$

where ω_{ox}, ω_{oy}, and ω_{oz} are the raw data outputs in static state; *N* is the number of sampled points (= sampling rate × 10 seconds).

The true angular velocities (ω_x, ω_y, and ω_z) from a gyroscope are considered to be linear according to the datasheets of gyroscopes. The sensitivity of a single gyroscope axis is computed with the values recorded while rotating the gyroscope 180° around that axis. The angular displacement by integrating the angular velocity is a sinusoidal signal. Those values are integrated over time and multiplied by 1/(sample rate). The signals of each gyroscope axis are then divided by the scaling factor to obtain the angular velocity in [°/s]. Then the scaling factors in three axes are described as:

$$\begin{pmatrix}S_{gx}\\ S_{gy}\\ S_{gz}\end{pmatrix} = \left(\frac{180^\circ}{\Delta t\cdot S_{gyro\_sensit}}\right)\Big/\begin{pmatrix}\sum_1^n \omega_{ox}\\ \sum_1^n \omega_{oy}\\ \sum_1^n \omega_{oz}\end{pmatrix}, \tag{6-4}$$

where S_{gyro_sensit} is the gyroscope's sensitivity scaling factor [unit: count/(°/s)], which can be found in the datasheet; and Δt is the sampling interval (unit: s).

Accelerometer Calibration

Accelerometer offsets, scaling factors, and cross-axis misalignment errors should also be compensated by the calibration process.

Thus the first order triple-axis gyroscope compensation equation is shown as follows:

$$\begin{bmatrix} a_x \\ a_y \\ a_z \end{bmatrix} = \boldsymbol{M} \begin{bmatrix} S_{ax} & 0 & 0 \\ 0 & S_{ay} & 0 \\ 0 & 0 & S_{az} \end{bmatrix} \begin{bmatrix} a_{ox} - b'_{ax} \\ a_{oy} - b'_{ay} \\ a_{oz} - b'_{az} \end{bmatrix}, \tag{6-5}$$

where S_{ax}, S_{ay}, and S_{az} are the scaling factors in three axes; b'_{ax}, b'_{ay}, and b'_{az} are the offsets in three axes; and $\boldsymbol{M}$ is the 3×3 cross-axis misalignment compensation matrix.

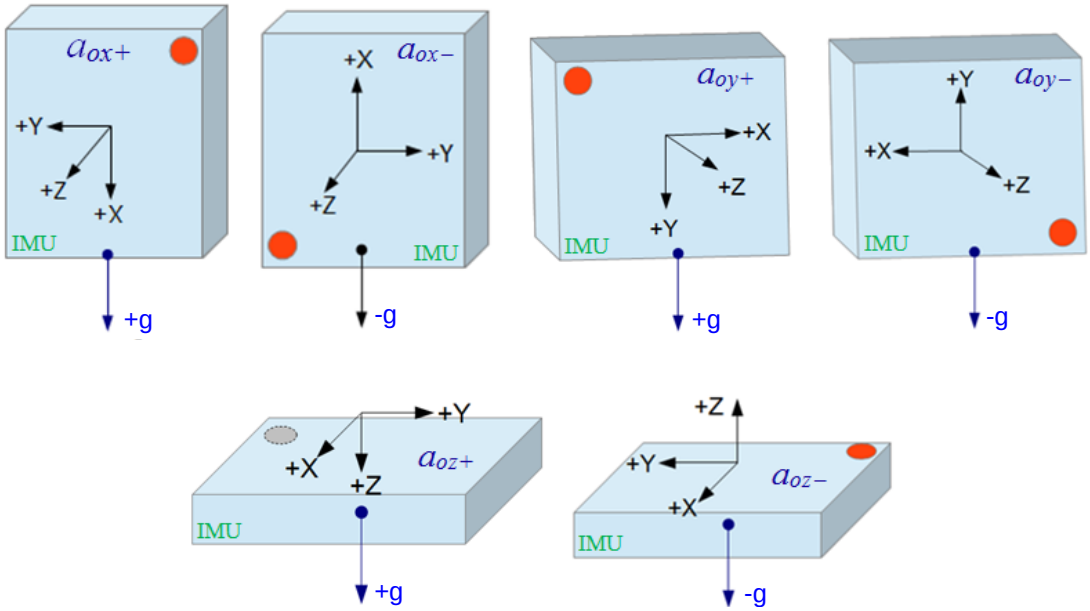

Figure 6-35: Positions of an IMU for calibrating accelerometer offsets.

The outputs of a triple-axis accelerometer include linear accelerations and gravitational accelerations. For the calibration of static offsets, the sensor is in a stable condition before being measured. Each axis of the accelerometer is placed parallel to gravity with both positive and negative sides. As Figure 6-35 shows, the true value of the related acceleration in the static state should be 1g or -1g. However, the outputs of the accelerometer include also bias (offsets). The recorded gravitational acceleration both with and against gravity, as shown in Figure 6-35, are described as follows:

$$(\boldsymbol{a}_{o+}, \boldsymbol{a}_{o-}) = \begin{bmatrix} a_{ox+} & a_{ox-} \\ a_{oy+} & a_{oy-} \\ a_{oz+} & a_{ox-} \end{bmatrix}. \tag{6-6}$$

The triple-axis accelerometer outputs are scaled to multiples of the gravitational constant (g). These values are used to calculate the sensitivity and offset of each axis. Then the offsets can be calculated with the values in Equation 6-2 as follows:

$$\begin{pmatrix} b'_{ax} \\ b'_{ay} \\ b'_{az} \end{pmatrix} = \frac{1}{2} \cdot (\boldsymbol{a}_{o+} + \boldsymbol{a}_{o-}) = \frac{1}{2} \cdot \begin{pmatrix} a_{ox+} + a_{ox-} \\ a_{oy+} + a_{oy-} \\ a_{oz+} + a_{oz-} \end{pmatrix}. \tag{6-7}$$

The scaling factors can be calculated with the values in Equation 6-2 as follows:

$$\begin{pmatrix} S_{ax} \\ S_{ay} \\ S_{az} \end{pmatrix} = \frac{1}{2} \cdot (\boldsymbol{a}_{o+} - \boldsymbol{a}_{o-}) = \frac{1}{2S_{acc\_sensi}} \cdot \begin{pmatrix} a_{ox+} - a_{ox-} \\ a_{oy+} - a_{oy-} \\ a_{oz+} - a_{oz-} \end{pmatrix}, \tag{6-8}$$

where S_{acc_sensi} is the sensitivity (unit: count/g) of the accelerometer.

The sensor outputs should be sampled at room temperature and the sensors should have been working for at least one hour before the measurement.

6.6.2 Calibration of Inertial Sensors

According to the calibration procedures in Chapter 3.6.3, the calibration results of the gyroscope (IMU3000) and the accelerometer (MMA8452Q) in the rigidity cuff are shown from Table 6-3 to Table 6-5.

Table 6-3 Offsets and sensitivities of the gyroscope in the rigidity cuff (IMU3000, 16-bit resolution: -32768–32767)

	X-Axis	**Y-Axis**	**Z-Axis**
Offset	-390	+161	+68
Sensitivity	0.9358	0.9491	0.9611

Table 6-4 Accelerometer outputs when its axes were oriented along/against the direction of gravity (MMA8452Q, 12- bit resolution: -2048–2047)

	X-Axis	**Y-Axis**	**Z-Axis**
Orientation along g-axis (1g)	991	1011	1008
Orientation against g-axis (-1g)	-1005	-974	-997

Table 6-5 Offset and sensitivity for the accelerometer (MMA8452Q, 12-bit resolution: -2048–2047)

	X-Axis	**Y-Axis**	**Z-Axis**
Offset	-7	+18	+5
Sensitivity	0.9746	0.9697	0.9785

6.6.3 Calibration of Force Sensor Boxes

According to Figure 5-8 in Chapter 5.2.2, the output of the force-to-voltage conversion was tied to a measuring resistor in a voltage divider configuration. The output voltage of a force sensor box (V_{out}) was shown as:

$$V_{out} = V_{cc} / \left[1 + \left(R_{FSR} / R_M\right)\right], \tag{6-9}$$

where V_{cc} was the power supply (+5 V); R_{FSR} was the resistor value of the force sensor box; and R_M was the value of the pull-down resistor (4.7 KΩ).

Equation 6-9 shows that the output of a force sensor box response for R_{FSR} is similar to an e-function. The force-resistance characteristic of a single FSR sensor (FSR149NS) is nonlinear and the response approximately follows an inverse power-law characteristic. However, a linear force-to-voltage relationship is needed in Equation 5-9 in Chapter 5.3.3. Hence, a regression analysis was applied to get the voltage-force function. Regression analysis was performed with the Curve Fitting Toolbox in MATLAB R2012a (Mathworks Inc., USA). Results of a two-term Gaussian regression were compared to one-term and four-term Gaussian functions.

Since the FSR output is nonlinear and sensor sensitivity varies, every force sensor box has to be respectively calibrated. As each force sensor box included four FSR sensors but had only one output, the calibration of FSRs was performed after the implementation of the two force sensor boxes.

As shown in Figure 6-36, 58 weight loads ranging from 5 grams to 6000 grams were applied at the center of the top side of each force sensor box. Since FSRs are prone to drift, only the value up to three seconds after applying the load could be used and the weight was released from the force sensor box after every single measurement. Therefore, 116 voltage values were acquired. The correlation of sensor outputs over weights was recorded.

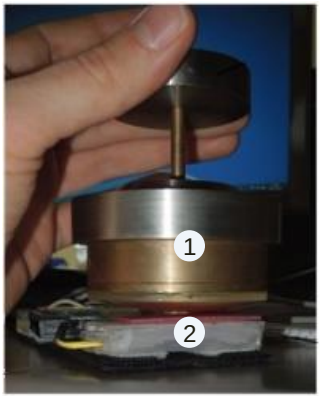

Figure 6-36: Setup of the force sensor box's calibration. Each force sensor box was tested with weights, while the weights were placed in the center top side of the force sensor box (Based on Dai *et al*, 2013a).

If the applied force was lower than 0.5 N, there was no change in the output of the force sensor box. However, for applying forces bigger than 0.5 N, the resistance of the force sensor box rapidly dropped and reached saturation when the applied force was more than 100 N. The FSR sensor tutorial (IEE International Inc., Luxemburg, 2011) states that the FSR sensor response to higher loads is similar to an e-function. Therefore, a Gaussian function was chosen for regression analysis:

$$f(x) = a_1 \cdot \exp\left[-\left(\frac{x-b_1}{c_1}\right)^2\right] + \ \ldots \ + a_n \cdot \exp\left[-\left(\frac{x-b_n}{c_n}\right)^2\right], \qquad (6\text{-}10)$$

where *x* was the output of the force sensor box and *f(x)* was the attached force.

To evaluate the performance of the Gaussian function, results were compared with fits for an e-function and polynomial functions (Abramowitz *et al*., 1965).

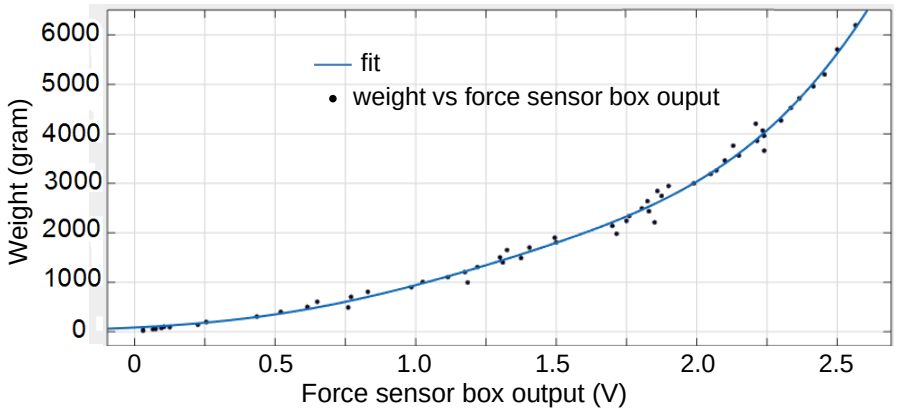

Figure 6-37: Two-term Gaussian regression plot of force sensor box 1: weight (g) versus the output of the force sensor box 1 (© TUM-MIMED, 2012).

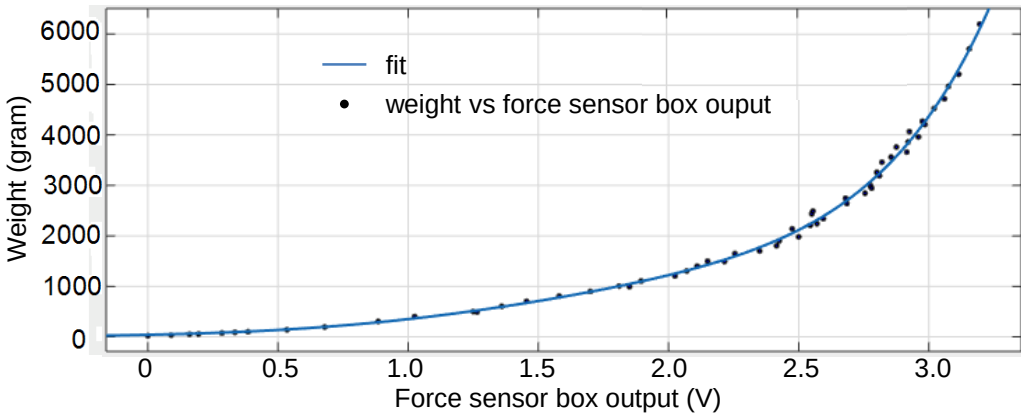

Figure 6-38: Two-term Gaussian regression plot of force sensor box 2: weight (g) versus output of the force sensor box 2 (© TUM-MIMED, 2012).

Using the MATLAB Curve Fitting Toolbox, one-, two-, and four-term Gaussian, e-Function, and Polynomial regression analyses were performed with the measurement data.

Figure 6-37 and Figure 6-38 show the regression plots of a two-term Gaussian regression function which fitted to the two force sensor box outputs, while Figure 6-39 shows a one-term Gaussian regression fitting and Figure 6-40 shows a four-term Gaussian regression fitting of the force sensor box 1.

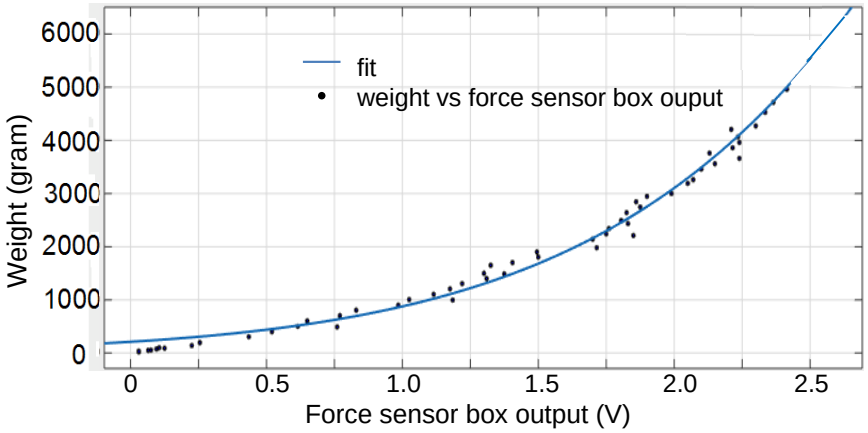

Figure 6-39: One-term Gaussian regression plot of force sensor box 1: weight (g) versus output of the force sensor box 1 (© TUM-MIMED, 2012).

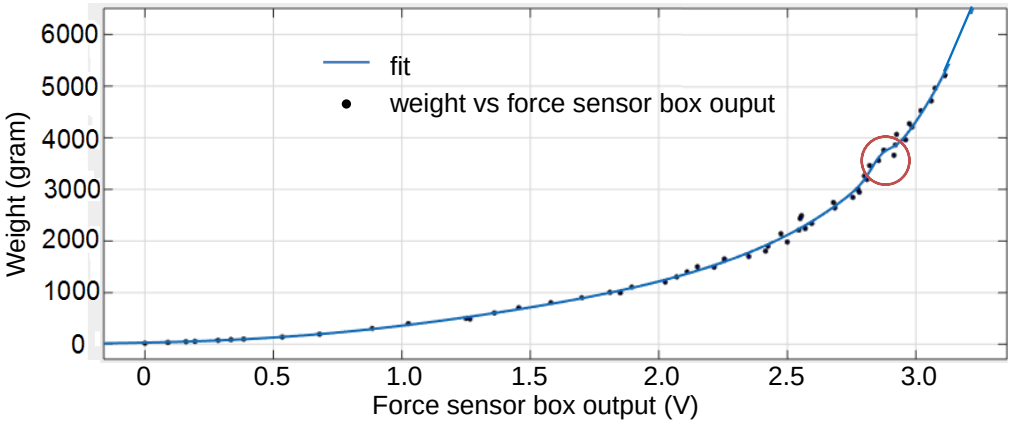

Figure 6-40: Four-term Gaussian regression plot of force sensor box 1: weight (g) versus output of the force sensor box 1. The red circle highlights the area with over-fitting (© TUM-MIMED, 2012).

As Figure 6-39 shows, one-term regression did not fit the response curve well, producing low values of correlation (r^2) (see Table 6-6). At the same time, the four-term regression was susceptible to outliers, which resulted in over-fitting (Figure 6-40).

Table 6-6 shows the results of the different curve fits applied to the data set. The selected fit has been highlighted. The MATLAB Curve Fitting toolbox was not able to find a one-term Gaussian fit for the dataset of force sensor box 2. Accordingly, the corresponding value in Table 6-6 is "no fit". In addition, there were no four-term e-Function fittings for the two force sensor boxes.

Table 6-6: Results of regression analysis: adjusted r^2 values (force sensor box 1/ force sensor box 2)

	Gaussian	**e-Function**	**Polynomial**
1-term	0.9904 / no fit	0.9896 / 0.9925	0.8908 / 0.7778
2-term	0.9937 / 0.9971	0.9931 / 0.9923	0.9826 / 0.9531
4-term	0.9934 / 0.9973	Not available in toolbox	0.9939 / 0.9961

As shown in Table 6-6, a two-term Gaussian function has the highest correlation with the measured data:

$$F(v_{out}) = a_1 \cdot e^{-(\frac{v_{out}-b_1}{c_1})^2} + a_2 \cdot e^{-(\frac{v_{out}-b_2}{c_2})^2}, \quad (6\text{-}11)$$

where $F(v_{out})$ was the calculated force value, v_{out} was the sensor box output voltage, and a, b, and c were coefficients.

The coefficients of Equation 6-11 could also be determined using the MATLAB Curve Fitting Toolbox. These parameters, which have been calculated using the two-term Gaussian regression, are given in Table 6-7.

Table 6-7: Coefficients of the two-term Gaussian regression for the two force sensor boxes (FSR boxes)

	a_1	b_1	c_1	a_2	b_2	b_3
FSR box 1	5.91e+04	1104	387.1	1020	322.6	195.5
FSR box 2	1.139e+18	7287	1159	734.6	445.6	253.4

6.7 Combined Version

Together with the tremor/bradykinesia assessment system and the rigidity assessment system, a portable monitoring system used to quantify all primary neurological symptoms in PD and ET was able to be implemented.

As shown in Figure 6-41, the combined system was built up based on the two prototypes (tremor/bradykinesia assessment system and rigidity assessment system).

Some components were replaced for the reason of a higher performance. The crystal oscillator frequency was set to 18.432 MHz instead of 11.0592 MHz. MPU6050 replaced MPU6150 for its better gyroscope noise performance. The active area of FSR149NS is too small (Ø4.03

mm) and therefore each force sensor box needed four force sensors. FSR402 has a 14.7 mm diameter active area coverage, thus only one force sensor was needed in the combined version.

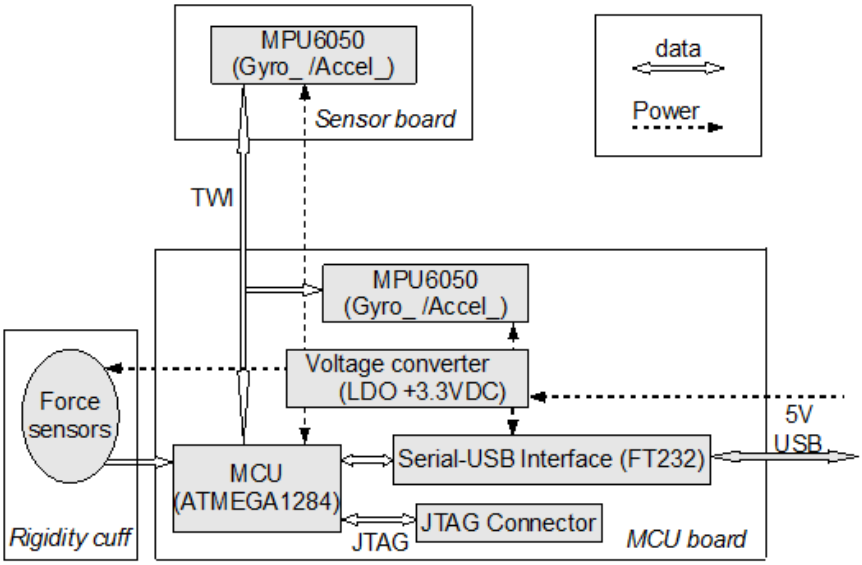

Figure 6-41: Internal architecture of the combined version.

Figure 6-42 shows the connection between the command module and the force sensor boxes. The force sensor boxes were connected to the microcontroller via an instrumentation amplifier.

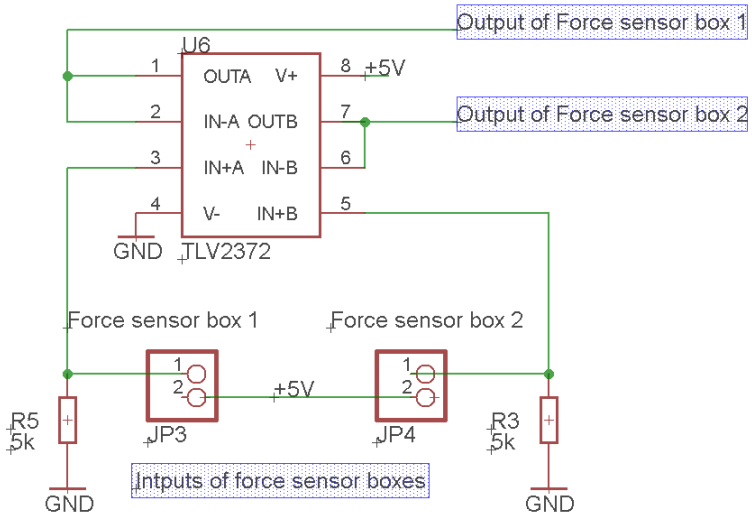

Figure 6-42: Interfaces between the force sensor boxes and command module (MCU board). The outputs of the two force sensor boxes were connected to an amplifier. TLV2372 (TI Inc., Dallas, USA) is a rail-to-rail input/output low power instrumentation amplifier.

For the tremor/bradykinesia assessment system and rigidity assessment system, the received sensor data in the computer were checked with an imitated tremor test by healthy subjects. The test result indicates that the missing points of sampling data (dropped packets) over the whole sampled data were less than 0.2% with a sampling rate of 50 Hz. However, sometimes there were disconnections between the command module and the computer. The assessment task was able to be interrupted by violent hand movement. In the combined version, one side of the USB cable was soldered directly to the printed circuit board of the command module, instead of using a USB connector in the command module.

A 10-pin header (FTSH-105-01-L-DV-K-A-P, Samtec Inc., Indiana, USA) was placed on the center of the command board as the JTAG programming connector, because of its small dimension and safe style (keyed).

Figure 6-43 shows the hardware of the combined version.

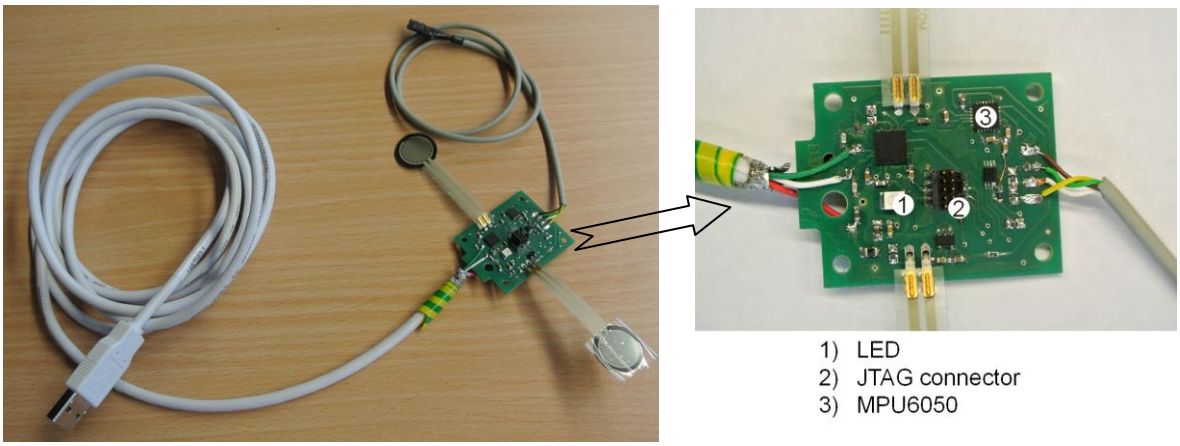

Figure 6-43: Prototype realization of the combined version.

Figure 6-44 shows the GUI which can be used to assess tremor, bradykinesia, and rigidity.

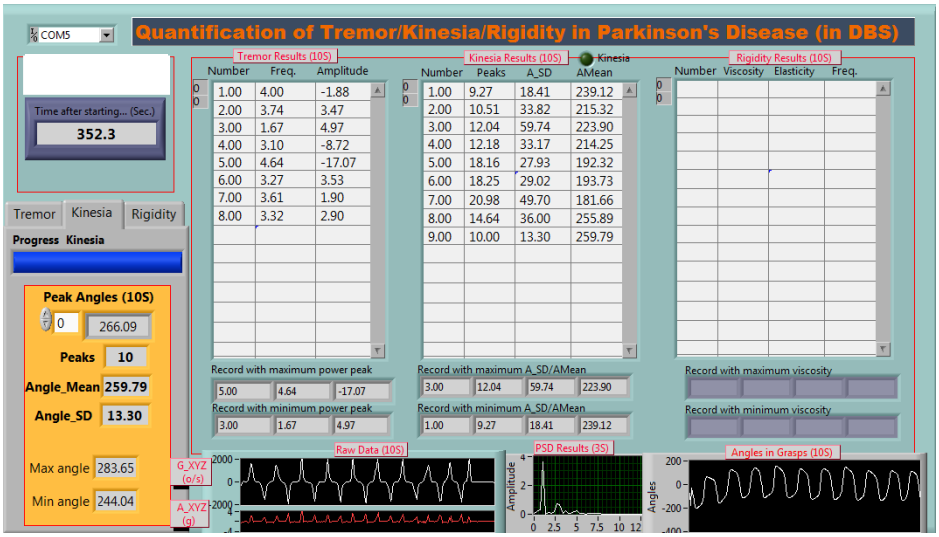

Figure 6-44: GUI of the combined version (Taken from Dai *et al.*, 2013a).

6.8 Conclusion

The prototype of the tremor/bradykinesia assessment system is presented. It was based on an IMU, which was attached on a finger, and could be combined with a textile glove.

The first prototype of a portable rigidity assessment system, which was attached to the wrist, was also presented. It was based on two force sensor boxes and an IMU. As a result, this system made it easy to perform passive elbow movement.

The combined version was implemented for quantification of all primary neurological symptoms in patients with PD or ET.

For possible hardware design in the future, a microcontroller with an embedded USB communication interface can provide a higher transmission rate between the computer and micro-

controller than the serial-to-USB converter. In addition, a system with a wireless interface instead of wired communication makes the system usable outside of the operating room and in places such as homes or sickrooms. As a result, the system can be used for bradykinesia assessment at home or in hospital for further tests.

The signal processing was mainly performed by the computer. The role of the microcontroller was simply to acquire and send the raw data to the computer.

The Kalman filter and DCM algorithm can be run on a microcontroller. As mentioned in the first section of this chapter, the nine-axis DCM algorithms can be run on an eight-bit microcontroller. However, the microcontroller needs more time consummation in this situation. Thus the sampling rate of the sensors is limited to a low value. In order to perform certain timing issues such as signal pre-proceeding by the side of the command module, two microcontrollers may be used: one as the master for sensor data acquisition and the other as the slave for signal processing. In addition, the sensor fusion can be embedded inside the sensor, which performs an orientation calculation. Then the angular displacement of tremor, grasping angles during a bradykinesia task, and elbow angles during a rigidity task can be easily acquired. The angles from the chip-based sensor fusion should be compared to the values acquired with the methods in this system.

Passive elbow movement is a movement in three dimensions. However, the force sensor boxes provided the different output only in a single axis. Thus the passive movement should be parallel to one axis of the Cartesian coordinate system.

Tremor/bradykinesia assessment systems with wireless communication interfaces can be used as mobile medical devices used before and after the DBS surgery. These prototype realizations are helpful for designs in the future.

7. Experiments and Discussion

IMU do not give position information, but most research projects use raw IMU data for signal processing in tremors and bradykinesia quantitative assessments. No previous studies have compared the assessment systems for neurological symptoms based on IMU with other medical motion tracking systems.

Before comparing this system's output with the patients' clinical ratings, it is necessary to evaluate the calculated technical parameters of this system. In order to do this, several experiments were carried out. Analytical verifications of the three test tasks of the glove monitoring system were performed. The verifications of analytical methods are presented in Chapters 7.1, 7.2, and 7.3, respectively.

After verifying the system, the tremor and bradykinesia assessment system was tested with tremor and bradykinesia tasks in the hospital. The experiments of tremor and bradykinesia assessments are presented in Chapter 7.5 and Chapter 7.6, respectively.

7.1 Verification of Analytical Methods for Tremor Assessment

The NDI Aurora electromagnetic tracking system is first introduced in Chapter 7.1.1. It was used for the verification of analytical methods for tremor, bradykinesia, and rigidity assessments.

The verification of tremor amplitude and frequency is presented in Chapter 7.1.2.

7.1.1 NDI Aurora Electromagnetic Tracking System

As shown in Figure 7-1 (a), an Aurora electromagnetic (EM) spatial measurement system (Northern Digital Inc., Waterloo, Canada) was used as the reference system. The Aurora® EM system is a navigation system designed specifically for medical applications.

As shown in Figure 7-1 (b), the Aurora's micro six-DOF EM sensor has a small dimension (Φ2.5 mm × L11 mm, line: 2 m) and can be attached to a finger or wrist.

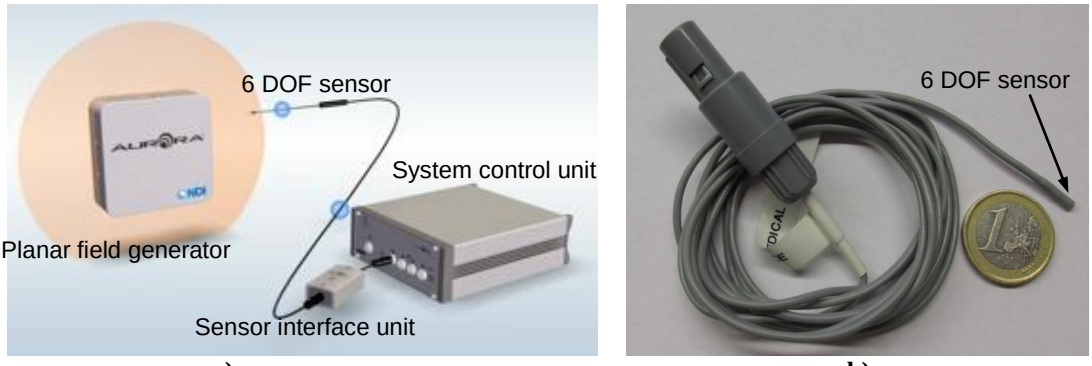

a) **b)**

Figure 7-1: a) Aurora electromagnetic (EM) tracking system; b) Aurora six-DOF sensor cable tool (© NDI, 2013).

The Aurora system's characterized measurement volume can be set to a dome volume (Φ480 mm × L660 mm) or cube volume (500mm × 500mm × 500mm). However, there is a 50 mm distance between the planar field generator and the characterized measurement volume. Fig-

ure 7-2 shows the characterized measurement volumes. The EM tracking in cube volume mode has higher accuracy than the dome volume mode. Thus the measurement volume was fixed to cube volume mode in this study. The accuracy parameters of the EM tracking system with a six DOF sensor are:

- Location: 0.48 mm (RMS), 1.40 mm (95% confidence interval).
- Orientation: 0.30º (RMS), 0.48º (95% confidence interval).

In this study, the sampling rate of the EM tracking system was 40 Hz. The IMUs of the glove monitoring system were sampled at 100 Hz.

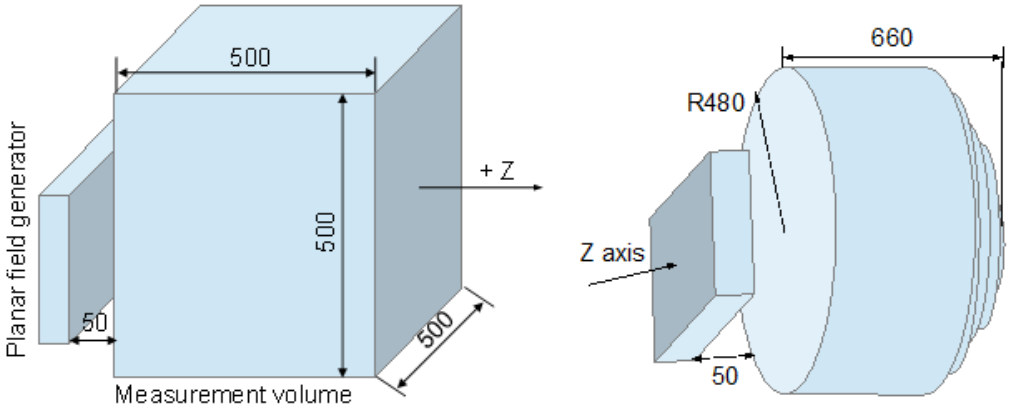

Figure 7-2: Characterized measurement volume (left: cube volume mode; right: dome volume mode).

Figure 7-3 shows the experimental setup of all verifications of analytical methods.

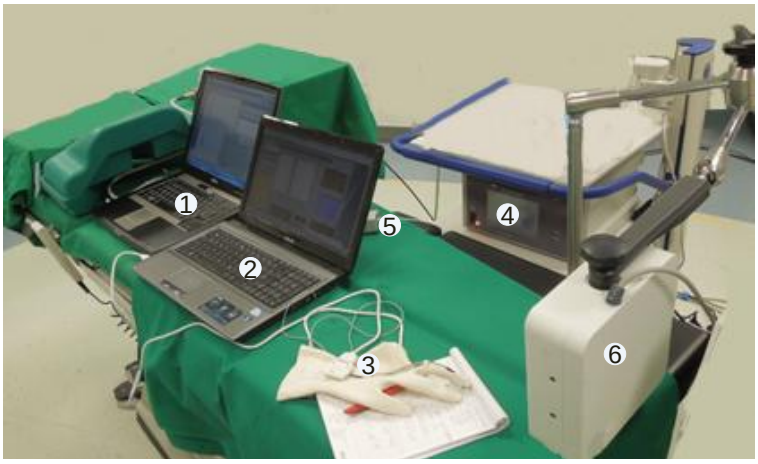

1) Laptop for EM tracking system
2) Laptop for glove monitoring system
3) Glove monitoring system and EM sensors
4) EM control unit
5) EM sensor unit
6) EM generator

Figure 7-3: Setup for the verification of analytical methods. An electromagnetic tracking system was run with the glove monitoring system at the same time. The graphical user interfaces of both systems were run on two laptops. The data transmissions of the two systems were both based on serial-USB communication.

7.1.2 Verification of Tremor Amplitude and Frequency

Motivation

IMU signals are angular velocity and linear acceleration; but a surgeon judges tremor severity according to the displacement of hand tremor. On the other hand, the EM tracking system can obtain position information directly. Therefore, the comparison of the analytical methods between EM signals and IMU signals was performed. Here the glove monitoring system refers to the tremor/bradykinesia assessment system.

Hypothesis

By comparing with those from the EM system, the tremor amplitude (peak powers) and dominant frequency of the glove monitoring system should meet the following requirements:

- Mean value and standard deviation of the differences between dominant frequencies: $f_{md} < 1.00 \pm 0.88$ Hz (Niazmand *et al.*, 2011b).
- Correlation coefficient of peak powers (tremor amplitude): $r > 0.95$ (Bland & Altman, 2003).

Materials

- NDI Aurora® EM tracking system with a six-DOF sensor (Northern Digital Inc., Canada)
- Tremor/bradykinesia assessment system (included a JTAG USB cable and a command module with a sensor board)
- Laptop installed with the application software of the EM system (Aurora Toolbox)
- Laptop with the application software of the tremor/bradykinesia assessment system (LabVIEW-based GUI for tremor/bradykinesia assessment; MATLAB R2008b for data analysis)

Method

The dominant tremor frequencies calculated by the tremor/bradykinesia assessment system and EM system were f_{tb} and f_{em} (see Chapter 5.3.1). Then the difference of their dominant frequencies in a single tremor task was represented by:

$$f_d = |f_{tb} - f_{em}|. \tag{7-1}$$

Therefore, f_{md} (mean and standard deviation of dominant frequency differences) can be calculated by the values of f_d (frequency differences) during all imitated tremor assessment tasks:

$$f_{md} = \left(\frac{1}{N}\sum_{i=1}^{N} f_{di}\right) \pm \left(\sqrt{\frac{1}{N} \cdot \sum_{i=1}^{N}\left[f_{di} - \left(\frac{1}{N}\sum_{i=1}^{N} f_{di}\right)\right]^2}\right), \tag{7-2}$$

where N was the amount of imitated tremor assessment tasks.

The tremor amplitude (peak powers based on the IMU signals) calculated by the tremor/bradykinesia assessment system was R, while the tremor amplitude (peak power based on the position data) judged by the EM system was E (see Chapter 5.3.1). Then the correlation coefficient between these two parameters was:

$$r = \frac{N\sum_{i=1}^{N}(R_i \cdot E_i) - \left(\sum_{i=1}^{N} R_i\right)\left(\sum_{i=1}^{N} E_i\right)}{\sqrt{N\left(\sum_{i=1}^{N} R_i^2\right) - \left(\sum_{i=1}^{N} R_i\right)^2}\sqrt{N\left(\sum_{i=1}^{N} E_i^2\right) - \left(\sum_{i=1}^{N} E_i\right)^2}}, \tag{7-3}$$

where N is the amount of imitated tremor assessment tasks.

Experimental Setup

As shown in Figure 7-4, together with the IMU in the tremor/bradykinesia assessment system, a six-DOF EM sensor was attached to the subject's middle finger for real-time finger motion tracking. Because of the limited EM tracking dimension, only the postural tremor task was

performed by nine healthy subjects (average age: 29±2.1 years). Each subject performed simulative postural tremors four times with different amplitudes (no tremor, slight, moderate, and severe). The glove monitoring system and Aurora EM system were running at the same time during the experiments. The raw sensor data from the EM sensor and IMU were respectively stored in the two laptops in real-time.

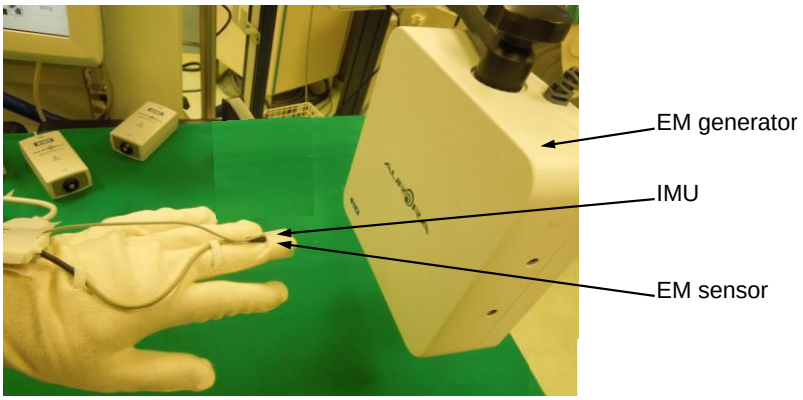

Figure 7-4: Setup for the verification of tremor quantification (Taken from Dai *et al.*, 2013a). The test subject performed "pill-rolling" action of the hand.

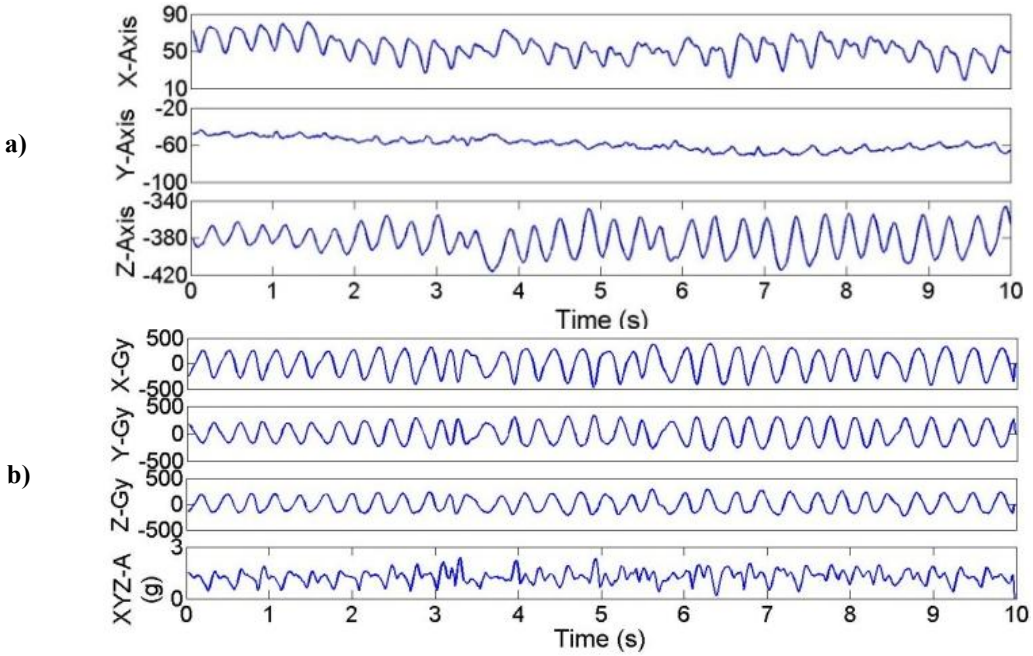

Figure 7-5: Raw signals measured with both the EM and tremor/bradykinesia assessment systems during an imitated tremor task (Taken from Dai *et al.*, 2013a). a) triple-axis EM localization signals (unit: mm); b) IMU signals: triple-axis gyroscope signals and a one-axis combined acceleration signal (gyroscope unit: °/s; accelerometer unit: g).

Figure 7-5 shows the ten-second signal waveform of both the EM sensor (localization signals) and IMU (angular velocity and acceleration). According to Equation 5-4 in Chapter 5.3.1, the acceleration readings in three axes were combined into an absolute linear acceleration and then the gravitational acceleration was partly removed.

Results and Discussion

The parameters obtained from the tremor/bradykinesia assessment system were compared to those calculated from the positional data, which were the outputs of the EM system, using the

PSD estimation method. The peak powers, which is regarded as tremor amplitude, and dominant frequencies from the two systems were compared.

The dominant frequencies between the two systems had little difference in the range from 2 to 6.5 Hz, even when the subjects did not perform a movement with stable tremor frequency.

As shown in Figure 7-6, for the postural tremor task, the dominant frequency of EM data is plotted against the dominant frequency of the IMU signals from the tremor/bradykinesia assessment system. The correlation coefficient (r) of dominant frequency between these two systems was 0.996.

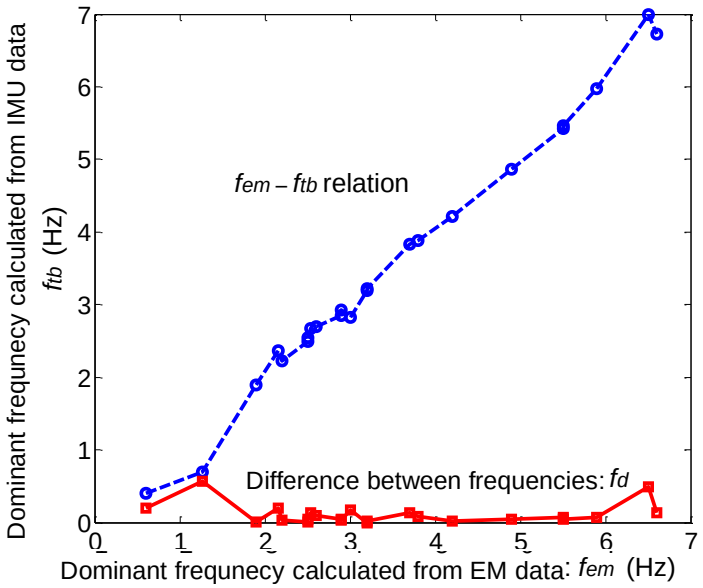

Figure 7-6: Correlation of the dominant frequencies in the imitated tremor tasks between the EM and tremor/bradykinesia assessment system (unit of the dominant frequency: Hz). The frequencies were calculated using the PSD estimation method (Based on Dai *et al.*, 2013a).

The maximum, mean, and standard deviation of the frequency differences between these two systems were 0.570 Hz, 0.115 Hz, and 0.144 Hz respectively. Therefore, f_{md} (0.115±0.144 Hz) was smaller than 1.00±0.88 Hz.

A linear correlation between the two systems' peak powers (tremor amplitude) could not be shown. The reason for this is believed to be that seven subjects did not realize the imitated tremor activity with a consistent amplitude and frequency during each timed task.

According to the experimental results, inconsistent movement made the peak power of the EM signals smaller when using the PSD method. When some sampling points in the EM signals were missed, the peak power increased. These two points are important for the calculation of tremor amplitude.

For the two subjects who performed a stable movement (i.e., means consistent amplitude and frequency as shown in Figure 7-5) the correlation between the two peak powers of the glove monitoring system and the EM tracking system is shown in Figure 7-7. The peak power of the glove monitoring system was calculated with both gyroscope and accelerometer signals using the PSD method, while the peak power of EM signals was calculated only from the position signals of the subject's finger. Figure 7-7 shows that the correlation between these two systems was approximately linear. The correlation coefficient between these two systems (r=0.97, p<0.001) was larger than 0.95.

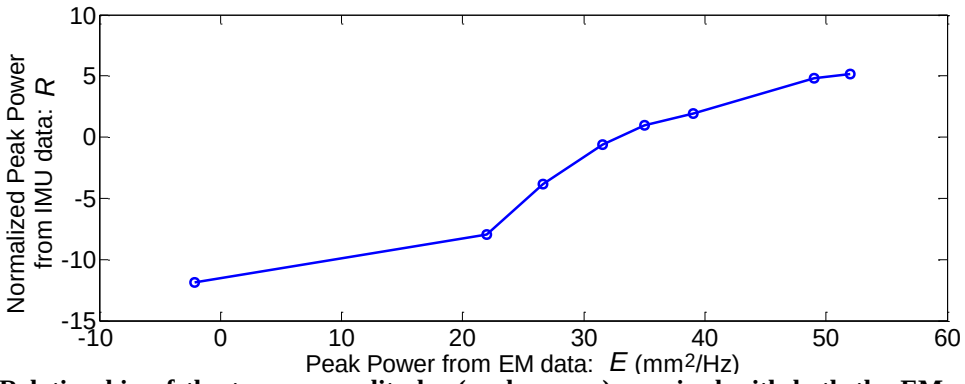

Figure 7-7: Relationship of the tremor amplitudes (peak power) acquired with both the EM and tremor/bradykinesia assessment system (Based on Dai *et al.*, 2013a). Two subjects each performed four imitated tremor tasks. The imitated tremor amplitudes varied in range from slight to severe for each subject.

For future research of the glove monitoring system, the RMS values of all sensor data should be calculated. Together, the RMS values and peak powers could be used to determine the tremor amplitude. The relation between the peak power of IMU signals and the consistency of IMU signals in PD patients should be studied in the future.

The basic changes in the EMG or MER signals caused by PD symptoms are increased tonic background activity and an alternating pattern of EMG or MER bursts. During the EMG or MER analysis of PD symptoms, special attention has been paid to the analysis of these bursts by measuring their counts, magnitudes, durations and frequencies (Rissanen *et al.*, 2007). For vigorous movement measurement, IMU provides good results. However, for slight motion disorders, the difference between EMG and IMU requires further verification.

7.2 Verification of Hand Grasping Angle Calculation

Motivation

As the bradykinesia quantification is based on hand grasping angles, the hand grasping angle calculation based on the integration of the triple-axis gyroscope signal is verified in this section. Here the glove monitoring system refers to the tremor/bradykinesia assessment system.

Hypothesis

By comparing with those from the EM tracking system, the angular displacements and dominant frequency of the hand grasps measured by the glove monitoring system should meet the following requirements:

- Mean value and standard deviation of the differences of dominant frequencies: $f_{md} < 1.00 \pm 0.88$ Hz (Niazmand *et al.*, 2011b).
- Mean difference of the angular ranges of hand grasps: $\overline{|\varphi|}_{md} < 0.1 \cdot \overline{|\varphi|}_{em}$.

Here $\overline{|\varphi|}_{em}$ is the mean angular range of hand grasps (peak-to-peak value) measured by the EM tracking system.

Materials

- An NDI Aurora® EM tracking system with a six-DOF sensor (Northern Digital Inc., Canada)

- A tremor/bradykinesia assessment system (included a JTAG USB cable and a command module with a sensor board)
- A laptop with the application software of the EM system (Aurora Toolbox)
- A laptop with the application software of the tremor/bradykinesia assessment system (LabVIEW-based GUI for tremor/bradykinesia assessment; MATLAB R2008b for data analysis)

Parameters

- Difference of the dominant frequencies from both the EM tracking system and the tremor/bradykinesia assessment system
- Mean difference of the hand grasping ranges between the EM tracking system and tremor/bradykinesia assessment system during a ten-second hand grasping task
- The standard deviation value of the differences of the hand grasping ranges from both the EM tracking system and tremor/bradykinesia assessment system during a ten-second hand grasping task

Methods

The dominant frequencies of hand grasps calculated by the tremor/bradykinesia assessment system and the EM tracking system were f_{tb} and f_{em} respectively (see Chapter 5.3.2). Then the difference of their dominant frequencies was:

$$f_d = |f_{tb} - f_{em}|. \tag{7-4}$$

As described in Equation 7-2, f_{md} (mean and standard deviation of frequency differences) could be calculated with the values of f_d during all bradykinesia assessment tasks.

The mean angular range of hand grasps calculated by the tremor/bradykinesia system and the EM tracking system were $\overline{|\boldsymbol{\varphi}|}_{tb}$ and $\overline{|\boldsymbol{\varphi}|}_{em}$ respectively (see Chapter 5.3.2). Then the difference of their mean angular ranges of hand grasps during a single bradykinesia task was:

$$\overline{|\boldsymbol{\varphi}|}_{d} = \left| \overline{|\boldsymbol{\varphi}|}_{tb} - \overline{|\boldsymbol{\varphi}|}_{em} \right|. \tag{7-5}$$

Therefore, $\overline{|\boldsymbol{\varphi}|}_{md}$ could be calculated with the values of $\overline{|\boldsymbol{\varphi}|}_{d}$ during all bradykinesia assessment tasks:

$$\overline{|\boldsymbol{\varphi}|}_{md} = \frac{1}{N}\sum_{i=1}^{N} \overline{|\boldsymbol{\varphi}|}_{di}, \tag{7-6}$$

where N was the amount of imitated bradykinesia assessment tasks (N=18 in this experiment).

Experiment Setup

As Figure 7-8 shows, the tremor/bradykinesia assessment system and the EM tracking system were used to measure the hand grasps by nine healthy subjects (average age: 29.0±2.1 years). Each test subject performed such tasks three times. The test subject's hand was in the measurement volume of the EM tracking system. A six-axis EM sensor and a sensor board (IMU) were attached to the middle finger.

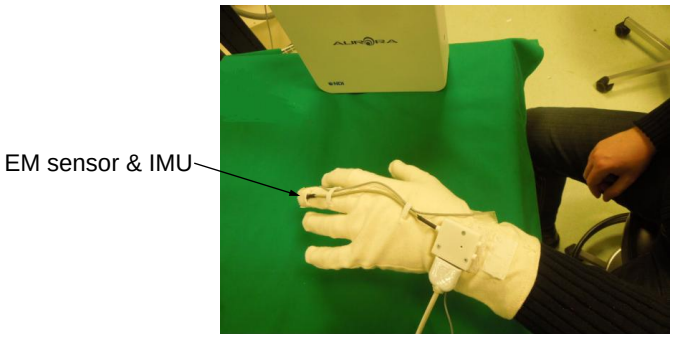

Figure 7-8: Setup for the verification of the bradykinesia quantification method.

Results and Discussion

As shown in Figure 5-14 in Chapter 5.3.2, only the gyroscope signal was used to calculate the bradykinesia parameters. Thus, the errors in the calculated grasping angles were mainly composed of the gyroscope drift and integration error. To reduce the errors in a short period of time, the gyroscope was calibrated upon system initiation. Figure 7-9 shows the raw data of the EM tracking system and the glove monitoring system for a ten-second bradykinesia task.

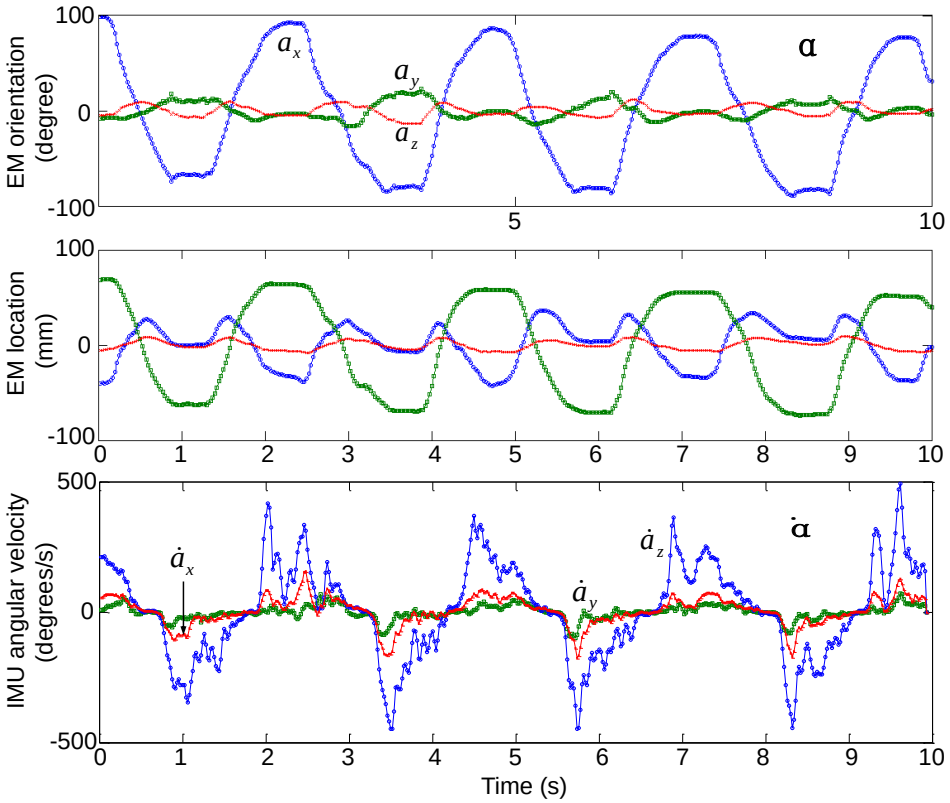

Figure 7-9: Raw sensor data both from the EM tracking system (location and orientation data) and the glove monitoring system (angular velocity) during the one-time bradykinesia task of a subject (Taken from Dai *et al.*, 2013a).

According to the analysis of the sensor signals of this experiment, three subjects performed hand grasping movements with different frequencies. Therefore, their data were removed.

The EM signals (three-dimensional orientation data) were processed using the FFT method to get the dominant frequency and the peak-detection method to obtain grasping ranges. The IMU signals (angular velocity) were processed using the methods described in Chapter 5.3.2.

Table 7-1 shows the differences of bradykinesia parameters between the EM tracking system

and the IMU-based glove monitoring system (six test subjects, each performed the task three times).

Table 7-1: Absolute differences of parameters between the EM tracking system and the IMU-based glove monitoring system (bradykinesia task)

Parameters	Frequency (Hz)	Mean range: $\overline{\lvert\varphi\rvert}$	SD of ranges: $\sigma_{\lvert\varphi\rvert}$
Max. Difference	0.70	22.18°	7.43°
Mean Difference	0.18	17.60°	3.65°
SD Difference	0.30	6.24°	3.14°

The difference of dominant frequencies (f_{md}) between the glove monitoring system and the EM tracking system (0.18±0.30 Hz) was smaller than 1.00±0.88 Hz.

The angular ranges of the finger movements were more than 200° in a single cycle during this experiment. Thus the difference in mean range between these two systems ($\overline{\lvert\varphi\rvert}_{md}$ =17.60°) was smaller than 10% of the mean angular ranges ($\overline{\lvert\varphi\rvert}_{em}$>200°) of the finger movement during the bradykinesia task.

As there were some bad fits in the results of the EM tracking system during hand grasping movements, another tracking system, such as an optical tracking system, can be used as the reference system in the future.

In order to improve the accuracy of the bradykinesia parameters, further signal processing methods must be carried out. The integration method of angular velocity plays a key role in the calculation of bradykinesia parameters. Also a modified DCM algorithm can be used in calculating the hand-grasping angle ranges.

7.3 Verification of Analytical Methods for Rigidity Assessment

7.3.1 Impact of Eccentric Application of Force on Force Sensor Box Outputs

Motivation

FSRs have a nonlinear characteristic. Therefore, in the situation that force is introduced outside the middle of the FSR's active area, the result is a lower output than when force is directly applied to the middle of the active area.

Similarly, when the applied force is performed more towards the edges of the force sensor box, the result is a lower output than when force is applied to the middle of the box. However, the magnitude of this effect remains unclear since the characteristics vary among FSRs and also depend on the chosen contact pad setup.

An experiment was carried out to obtain the deviation between the calculated force value and its real value (weight value) when an examiner pressed different parts of the force sensor boxes.

Hypothesis

According to the datasheet of FSR149NS, its accuracy ranges from 5% to 25%. Therefore, the following requirements should be met:

- Accuracy (relative deviation): *Val* < 25%.

Materials

- A series of iron weight plates (250–3000 grams)
- A rigidity assessment system (included a rigidity cuff and a USB cable)
- A laptop with the application software of the rigidity assessment (Visual C# 2010-based GUI for rigidity assessment and MATLAB R2008b for data analysis)

Parameters

The difference between the measured value and the attached weight load was defined as: *Val*

Methods

The relative deviations were calculated according to the following formula:

$$Val = \left[F(out) - F(weight)\right]/F(weight), \tag{7-7}$$

where *F(out)* was the measured force value and *F(weight)* was the weight value attached to the force sensor box. The unit of *F(weight)* was also gram.

The mean absolute value of the relative deviations at a certain point or for a certain weight was expressed as:

$$\overline{|Val|} = \left(\sum_{i=1}^{N}|Val_i|\right)/N, \tag{7-8}$$

where *N* was the number of values at a certain point or for a certain weight in different points.

Experiment Setup

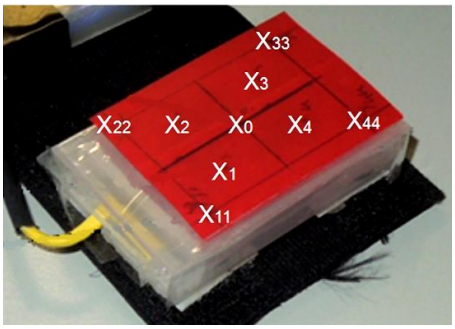

Figure 7-10: Plot with depressed points on force sensor box 1, in which X_0 is the central point of the pressing area. These same points were marked on the force sensor box 2 as well (© TUM-MIMED, 2012).

As Figure 7-10 shows, four FSR sensors were located underneath the points marked with X_{11}, X_{22}, X_{33}, and X_{44}. Points X_1, X_2, X_3, and X_4 were located at the midways between the center X_0 and X_{11}, X_{22}, X_{33}, and X_{44}, respectively.

Similarly to the calibration of force sensor boxes in Chapter 7.1.2, a series of weight loads were applied to the force sensor boxes. However, in this experiment, the force was not only applied to the central point of the force sensor boxes but also to the edges. Ten weight loads ranging from 250 grams to 3000 grams were exerted on the marked points, shown in Figure

7-10, of each force sensor box. As a result, 90 voltage values for each force sensor box were acquired.

Derivation Values of the Measurements in Different Points

Table 7-1: Relative deviations of force sensor box 1 and the mean absolute values of the relative deviations. The applied points with the biggest relative deviation are highlighted.

Force [N]	**Relative deviation**									$\overline{\lvert Val \rvert}$
	X_1	**X_{11}**	**X_2**	**X_{22}**	**X_3**	**X_{33}**	**X_4**	**X_{44}**	**X_0**	
2.47	14%	49%	39%	47%	14%	-3%	-38%	-59%	8%	30%
3.45	32%	35%	29%	22%	8%	-6%	-35%	-70%	-1%	27%
6.29	19%	29%	17%	19%	7%	-15%	-39%	-74%	-1%	24%
5.10	24%	34%	23%	9%	8%	-10%	-45%	-72%	12%	26%
9.90	13%	15%	19%	-11%	1%	-24%	-33%	-73%	7%	22%
14.74	6%	8%	9%	-5%	-16%	-37%	-41%	-73%	5%	22%
19.68	0%	-9%	3%	-9%	-23%	-41%	-32%	-77%	5%	22%
24.57	-10%	-12%	1%	-19%	-31%	-53%	-33%	-53%	-2%	24%
38.55	-17%	-37%	-7%	-34%	-45%	-48%	-40%	-62%	-11%	33%
30.05	-11%	-22%	-3%	-10%	-34%	-43%	-36%	-59%	-12%	26%
$\overline{\lvert Val \rvert}$	15%	25%	15%	19%	19%	28%	37%	67%	6%	

Table 7-2: Relative deviations of force sensor box 2 and the mean absolute values of the relative deviations. The applied points with the biggest relative deviation are highlighted.

Force [N]	**Relative deviation**									$\overline{\lvert Val \rvert}$
	X_1	X_{11}	X_2	X_{22}	X_3	X_{33}	X_4	X_{44}	X_0	
1.49	15%	-6%	8%	-5%	-1%	-16%	2%	-11%	5%	8%
2.47	4%	-10%	5%	-10%	-6%	-24%	17%	-14%	13%	11%
3.45	5%	-14%	8%	4%	-4%	-12%	10%	-17%	13%	10%
6.29	6%	-11%	6%	2%	-6%	-9%	6%	-32%	7%	9%
5.10	3%	-12%	9%	15%	6%	-6%	11%	-14%	8%	9%
9.90	2%	2%	-1%	-17%	-13%	-17%	-1%	-19%	14%	10%
14.74	3%	-1%	-10%	-9%	-13%	-25%	-11%	-8%	8%	10%
19.68	4%	1%	-14%	-14%	-29%	-33%	-19%	-41%	2%	17%
24.57	-3%	-14%	-23%	-28%	-25%	-41%	-31%	-42%	1%	23%
$\overline{\lvert Val \rvert}$	5%	8%	9%	12%	11%	20%	12%	22%	8%	

In the first step, the recorded sensor output was normalized to values of Gramm using Equa-

tion 6-1. Table 7-1 and Table 7-2 show the relative deviations which were calculated according to the Equations 7-7 and 7-8.

When the weights, ranging from 2.47 to 30.05 N, were applied to the center of both force sensor boxes ten times, the average deviations of two force sensor boxes were 6% and 8%, respectively.

Summary

When force was applied to the center of the force sensor boxes, the relative deviations were moderate ($|Val|$<15%). However, if the force was applied to the edges of the force sensor boxes, two effects, which impaired the output, could be observed. Firstly, values measured when applying force more to the edges of the sensor box tended to be lower than when force was applied to the center. This was likely due to the nonlinear characteristics of the sensors. Secondly, when force was applied to the edges, the underlying sensor beared a greater share of the total force and was already closer to saturation than when it was during centric application of force.

However, this effect seems to be influenced by the differences in sensitivity of FSRs. Even though the FSRs had been selected to match in terms of characteristics, deviations depended strongly on which of the force sensor was exposed to the greatest share of total load. As it can be seen in column X_{44} of Table 7-1 (highlighted), the FSR 4 in force sensor box 1 had a very low sensitivity compared to the other FSRs and therefore influenced the results.

In order to avoid such problem, it is necessary to either select the FSRs more carefully or connect each FSR in the force sensor boxes to a single analog input (ADC) pin of the microcontroller and perform individual calibration of each single FSR in the two force sensor boxes.

In addition, the weight values ranged only from 2.47 to 30.05 N. A larger weight range (30–80 N) should be verified in the future research.

7.3.2 Verification of Wrist Angle Calculation

Motivation

As the torque of elbow passive movement is based on wrist angular displacement, the verification of the elbow angle calculation is introduced in this section. The examiner can hold the patient's elbow to perform straight movement along a single axis, and then only the movement around the EM generator's Z-axis was verified in this experiment.

Hypothesis

The calculation of the elbow's angular displacement during passive movement was based on the sensor fusion (see Chapter 5.3.2). By comparing with those from the EM system, the angular displacements of the elbow movement measured by the glove monitoring system should meet the following requirement:

- Mean difference of the angular displacements of the two systems during all tested rigidity tasks (elbow movement)

$$\overline{|\alpha|}_{mz} < 0.1 \cdot \overline{|\varphi|}_{emz}.$$

Here $\overline{|\alpha|}_{emz}$ is the mean angular range of the ten-second elbow movement (peak-to-peak value in Z-axis) measured by the EM tracking system.

Materials

- An NDI Aurora® EM tracking system with a six-DOF sensor (Northern Digital Inc., Canada)
- A rigidity assessment system (included a rigidity cuff and a USB cable)
- A computer installed with MATLAB R2008b (Mathworks Inc., USA), EM application software (Northern Digital Inc., Canada), and rigidity assessment software (Visual C# 2010, Microsoft Inc., USA)

Parameters

- Maximum difference of the calculated elbow angles from both the EM tracking system and the rigidity assessment system during all the ten-second rigidity assessment tasks
- Mean difference of the calculated elbow angles from both the EM tracking system and the rigidity assessment system during all the ten-second rigidity assessment tasks
- Standard deviation of the differences of the calculated elbow angles from both the EM tracking system and the rigidity assessment system during all the ten-second rigidity assessment task

Methods

Z-axis elbow angle at a sampled point of the EM tracking system was α_{emz}, which was acquired directly from the NDI EM tracking system. At the same time, the Z axis elbow angle measured by the rigidity assessment system was α_{rz}, which was calculated using the six-axis DCM algorithm based on the IMU signals (see Chapter 5.3.2).

Therefore, the difference of angular displacements in a sampled point was:

$$\alpha_{zd} = (\alpha_{rz} - \alpha_{emz}). \tag{7-9}$$

The mean difference of the angular displacements during all the ten-second elbow movements was:

$$\overline{|\alpha|}_{mz} = (\sum_{i=1}^{N} |\alpha_{zdi}|)/N, \tag{7-10}$$

where *N* was the number of all sampled points. For one time rigidity assessment, the sampled points were 1000. There were five valid measurements in this experiment. Thus *N* was 5000.

The calculation of $\overline{|\varphi|}_{emz}$ is the same as the method described in Chapter 5.3.2.

Setup

Only one test subject (age: 27 years) was involved in this experiment. He performed the rigidity task six times. As shown in Figure 7-11, a six-DOF EM sensor attached to the wrist was used in the elbow-motion-tracking experiment. With the help of an examiner, the subject per-

formed elbow flexion and extension movements around the Z axis of the EM generator, while the end of the elbow acted as a fulcrum.

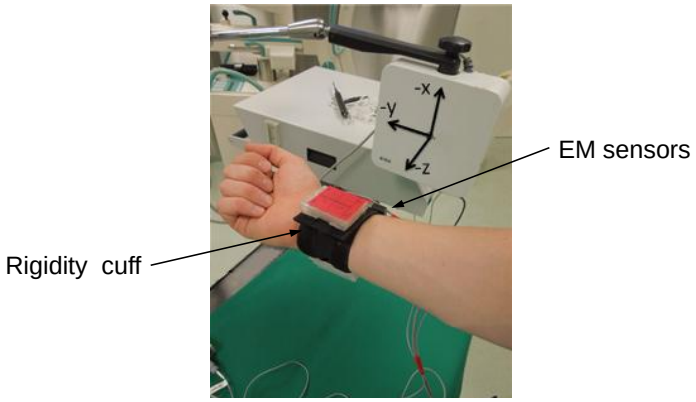

Figure 7-11: Setup for the verification of elbow angle calculation. The subject performed the same elbow movement (around the Z-axis) during the rigidity task. An EM sensor was attached to the wrist (Based on Dai *et al.*, 2013a).

The elbow's angle values, which were obtained from the EM system directly, were compared to the elbow angles calculated using the DCM method with the IMU data.

Results

Figure 7-12 shows the angular displacements of elbow's movement both from the IMU based rigidity assessment system (DCM fusion algorithm) and from the EM tracking system in the second measurement. Their difference and the maximum difference over a ten-second task are also shown in Figure 7-12.

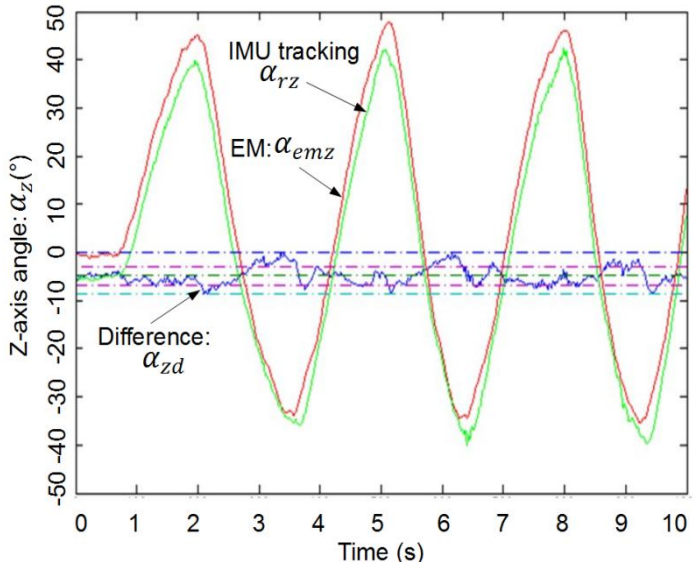

Figure 7-12: Plot of DCM fusion (IMU tracking) versus EM tracking. The elbow movement during a rigidity assessment task was measured with both IMU and EM sensors. IMU signals were processed using the DCM algorithm. The EM tracking values (angles) were directly obtained from the EM tracking system (Based on Dai *et al.*, 2013a).

In the sensor data of the sixth measurement, too many sampling points from the EM data were missing because of an error in the NDI toolbox; thus only five measurements were analyzed. Table 7-3 shows the absolute differences between the EM tracking system and the rigidity assessment system from all the five measurements.

Table 7-3: Absolute differences between the EM tracking system and the IMU based rigidity assessment system

Test Number	1	2	3	4	5
Max. Difference	9.41°	8.27°	12.50°	9.34°	9.90°
Mean Difference	4.40°	4.90°	4.86°	4.70°	4.87°
SD Difference	1.69°	1.82°	2.01°	1.96°	2.05°

The maximum, mean value, and standard deviation of the differences between these two systems in all test subjects were 12.50°, -4.74°, and 1.91° respectively. The angular ranges of elbow movements were about 80° during this experiment. Thus the mean difference ($\overline{|\alpha|}_{mz}$ = -4.74±1.91°) was smaller than 10% of the elbow angular range ($\overline{|\varphi|}_{emz}$ >80°).

7.3.3 Verification of Mechanical Impedance Components

Motivation

In order to acquire the correlation between the UPDRS ratings and mechanical impedance, first the correlation of elastic stiffness and viscosity with the rigidity severity should be investigated. In the presented experiment, the rigidity assessment algorithm was verified.

Hypothesis

For Cohen's *d*, an effect size of 0.8 to infinity denotes a "large" effect (Nakagawa *et al.*, 2007). Therefore, the following requirements should be met:

- Effect size $d > 0.8$.
- *p*-value < 0.05.

Materials

- A rigidity assessment system which includes a rigidity cuff and a USB cable
- A computer installed with MATLAB R2008b and rigidity assessment software (Visual C# 2010)
- A wooden folding ruler in hard wood (scale range: 1 m)

Parameters and Methods

To assess if the proposed system was able to detect an increase in mechanical rigidity at a significant level, the four sample reference data were t-tested against the four sample data for every test subject. Hence a one-side paired t-test between reference state (relaxed) and imitated rigid state of each volunteer was performed. The difference between the elasticity or viscosity between the relaxed state and imitated rigidity state was described as:

$$X = Y - Z \,, \tag{7-11}$$

where

Y=Elasticity (or viscosity) while the test subjects contracted arm muscles;

Z=Elasticity (or viscosity) while the test subjects kept muscles relaxed.

The calculations of elasticity and viscosity are described in Chapter 5.3.3.

The standard deviation, t-test formula, and effect size of *X* are described as Equations 7-12, 7-13, and 7-14, respectively.

$$\text{Standard deviation of } X\text{: } S(X)=\sqrt{\frac{1}{N}\sum_{i=1}^{N}(X_i-\bar{X})}\ ; \tag{7-12}$$

$$\text{One-side paired t-test: } t=\frac{\bar{X}}{S(X)/\sqrt{N}}\ ; \tag{7-13}$$

$$\textit{Cohen's}\quad d=\bar{X}/S(X)\ ; \tag{7-14}$$

where *S(x)* was the standard deviation of *X*, *N* was the number of measurements, and $\bar{X}$ was the average value of *X*.

Experimental Setup

As Figure 7-13 shows, nine healthy volunteers (average age: 24.4±4.2 years) were tested with the rigidity assessment system, yielding eight measurements each. During the first four reference movements, the volunteers were asked to relax (i.e., with no rigidity), while in the next four movements they were asked to imitate rigidity.

Figure 7-13: Experiment with the rigidity assessment system (Based on Dai *et al.*, 2013b).

Table 7-4: Ranges and frequencies of four times elbow movements for a test subject during the rigidity assessment tasks

Number	Range	Frequency
1	60°	0.5 Hz
2	60°	1.0 Hz
3	120°	0.5 Hz
4	120°	1.0 Hz

Also, during the assessments, the examiner tried to perform different elbow movement ranges and frequencies according to Table 7-4.

Results

Figure 7-14 shows the torque-displacement plots both in normal condition (i.e., relaxed state) and imitated rigidity condition.

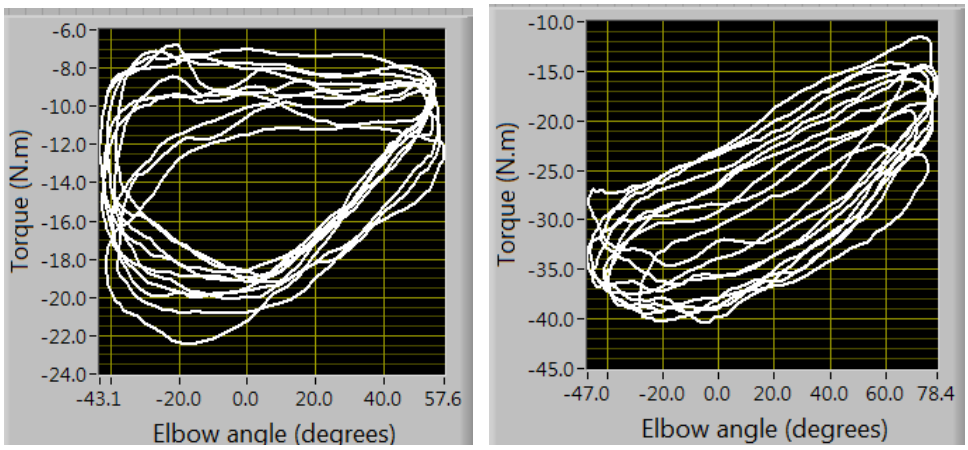

a) **b)**

Figure 7-14: Torque-displacement plots (Taken from Dai *et al.*, 2013b). a) normal condition (relaxed), elbow movement range: 100°, dominant frequency: 1.2 Hz; b) imitated rigidity condition, elbow movement range: 120°, dominant frequency: 1.1 Hz.

The viscosity values, elasticity values, and the frequencies during this experiment were calculated with the algorithms stated in Chapter 5.3.3.

The viscosity and elasticity were converted to absolute values before calculation. The average value of viscous modulus with no rigidity (i.e., relaxed state) was 0.26±0.08 N·m/degree, and 0.78±0.45 N·m/degree in the imitated rigidity state. The average value of elastic modulus with no rigidity (i.e., relaxed state) was 0.99±0.53 N·m/degree, and 3.78±2.85 N·m/degree in the imitated rigidity state.

Table 7-5: Evaluation of the viscosity. The insignificant value (p>0.05) is highlighted with yellow.

Subject	**1**	**2**	**3**	**4**	**5**	**6**	**7**	**8**	**9**	**Mean value**
$\bar{X}$	7.1	12.3	5.4	7.8	12.1	8.1	3.1	4.0	4.8	4.81
S(X)	3.7	6.3	1.45	3.7	2.8	3.6	2.9	1.2	1.4	1.35
Effect size (d)	1.91	1.94	3.74	2.13	4.40	2.26	1.07	1.35	3.55	1.65
p-value	0.015	0.015	0.002	0.012	0.002	0.01	0.061	0.036	0.003	<< 0.001

Table 7-5 and Table 7-6 show the viscosity and elasticity of the subjects assessed by the rigidity assessment system, respectively.

Table 7-6: Evaluation of the elasticity. The insignificant value (p>0.05) is highlighted with yellow, while the negative elasticity is highlighted with green.

Subject	**1**	**2**	**3**	**4**	**5**	**6**	**7**	**8**	**9**	**Mean value**
$\bar{X}$	0.94	1.00	0.54	0.80	2.39	0.14	0.58	-0.26	0.65	0.75
S(X)	0.44	0.21	0.27	0.12	0.71	0.13	0.23	0.12	0.13	0.75
Effect size (d)	2.11	4.78	1.99	6.77	3.34	1.04	2.43	-2.20	4.81	1.00
p-value	0.012	0.001	0.014	<0.001	0.003	0.065	0.008	-	0.001	<<0.001

For eight of the nine test subjects, the proposed system was able to detect a significant change in viscosity (p<0.05). For eight of the nine test subjects, a significant change of the elbow joint elasticity (p<0.05) was also detected. The effect size (Cohen's d) of viscosity and elasticity between normal state and imitated rigidity were therefore, "large", at 1.61 and 1.36 (d>0.8), respectively.

Influence of Angular Range and Frequency of the Elbow Movement

The viscosity and elasticity versus elbow ranges and frequencies are shown in Figure 7-15 to Figure 7-18, which were produced using the freely available statistical software package R (version 2.15.2).

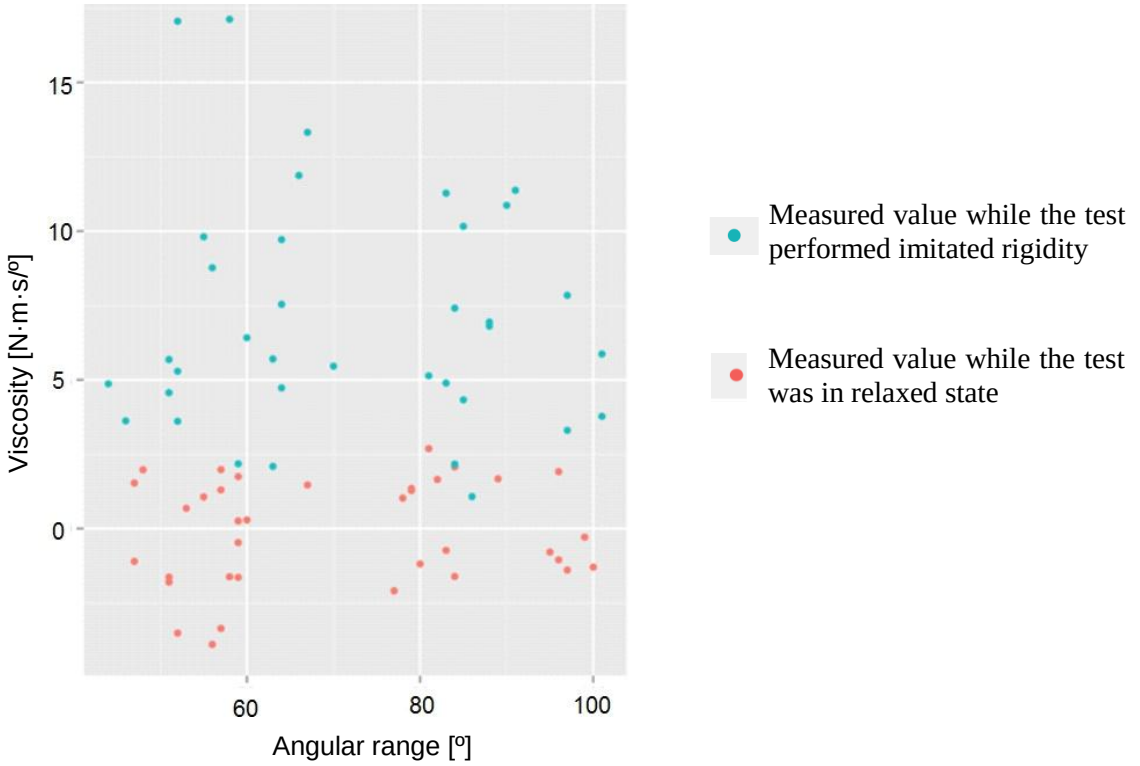

Figure 7-15: Plot of viscosity against the range of passive elbow movement (© TUM-MIMED, 2012).

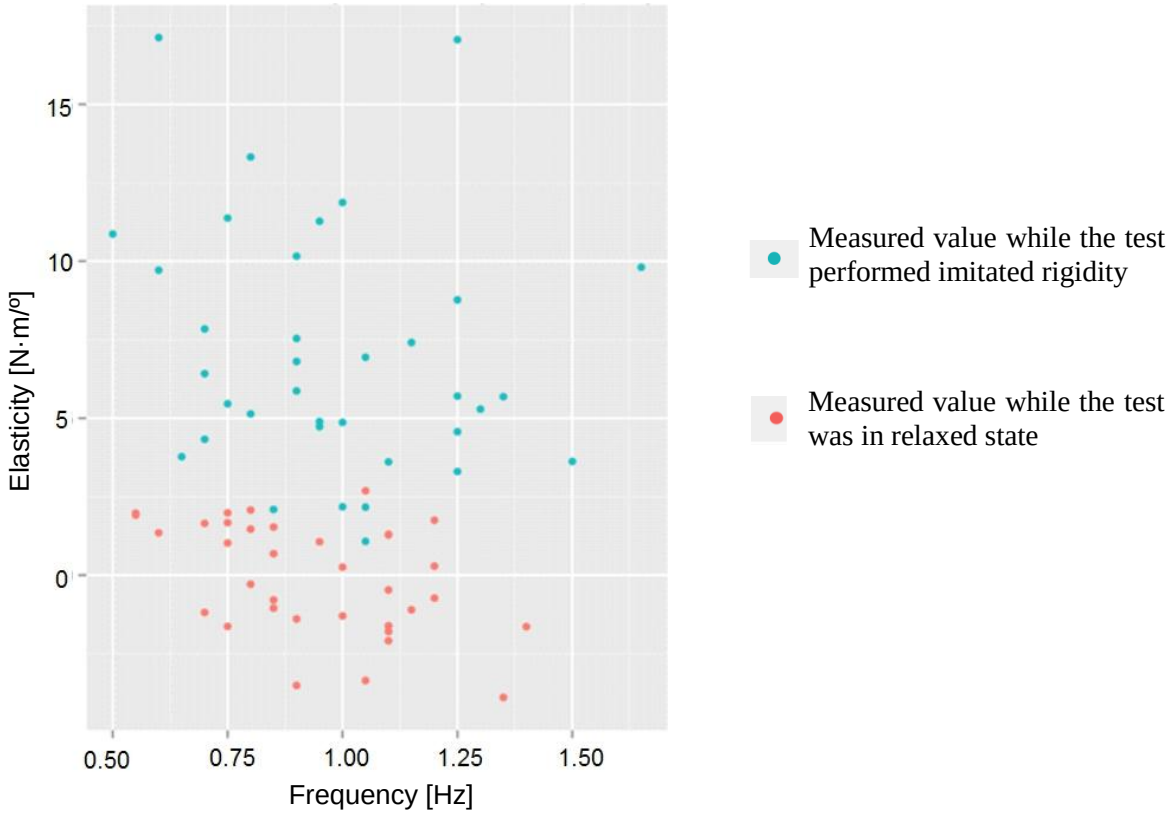

Figure 7-16: Plot of elasticity versus the range of passive elbow movement (© TUM-MIMED, 2012).

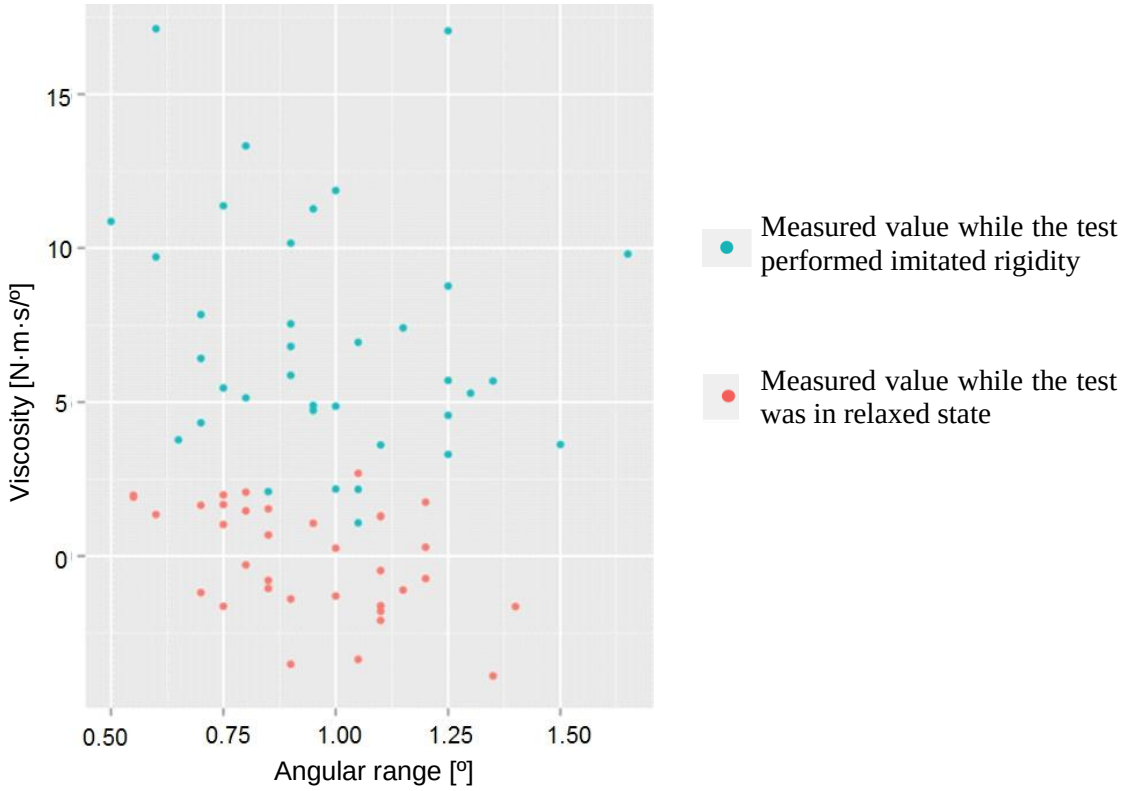

Figure 7-17: Plot of viscosity over the frequency of passive elbow movement (© TUM-MIMED, 2012).

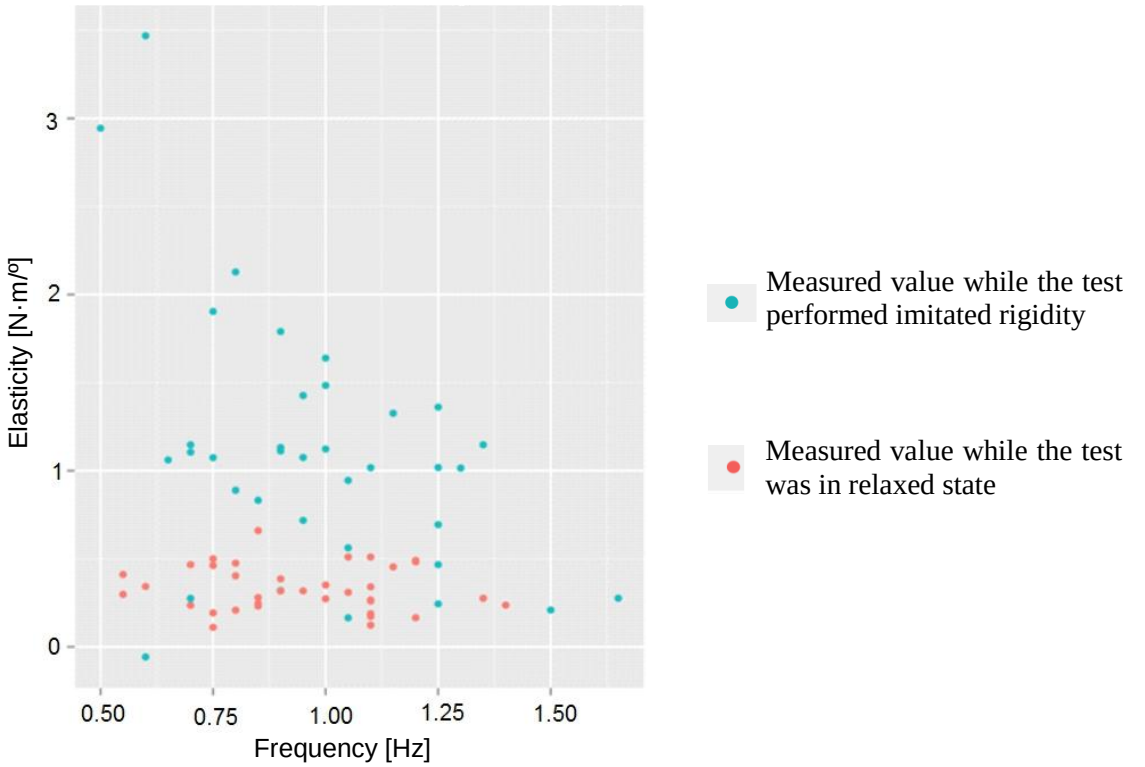

Figure 7-18: Plot of elasticity over the frequency of passive elbow movement (© TUM-MIMED, 2012).

The result shows that the frequencies and ranges of these passive elbow movements were not exactly the same as the settings in Table 7-7, because it was very difficult for the examiner to keep accurate movement frequency or range in an assessment task. The mean and SD values of viscous modulus and elastic modulus in different movement ranges and frequencies are displayed in Table 7-7.

Table 7-7: Mean and standard deviation of the absolute viscosity and elasticity

	Range		**Frequency**	
	≈ 60°	*≈ 120°*	*≈ 0.5 Hz*	*≈ 1 Hz*
Viscosity (normal)	0.28±0.08	0.23±0.09	0.25±0.08	0.26±0.09
Viscosity (rigid)	0.79±0.46	0.77±0.44	0.80±0.55	0.76±0.39
Elasticity (normal)	1.15±0.83	0.82±0.51	0.81±0.51	1.18±0.62
Elasticity (rigid)	3.55±3.43	4.01±2.47	3.55±2.95	4.02±2.96

The result shows that the frequency and range of elbow movement had little effect on the viscosity. In contrast, movement frequency had a greater effect on the elasticity, which might have negative influences when the examiner flexed and extended the forearm at different speeds. As a result, if the neurologist wants to obtain the mechanical impedance according to the formula of mechanical impedance (see Chapter 5.3.3), it is important to keep the same frequency. Compared with normal state (relaxed), elasticity varies largely in the imitated rigidity state.

According to the formula of mechanical impedance, elasticity depends on the movement frequency and range, and other factors. Thus, the mean value of elastic modulus had a large standard deviation. Another reason is that the test subjects did not perform imitated rigidity in the same state, which means the imitated rigidity varied.

7.4 Experiment of Tremor Assessment

Clinical experiments of patients with tremors were carried out with the glove monitoring system. The glove monitoring system in this section refers to the tremor/bradykinesia assessment system (prototype for tremor and bradykinesia assessments).

Hypothesis

The tremor amplitude correlation between the glove monitoring system and the clinical ratings should meet the requirement:

- Correlation coefficient $r > 0.84$ (Giuffrida *et al*., 2009).

Materials

- A tremor/bradykinesia assessment system (included a command module with a sensor board, and a JTAG USB cable)
- A computer installed with MATLAB R2008b (MathWorks Inc., USA) and the GUI (LabVIEW 2010 Evaluation Version, National Instruments Corp., USA) of the tremor/bradykinesia assessment system.

Parameters and Evaluation Methods

As described in Section 5.3.1, the tremor amplitude calculated by the glove monitoring system was *R*, while the tremor amplitude judged by the surgeon was *D*. Then the correlation coefficient between these two parameters was:

$$r = \frac{N\sum_{i=1}^{N}(R_i \cdot D_i) - \left(\sum_{i=1}^{N} R_i\right)\left(\sum_{i=1}^{N} D_i\right)}{\sqrt{N\left(\sum_{i=1}^{N} R_i^2\right) - \left(\sum_{i=1}^{N} R_i\right)^2}\sqrt{N\left(\sum_{i=1}^{N} D_i^2\right) - \left(\sum_{i=1}^{N} D_i\right)^2}}, \tag{7-15}$$

where *N* is the amount of assessed patients.

For the valid state detection (see Chapter 5.3.1), only the gyroscope signal was utilized. Parameters for the valid state detection both in the frequency domain and time domain were:

$$V_f = \frac{Peak\ power}{Power\ estimation\ in\ all\ frequency\ points}; \tag{7-16}$$

$$V_t = \frac{Standard\ deviation\ (\boldsymbol{G_{p-p}})}{Mean\ (\boldsymbol{G_{p-p}})}, \tag{7-17}$$

where $\boldsymbol{G_{p-p}}$ was the matrix of peak-to-peak values of the triple-axis gyroscope signals during a ten-second tremor task, peak power was the power estimation around the dominant tremor frequency (±0.3 Hz).

Experiment Setup

A total of five patients with tremors were tested with this wearable system. The tremor severi-

ty of these patients ranged from 1 to 3 (UPDRS tremor scores: *D*). The measurements in these patients were performed after stopping their medication for more than 24 hours.

Rest, postural, and action tremor assessment tasks were performed. However, for each patient, only the hand side with a more severe tremor was assessed. Each tremor assessment task lasted for ten seconds.

The tremor amplitude was represented the tremor severity in this system. Time-frequency analyses and statistical analyses were carried out based on the IMU signals. The valid state detection algorithm was performed for each assessment task.

As shown in Figure 7-19, a PD patient performed three tremor assessment tasks in turn according to the instructions of a surgeon.

a) **b)** **c)**

Figure 7-19: Experiments with the tremor/bradykinesia assessment system. a) rest tremor; b) postural tremor; c) action tremor.

Each patient performed 3–5 times each task repeatedly. Each task lasted ten seconds.

Results

Figure 7-20 shows the IMU signals of the glove monitoring system and their power spectra for a PD patient with slight rest tremor (*D*=1). In Figure 7-20 (a), the tremor occurred only for several seconds and with varying amplitude. In Figure 7-20 (b), there was only a small amplitude fluctuation during the ten-second period.

The tremor amplitude calculation with PSD method depends on the precondition that the tremor movement is stable and the power estimation around the dominant frequency is sharp. Therefore, the signals in Figure 7-20 (b) were able to be used to calculate the tremor amplitude. The assessment tasks which had bigger tremor amplitude fluctuation than Figure 7-20 (b) were discarded during signal processing because the tremors were not in a stable condition. Although Heldman *et al.* (2011b) indicated that the tremor amplitude calculated with PSD correlated well with clinical ratings even for a broad power spectra distribution, the power distribution in other frequency points still influenced the tremor amplitude calculation in these measurements.

As shown in Figure 7-20, (d) is the normal situation in frequency domain while (c) is not good for tremor calculation with the PSD method (Timmer *et al.*, 1997).

For the action tremor assessment, it was difficult to separate the active movement with tremor even with different band-pass filters. Its power spectrum included multiple frequency components. A better signal filter should be adopted in the future (Timmer, *et al.* 1993).

When performing the signal processing algorithms, the rest and postural tremor tasks were assessed as valid state or invalid state for PSD estimation. The amplitude of action tremor was not included in the present results.

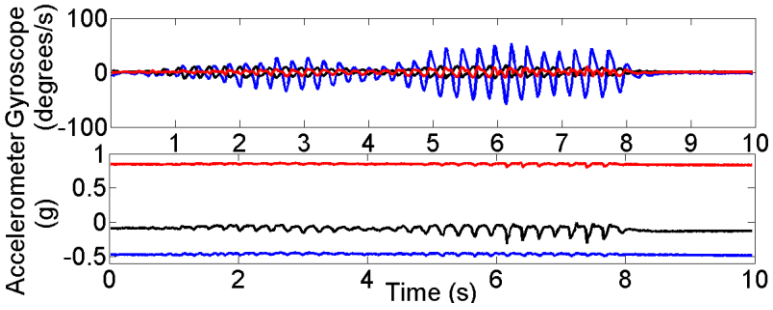

a) invalid state in time domain (V_t = 0.64);

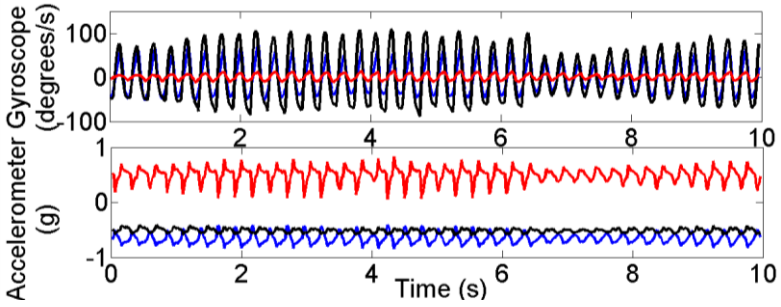

b) valid state in time domain (V_t = 0.23);

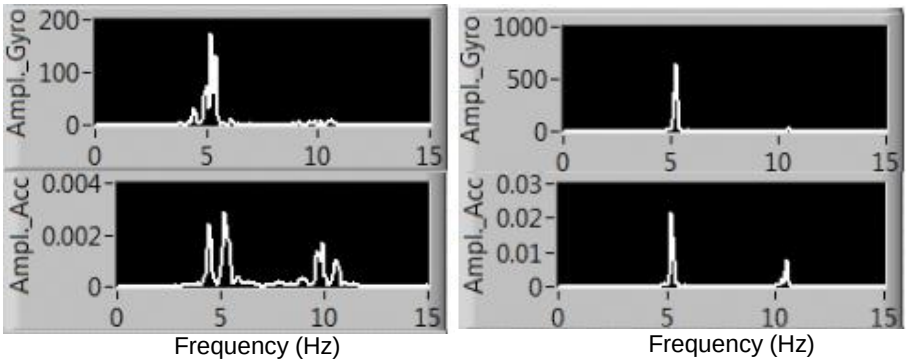

c) invalid state in frequency domain (V_f = 69.4%); **d) valid state in frequency domain (V_f = 91.3%).**

Figure 7-20: Tremor state of a PD patient (UPDRS tremor score: *D*=1). a) and b): waveforms of triple-axis raw accelerations and triple-axis angular velocities (rest tremor); c) and d): combined power spectra of the triple-axis acceleration signals (bottom chart) and the combined power spectra of the angular velocity signals (upper chart). b) and d) are for the same tremor assessment task.

In order to investigate the correlation between the inertial sensor outputs and clinical ratings, the outputs of the gyroscope and the accelerometer were analyzed independently as well. As shown in Table 7-8, the parameters, calculated with the sensor signals, were compared to the judgments of a surgeon according to the UPDRS and TETRAS ratings. These results were from the average values of valid rest and postural tremor tasks.

Table 7-8 shows that the gyroscope signal had a stronger correlation (r=0.92) with the clinical scores than the accelerometer signal (r =0.81).

Both the RMS value of the gyroscope signal and peak power from all IMU outputs have the biggest correlation with the clinical scores (r=0.92). In the program of the glove monitoring system, the frequency range of peak power was 0.6 Hz. Thus, the frequency range should be wider in the next version of this glove monitoring system.

Table 7-8: Results for rest and postural tremor assessments. Here *acc.* represents accelerometer; *gyro.* means gyroscope; *RMS* means root-mean-square; *ln* means natural logarithm; *R* is the predicated tremor score from the glove monitoring system; *r* denotes the correlation coefficient between the relative parameters calculated by the IMU signals and clinical scores judged by the surgeon.

Subject	ln (acc. power)	ln (gyro. power)	ln (acc. RMS)	ln (gyro. RMS)	*R*	Clinical Score (*D*)
Patient 1	-8.52	-6.27	-2.95	0.30	-5.41	0
Patient 2	-7.42	0.78	-2.42	1.93	-4.01	0.5
Patient 3	-3.06	7.05	-0.92	3.92	1.27	1
Patient 4	-4.10	7.37	-1.40	4.14	1.36	1.5
Patient 5	-2.72	7.87	-0.58	4.31	1.99	2.0
r	0.24	0.83	0.81	0.92	0.92	

It can also be seen from Table 7-8 that the proportion of rotational movement and translation movement of a tremor [*ln(gyro. Power)* versus *ln(acc. Power)*] varies from patient to patient. More tremor measurements are needed to acquire further symptom information and better regression coefficients.

Figure 7-21 shows the dominant tremor frequencies of a patient during three times rest tremor tasks (numbers 1 to 3) and three times postural tremor tasks (numbers 4 to 6). The difference of dominant frequencies from gyroscope and accelerometer was small (<0.2 Hz). For all the measured patients, the dominant tremor frequency was constant or with small fluctuations even if the tremor amplitude changed during ten-second task period.

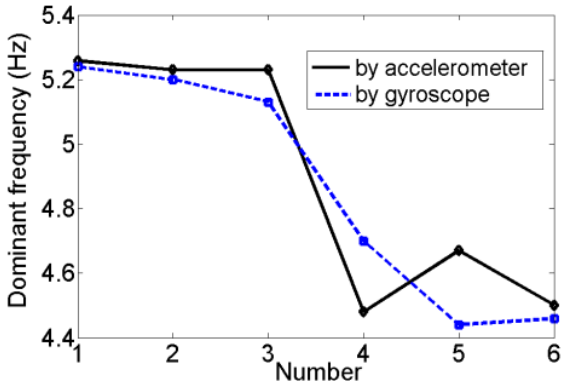

Figure 7-21: Dominant tremor frequency of a PD patient (UPDRS tremor score *D*=1) during the assessment tasks of rest tremor (numbers 1 to 3) and postural tremor (numbers 4 to 6). The dominant tremor frequencies were calculated from accelerometer signals and gyroscope signals, respectively.

Discussion

Results indicate that the tremor frequency was stable for all patients; however, the tremor amplitude fluctuated all the time. The quantitative assessment of tremor, with an IMU and adaptive algorithms, provided an objective rating to classify rest or postural tremor severity even with a small scale.

7.5 Experiment of Bradykinesia Assessment

Motivation

For the measurements in a healthy subject or a patient with mild bradykinesia, the signals obtained from the gyroscope have a consistent amplitude and frequency and appear sinusoidal. However, the signals from a patient with severe bradykinesia have a much lower and inconsistent amplitude and frequency.

Thus the mean and standard deviation of amplitude and frequency during bradykinesia measurement tasks represent the parameters of bradykinesia.

The prototype should be tested both with healthy volunteers and PD patients to demonstrate a difference between the PD patients and healthy subjects. The glove monitoring system in this section refers to the tremor/bradykinesia assessment system.

Hypothesis

The correlations of bradykinesia parameters between the glove monitoring system and clinical ratings should meet the following requirement:

- Correlation coefficient $r > 0.79$ (Giuffrida *et al*., 2009).

Parameters and Evaluation Methods

As described in Section 5.3.2, the bradykinesia parameter calculated by the glove monitoring system is *R*, while the severity of bradykinesia judged by the surgeon is *D*. Then the correlation coefficient between these two parameters is

$$r = \frac{N\sum_{i=1}^{N}(R_i \cdot D_i) - \left(\sum_{i=1}^{N} R_i\right)\left(\sum_{i=1}^{N} D_i\right)}{\sqrt{N\left(\sum_{i=1}^{N} R_i^2\right) - \left(\sum_{i=1}^{N} R_i\right)^2}\sqrt{N\left(\sum_{i=1}^{N} D_i^2\right) - \left(\sum_{i=1}^{N} D_i\right)^2}}, \tag{7-18}$$

where *N* is the amount of assessed patients.

Along with dominant frequency of hand grasping, mean and SD values of hand grasping ranges ($|\varphi|$) were regarded as bradykinesia parameters. In addition, we defined the product of dominant frequency and mean range as the modified mean range.

Materials

- A tremor/bradykinesia assessment system which included a JTAG USB cable and a command module with a sensor board
- A computer installed with the GUI of the tremor/bradykinesia assessment system (LabVIEW 2010 Evaluation Version, National Instruments Corp., USA) and MATLAB R2008b (Mathworks Inc., USA)

Experiment Setup

Three healthy volunteers (average age: 49.0±16.6 years) and five PD patients (average age: 75.5±11.1 years) should execute hand grasping movement as quickly and widely as possible for ten seconds, and repeat the assessment task three times for each subject. However, a severe PD patient (UPDRS bradykinesia score *D*=4) was unable to perform the bradykinesia

task.

One time grasping movement included several grasp cycles, which was the number of peak-to-peak ranges.

An IMU, which was attached to the middle finger, was used to measure the angular displacement of the middle finger movement during the bradykinesia assessment task. The dominant grasping frequency, mean, and standard deviation of hand grasping ranges were used as the severity features of bradykinesia.

The bradykinesia parameters, calculated by the glove monitoring system, were compared to the ratings of a surgeon.

Results and Discussion

Figure 7-22 shows three ten-second waveforms of hand grasps and their PSD figures. For some patients, as shown in Figure 7-22 (b), action tremor appeared during the bradykinesia assessment task.

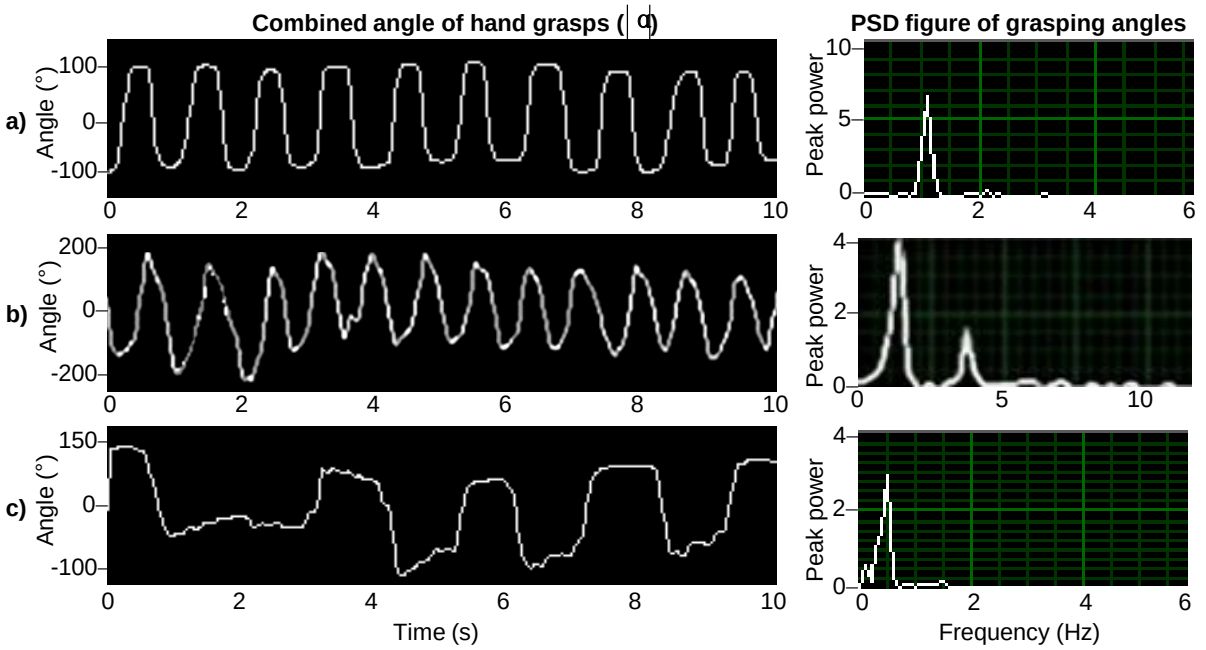

Figure 7-22: Ten-second hand grasps and their PSD figures. a) healthy subject, age: 72 years; b) PD patient with tremor and bradykinesia, age: 82 years, UPDRS bradykinesia score *D*= 1; c) PD patient, age: 86 years, UPDRS bradykinesia score *D*= 3. The peak powers in the figure were calculated on a weighted scale.

In addition, as shown in Figure 7-22 (c), there was a delay time for a patient with severe bradykinesia to start the hand grasping movement after the instruction from the examiner. This situation is the symptom of akinesia (difficulty initiating movement).

The three healthy subjects had a dominant frequency of 1.16 Hz and a standard deviation of 0.11 Hz. The parameter values are presented in Table 7-9. Table 7-9 shows that the patients with severe bradykinesia executed grasping movements with lower dominant frequencies.

As Table 7-9 shows, the dominant frequency of hand grasps and the modified mean range had the higher correlations with the UPDRS score (r=-0.94 and -0.86 respectively).

Table 7-9: Results of bradykinesia assessment tasks. *Freq.* represents frequency; *r* denotes the correlation coefficient between the relative parameters and clinical scores.

Subjects	Dominant Freq.	Mean Range	SD Ranges	Modified Mean Range	UPDRS Score (*D*)
Healthy 1	1.09 Hz	202.3°	10.6°	220.5 Hz·°	0
Healthy 2	1.29 Hz	255.4°	11.5°	329.5 Hz·°	0
Healthy 3	1.10 Hz	289.8°	19.8°	318.8 Hz·°	0
Patient 1	0.88 Hz	241.6°	10.2°	212.6 Hz·°	1
Patient 2	0.60 Hz	181.7°	9.47°	109.0 Hz·°	1
Patient 3	0.44 Hz	212.8°	21.0°	93.6 Hz·°	2
Patient 4	0.32 Hz	221.8°	3.6°	71.0 Hz·°	3
r	-0.94	-0.36	-0.32	-0.86	

There were also subjects, such as Healthy 1 and Patient 1, whose mean grasping range deviated from the normal situation. The reason may be the age of subjects. The healthy subject was too old to reach great amplitudes during hand grasping movements. On the other hand, the PD patient with a smaller age was able to grasp at a higher amplitude. Therefore, the obtained parameters need to be modified according to the subject's age. For the SD values of the grasping ranges, there was only a small correlation coefficient (r=-0.32) to the UPDRS ratings in this experiment.

As a conclusion, the difference of the parameters between the healthy subjects and PD patients was significant. Further clinical measurements should be performed in the future.

7.6 Conclusion

As a force sensor box of the rigidity assessment system had four FSRs and the force-resistance characteristic was nonlinear, a two-term Gaussian regression function was used for each force sensor box calibration.

A better cognition of the analytical methods in this system was achieved with these verification results, providing the necessary science and engineering to guide future signal processing methods. Then the clinical experiments could be performed.

The verification experiment of tremor amplitude and frequency indicates that the dominant tremor frequencies from both systems had little difference (0.115±0.144 Hz). For the imitated tremor task with consistent movement, the calculated tremor amplitude using the IMU based system correlated well with the tremor amplitude from the EM system (r=0.97). The results of clinical experiment indicate that the tremor amplitude calculation with the PSD method was valid only in the constant state. Thus the tremor tasks were divided into valid state and invalid state. Rest and postural tremors in valid state were correlated with the UPDRS scores (r=0.92). For the action tremor amplitude calculation, quadratic mean method or other algorithms should be employed. The dominant tremor frequency of a patient for one type of tremor task had small fluctuations even in an invalid tremor state (r=0.996) (Elble *et al.*, 2006).

Further measurements are needed to modify the regression coefficients in the regression function for tremor calculation.

The difference between parkinsonian tremor and ET needs to be investigated.

The analysis as to whether there are single or multiple dominant frequencies during tremor assessment tasks also needs to be performed (Mostile *et al.*, 2010).

The clinical experiment indicates that the components of rotational and linear movements of different subjects' tremors were different.

According to the results of clinical measurements, the dominant frequency and modified mean range of hand grasps correlated well with the UPDRS ratings. Their correlation coefficients were 0.94 and 0.86 respectively.

As quantitative rigidity assessment in PD is difficult and depends on many factors, a comparison experiment was carried out. Elastic and viscous values will be obtained through a least squares estimation with all the data. Nine healthy subjects were tested with this system in two experimental conditions: 1) normal state (relaxed); and 2) imitated rigidity state. In addition, the subjects performed the assessment task with different frequencies and elbow movement ranges. The result indicates that viscosity and elasticity in the imitate rigidity condition are bigger than the normal condition (relaxed state). The effect sizes (Cohen's *d*) of the viscosity and elasticity between normal state and imitated state are 1.61 and 1.36 respectively, which means the difference is significant. Thus, this system can detect the ON-OFF fluctuations of parkinsonian rigidity. Both the wrist movement angle and frequency have a small effect on the viscosity, but have an elevated effect on the elasticity.

The future research consists of carrying out measurements with more PD patients. With the measurement data, the correlation between mechanical impedance (viscosity, elasticity, and movement frequency) and UPDRS scores can be determined. After that, the system can be used for rigidity assessment in PD.

Nevertheless, attention must be paid to the signal processing methods:

- Influence of noise in tremor assessment when the PD patient has a slight tremor.
- Inconsistent movement and its influence in tremor amplitude during the tremor assessment task, especially for peak power calculation with the PSD estimation.
- Combination of the six-axis signals in both a gyroscope and an accelerometer, which represent the rotational and the linear movement respectively.
- Correlation between different sensor signals and the UPDRS ratings.
- Repeatability of parameters with the same patient at different times.
- Accurate quantification action tremor.

8. Conclusions and Outlook

8.1 Conclusions

A portable monitoring system used to quantify all primary neurological symptoms in the PD and ET during the DBS surgery is presented in this thesis.

According to the requirements of neurosurgeons, the concept of a glove monitoring system used in DBS surgery is presented. This system is focused on the symptom assessments of PD and ET.

According to the definitions of UPDRS and TETRAS scores and the situation during DBS surgery, several of such tasks were chosen to detect the stimulating effects of the electrical stimulation. Each assessment lasts for ten seconds. Passive flexion and extension of the elbow is used to assess rigidity in this study. Tremor, bradykinesia, and rigidity assessments are performed in a system based on IMUs and FSRs. An IMU can be used to measure both the rotational and linear movement, using the combination of a triple-axis accelerometer and a triple-axis gyroscope. This system consists of a glove part and a computer part. The communication between these two parts is based on a USB cable. The measured parameters in different electrode placements and stimulating intensities are listed in the GUI for comparison.

The positions of sensors are the wrist and fingers. All the sensors have no contact with the human body.

The first version of the glove monitoring system based on the above concept includes two portable prototypes: one for tremor/bradykinesia assessment and the other for rigidity assessment. A wearable textile glove, two inertial measurement units (IMUs), two force sensor boxes, a computer, and other components were included in the prototypes. The prototype of the tremor/bradykinesia assessment system was based on an IMU attached to a finger. The first prototype of the rigidity assessment system was based on two force sensor boxes and an IMU on the wrist.

The verification of the analytical methods of the two prototypes was performed, compared with an EM system. Because the quantitative rigidity assessment of PD patients is difficult and depends on many factors, a comparison experiment was carried out. An examiner flexed and extended the elbow joint of nine volunteers through a rigidity assessment cuff attached around the wrist, both with the relaxed state and imitated rigidity state. The result indicates that viscosity and elasticity in the imitated rigidity condition were bigger than they were in normal conditions (relaxed state).

This system was tested in the hospital but outside the operating room first. Five patients were tested with the tremor/bradykinesia monitoring system. The tremor measurement results indicated that the tremor amplitude calculation with the PSD method was valid only in the constant state, which was regarded as a valid state. For the action tremor amplitude calculation, the quadratic mean method or other algorithms should be employed. The dominant tremor frequency of a patient for one type of tremor task included small fluctuations even in an invalid tremor state. The bradykinesia measurement results indicate that the dominant frequency and modified mean range of hand grasps correlate well with the severity of bradykinesia.

As a result, the prototype for tremor and bradykinesia assessment can quantify tremor and bradykinesia. However, few patients were measured in this study. More measurements of patients with PD and ET are needed.

The prototype for rigidity assessment can detect the ON-OFF fluctuations of parkinsonian rigidity. With further measurement data, the correlation between the UPDRS score and mechanical impedance (viscosity, elasticity, and movement frequency) and UPDRS score can be determined.

Based on the disadvantages of the first version of the glove monitoring system and the suggestions from the surgeons, a combined prototype for the assessment of all three primary symptoms was also presented.

8.2 Outlook

In this thesis, the glove monitoring system in the DBS application is present. It is the world's first objective assessment system for the quantification of three primary symptoms of PD and ET.

However, there are still some approaches to improve the system in the next step:

1) Further clinical measurements should be performed to modify the regression coefficients in the algorithms with the combined prototype.

2) Further signal processing algorithms need to be developed based on the hardware and the measurement data. Automatic calibration algorithms during symptom assessments can be adopted in addition to the initial calibration procedures.

3) The difference between parkinsonian tremor and ET needs to be further investigated.

4) The analysis as to whether there are single or multiple dominant frequencies during tremor tasks also needs to be performed (Post *et al.*, 2005).

5) The multi-symptom phenomenon in a single assessment task should be investigated.

6) Nine-axis sensor fusion algorithms and other statistical methods can be incorporated into future designs, especially for the tremor quantification, to get better performance.

Although this system is supposed to be used during DBS surgery, there is no clinical measurement in the operating room yet. Thus, there is still much work to be done in the near future:

1) Dyskinesia assessment is important to detect the side effects of DBS surgery. It should be integrated into the system in the next version.

2) For the comparison of slight symptoms during DBS surgery, much work should be done. Because the symptoms fluctuate all the time, it is important to measure the stable parameters.

3) A series of validations and modifications of this system should be carried out according to the requirements of DBS surgery.

4) This system can be combined with the MRI, MER or iMRI systems for the application of DBS surgery. The effective combination of these different systems will result in a more complete and accurate severity quantification of the symptoms of PD and ET.

5) Clinical experiments should be performed during DBS surgery.

Only after further experiments and compulsory validations both outside and inside the operating room is this system supposed to help select the optimal target location and the settings of the stimulation parameters of the DBS electrodes during and after DBS surgery.

In addition, a glove monitoring system with a wireless communication interface can be implemented for the extended applications, for example, the assessments of symptoms before and after DBS surgery or at the patients' home.

9. Glossary

ADC	An *analog-to-digital converter* converts a continuous voltage to a digital value that represents the voltage.
AHRS	An *attitude heading reference system*, which are either solid-state or MEMS gyroscopes, accelerometers, and magnetometers on all three axes, provide heading, attitude, and yaw information. A form of nonlinear estimation, such as a Kalman filter, is typically used to compute the solution from these multiple sources.
CE	*Consumer electronics* are electronic devices intended for everyday use. Apple Inc. has invented the consumerization of information technology in the 2010s.
CNS	The *central nervous system*, which consists of the brain and the spinal cord, contains the majority of the nervous system.
DBS	*Deep-brain stimulation* is a surgical procedure used for some types of disabling neurological symptoms, which includes PD, ET, dystonia, and chronic pain.
DCM	A *direction-cosine-matrix* (rotation matrix) is a 3x3matrix containing the cosines of the rotation (each of the 9 possible pairs of axes) of one frame relative to another.
DOF	The *degree of freedom* of a mechanical system is the number of parameters that may vary independently.
EM	*The electromagnetic tracking system* is a spatial measurement system which determines the location and orientation of an object that is attached to sensor coils.
ET	*Essential tremor is* a common progressive neurological movement disorder and appears in the arms or hands only in the state of movement such as eating or writing.
FSR	*Force sensing resistor* is a passive component whose resistance changes when a force or pressure is applied.
GPi	*Globus pallidus or paleostriatum* is a sub-cortical structure of the brain which performs the regulation of voluntary movement.
GUI	The *graphical user interface* represents the information and interactions available to a user through graphical icons and visual indicators and as opposed to text-based interfaces.

iMRI	*Interventional MRI* is a real-time MRI which can be used in surgery conditions. Asleep iMRI-guided DBS implantation has many advantages. The electrodes are positioned with the patient asleep in an MRI scanner instead of awake in the operating room.
IMU	*Inertial measurement unit* is a single unit that measures a subject's velocity, orientation, and gravitational forces in three dimensions, using a combination of accelerometers and gyroscopes. It is the main component of an inertial navigation system.
LID	*Levodopa-induced dyskinesia* is a form of dyskinesia associated with anti-parkinsonian medications (Levodopa). It often involves the presence of involuntary movement (chorea, dystonia, and athetosis) and diminished voluntary movements. DBS can reduce LID or reduce L-DOPA dosage.
MBRS	The *Modified Bradykinesia Rating Scale* rates the bradykinesia expressions of speed, amplitude, and rhythm separately, while the UPDRS rates bradykinesia as a whole. Thus more information is provided for different PD patients.
MCU	A *microcontroller* (µC, uC or MCU) is a small computer on a single chip containing a processor core, memory, an I/O control unit, and a clock.
MEMS	*Microelectromechanical systems* or *micro systems technology* is a technology that can be defined as miniaturized mechanical and electro-mechanical elements (i.e., devices and structures) of small scale that are made using the techniques of microfabrication. Their general components are a microprocessor and several components that interact with the surroundings such as microsensors.
MER	*Microelectrode recording* is a neurosurgical technique of single neuron activity. MER is realized with the patient awake and interacting by performing a series of motor tasks so that the neurophysiological mapping of the target is enhanced by functional mapping to localize the optimal target of the DBS electrode.
MF	*Motor fluctuations* (or ON-OFF fluctuations) refer to the state changes between symptoms controlled (ON state) and symptoms not controlled (OFF state, symptoms are poor or not responding to the medication).
MRI	*Magnetic resonance imaging* is a radiology medical imaging technique used to visualize body structures in detail.
PD	*Parkinson's disease* is a central nervous system disease that leads to movement disorders such as tremor, stiffness, and diffi-

	culty with walking and balance. It appears mainly in people more than 60 years old, and the risk of developing PD goes up with age.
PSD	The *power spectral density* describes how the power estimation of a signal or time series is distributed on the frequency domain. The PSD is the Fourier transform of the autocorrelation function of the signal which is a wide-sense stationary random process. If the signal is not stationary, then its autocorrelation function is a function of two variables. A similar technique, instead of PSD, may be used to estimate a time-varying spectral density.
QFN	The *Quad Flat No-Lead* is a surface mount plastic package with leads located on four sides of the bottom package.
RFI	The *radio frequency interference* refers to the information being transmitted across unshielded copper cable, which can be interfered with by the noise caused by other radio frequencies.
RMS	The *root mean square* (quadratic mean) is a statistical measure of the magnitude (the average of the squares) of a randomly varying quantity.
STN	The *subthalamic nucleus* is a small lens-shaped nucleus in the brain, a component of the basal ganglia control system, and is involved in action selection.
TETRAS	The *Essential Tremor Rating Assessment Scale* consists of 10 items in which action tremor is rated 0–4 in 0.5 intervals. It excellently rates ET in term of estimated tremor amplitude.
TWI	The *two-wire interface* protocol, which is the same as the IIC protocol, uses two wires for serial data transmission between two or more chips in asynchronous mode.
UPDRS	The *Unified Parkinson's Disease Rating Scale* is a clinical rating scale used to evaluate the symptom severities of PD by interview and clinical observation. Other rating scales for PD, such as the Hoehn and Yahr scale and the Schwab and England Activities of Daily Living Scale, are included in the revised UPDRS.
USB	The *universal serial bus* (USB) is an industry standard that defines the cables, connectors, and communications protocols used in a 4-pin interface for connection, communication, and power supply between a computer and another electronic device.

10. Bibliography

Abramowitz, M & Stegun, I.A. (1964): Handbook of mathematical functions with formulas, graphs, and mathematical tables, *New York*: Dover.

Allen, D.P.; Playfer, J.R.; Aly, N.M.; Duffey, P.; Heald, A.; Smith, S.L. & Halliday D.M. (2007): "On the use of low-cost computer peripherals for the assessment of motor dysfunction in Parkinson's disease--quantification of bradykinesia using target tracking tasks", *IEEE Trans. Neural. Syst. Rehabil. Eng.*, vol. 15, no. 2, pp. 286–294.

Bamberg, S.; Benbasat, A.Y.; Scarborough, D.M.; Krebs, D.E. & Paradiso, J.A. (2008): "Gait analysis using a shoe-integrated wireless sensor system", *IEEE Trans. Inf. Technol. Biomed.*, vol. 12, no. 4, pp. 413–423.

Bittar, R.G.; Burn S. C.; Bain, P.G.; Owen, S.L.; Joint, C.; Shlugman, D. & Aziz, T.Z. (2005): "Deep brain stimulation for movement disorders and pain", *Journal of clinical Neuroscience*, vol. 12, no. 4, pp. 457–463.

Bland, J.M. & Altman, D.G. (2003): "Applying the right statistics: analyses of measurement studies", *Ultrasound Obstet. Gynecol.*, vol. 22, pp. 85–93.

Bour, L.J.; Contarino, M.F.; Foncke, E.M.; de Bie R.M.; van den Munckhof, P.; Speelman, J.D. & Schuurman, P.R. (2010): "Long-term experience with intraoperative microrecording during DBS neurosurgery in STN and GPi.", *Acta Neurochir.*, vol. 152, pp. 2069–2077.

Burkhard, P.R.; Langston, J.W. & Tetrud, J.W. (2002): "Voluntarily simulated tremor in normal subjects", *Neurophysiol. Clin.*, vol. 32, no. 2, pp. 119–126.

Burkhard, P.R.; Shale, H.; Langstom, J.W. & Tetrud, J.W. (1999): "Quantification of dyskinesia in Parkinson's disease: validation of a novel instrumental method", *Mov. Disord.*, vol. 14, no. 5, pp. 26–27.

Carmeli, E.; Vatine, J.J.; Peleg, S.; Bartur, G. & Elbo, E. (2009): "Upper limb rehabilitation using augmented feedback: Impairment focused augmented feedback with HandTutor", *Virtual Rehabilitation International Conference*, pp. 220.

Charles S.M. (2003): "Parkinson's Disease: Overview and Current Abstracts", *New York*: Nova Science Pub Inc., pp. 7–9.

Chaudhuri, K.R. & Ondo, W.F. (2011): "Handbook of Movement Disorders", *London*: Springer Healthcare Ltd, pp. 1–2.

Chwaleba, A.; Jakubowski, J. & Kwiatos, K. (2003): "The measuring set and signal processing method for the characterization of human hand tremor", *International Conference on CAD Systems in Microelectronics (CADSM)*, pp. 149–154.

Crawford, P. & Zimmerman, E.E. (2011): "Differentiation and diagnosis of tremor", *American Family Physician*, vol. 83, no. 6, pp. 697–702.

Czabke, A.; D'Angelo, L.T.; Niazmand, K.; & Lueth, T.C. (2009): " Ein kompaktes System zur Erfassung und Dokumentation von Bewegungsgewohnheiten", *Conference on Ambinent Assisted Living -AAL*, Berlin, pp. 1–5.

Dai, H.; Otten, B.; Mehrkens, J.H.; D'Angelo, L.T. & Lueth, T.C. (2013a): "A novel glove monitoring system used to quantify neurological symptoms during deep-brain stimulation surgery", *IEEE Sensors Journal*, vol. 13, no. 9, pp. 3193–3202.

Dai, H.; Otten, B.; Mehrkens, J.H. & D'Angelo, L.T. (2013b): "A portable system for quantitative assessment of parkinsonian rigidity", *IEEE EMBC Conf.*, pp. 6591–6594.

D'Angelo, L.T.; Czabke, A.; Niazmand, K. & Lueth, T.C. (2010): "ART–a new concept for an activity recorder and transceiver", *IEEE EMBS Conf.*, Buenos Aires, pp. 2132–2135.

D'Angelo, L.T.; Michael, S.; Paul, N. & Lueth, T.C. (2011): "A sensor network to iPhone interface separating continuous and sporadic processes in Mobile Telemedicine", *IEEE EMBS Conf.*, Boston, pp. 1528–1531.

Deuschl, G.; Bain, P. & Brin, M. (1998): "Consensus statement of the movement disorder society on tremor", *Movement Disorders*, vol. 13, pp. 2–23.

Dipietro, L., Sabatini, A.M. & Dario, P. (2008): "A survey of glove-based systems and their applications", *IEEE Transactions on Systems, Man and Cybernetics*, vol. 4, pp. 461–482.

Edwan, E.; Zhang, J.Y.; Zhou, J.C. & Loffeld, O. (2011): "Reduced DCM based attitude estimation using low-cost IMU and magnetometer triad", *8th Workshop on Positioning Navigation and Communication (WPNC)*, pp. 1–6.

Elble, R.J.; Pullman, S.L.; Matsumoto, J.Y.; Raethjen, J.; Deuschl, G.; Tintner, R. & Tremor Research Group (2006): "Tremor amplitude is logarithmically related to 4- and 5-point tremor rating scales", *Brain*, vol. 129, no. 10, pp. 2660–2666.

Elble, R.J. & Deuschl, G. (2011): "Milestones in tremor research", *Movement Disorders*, vol. 26, no. 6, pp. 1096–1105.

Ellermeier, W. & Faulhammer, G. (2000): "Empirical evaluation of axioms fundamental to Stevens's ratio-scaling approach: I. Loudness production", *Perception & Psychophysics*, vol. 62, no. 8, pp. 1505–1511.

Espay, A.J.; Giuffrida, J.P.; Chen, R.; Payne, M.; Mazzella, F.; Dunn, E. *et al.* (2011): "Differential response of speed, amplitude, and rhythm to dopaminergic medications in Parkinson's disease", *Movement Disorders*, vol. 26, no. 14, pp. 2504–2508.

Endo, R.; Yokoe, M.; Fukawa, K.; Sakoda, S. & Akazawa, K. (2007): "Measurement system of finger-tapping contact force for quantitative diagnosis of Parkinson's disease", *IEEE EMBS Conf.*, pp. 1354–1357.

Endo, T.; Okuno, R.; Yokoe, M.; Akazawa, K. & Sakoda, S. (2009): "A Novel method for systematic analysis of rigidity in Parkinson's disease", *Movement Disorders*, vol. 24, pp. 2218–2224.

Gowers, W.R. (1886): "A Manual of Diseases of the Nervous System", *London*: J. & A. Churchill.

Giovannoni, G.; Schalkwyk, J.; Fritz, V.U. & Lees, A.J. (1999): "Bradykinesia akinesia incoordination test (BRAIN TEST): an objective computerized assessment of upper limb motor function", *Journal of Neurol Neurosurg Psychiatry*, vol. 67, pp. 624–629.

Giuffrida, J.P.; Riley, D.E.; Maddux, B.N. & Heldman, D.A. (2009): "Clinically deployable Kinesia technology for automated tremor assessment", *Movement Disorders*, vol. 24, pp. 723–730.

Hauser, R.A.; Friedlander, J.; Zesiewicz, T.A.; Adler, C.H.;Seeberger, C.H.; O'Brien C.F.; *et al.* (2000): "A home diary to assess functional status in patients with Parkinson's disease with motor fluctuations and dyskinesia", *Clinical Neuropharmacology*, vol. 23, no. 2, pp. 75–81.

Heldman, D.A.; Giuffrida, J.P.; Chen, R.; Payne, M.; Mazzella, F.; Dunn, E. *et al.* (2011a): "The modified bradykinesia rating scale for Parkinson's disease: reliability and comparison with kinematic measures", *Movement Disorders*, vol. 26, pp. 1859–1863.

Heldman, D.A.; Jankovic, J.; Vaillancourt, D.E.; Prodoehl, J.; R.J. Elble & Giuffrida, J.P. (2011b): "Essential tremor quantification during activities of daily living", *Parkinsonism & Related Disorders*, vol. 17, no. 7, pp. 537–542.

Hess, C.W. & Pullman, S.L. (2012): "Tremor: clinical phenomenology and assessment techniques", *Tremor and Other Hyperkinetic Movements*, vol. 2, pp. 1–15.

Hurtado, J.M.; Charles, C.M.; Tamas, L.B. & Sigvardt, K.A. (1999): "Dynamics of tremor-related oscillations in the human globus pallidus: A single case study", *Proc. Natl. Acad. Sci. U.S.A*, vol. 96, no. 4, pp. 1674–1679.

Iacono, R.P.; Lonser, R.R.; Maeda, G.; Kuniyoshi, S.; Warner, D.; Mandybur, G, & Yamada S. (1995): "Chronic anterior pallidal stimulation for Parkinson's disease", *Acta Neurochir.*, vol. 137, pp. 106–112.

Iba´nez, J.; Serrano, J.I.; del Castillo, M.D. & Barrios, L.J. (2010): "An asynchronous BMI system for online single-Trial detection of movement intention", *IEEE EMBS Conf.*, pp. 4562–4565.

Jankovic, J. (2008): "Parkinson's disease: clinical features and diagnosis", *J. Neurol. Neurosurg Psychiatry*, vol. 79, no. 79, pp. 368–376.

Kazi, S.; Azizan, A.; Zain, Z.M.D. & Mailah, M. (2010): "Performance evaluation of smart glove applied to experimental rig to control human hand tremor for Parkinson disease", *ACE Proceedings of the 9th WSEAS international conference on Applications of computer engineering*, pp. 306–315.

Keijsers, N.L.; Horstink, M.W.; van Hilten, J.J.; Hoff, J.I. & Gielen, C.C. (2000): "Detection and assessment of the severity of Levodopa-induced dyskinesia in patients with Parkinson's disease by neural networks", *Movement Disorders*, vol. 15, no. 6, pp. 1104–1111.

Kim, J.W.; Lee, J.H.; Kwon, Y.; Kim, C.S.; Eom, G.M.; Koh, S.B.; Kwon, D.Y. & Park, K.W. (2011a): "Quantification of bradykinesia during clinical finger taps using a gyroscope in patients with Parkinson's disease", *Medical Biology Engineering Computation*, vol. 49, pp. 365–371.

Kim, J.W.; Kwon, J.; Kim, Y.M.; Chung, H.Y.; Eom, G.M.; Jun, J.H.; *et al.* (2011b): "Analysis of lower limb bradykinesia in Parkinson's disease patients", *Geriatrics & Gerontology International*, vol. 12, no. 2, pp. 257–264.

Kringelbach, M.L.; Jenkinson, N.; Owen, S.L.F. & Aziz, T.Z. (2007): "Translational principle of deep brain stimulation", *Nature Reviews Neuroscience*, vol. 8, no. 8, pp. 623–635.

Levin, J.; krafczyk, S.; Valkovic, P.; Eggert, T.; Claasssen, J. & Bötzl, K. (2009): "Objective measurement of muscle rigidity in Parkinsonian patients treated with subthalamic stimulation", *Movement Disorders*, vol. 24, no. 1, pp. 57–63.

LeMoyne, R.; Mastronianni, T.; Cozza, M.; Coroian, C. & Grundfest, W. (2010): "Implementation of an iPhone for characterizing Parkinson's disease tremor through a wireless accelerometer application", *IEEE EMBS Conf.*, pp. 4954–4958.

LeMoyne, R.; Coroian, C. & Mastronianni, T. (2009): "Quantification of Parkinson's disease characteristics using wireless accelerometers", *IEEE Complex Medical Engineering Conf. (CME/ICME)*, pp. 1–5.

Lötters, J.C.; Schipper, J.; Veltink, P.H.; Olthuis, W. & Bergveld, P. (1998): "Procedure for in-use calibration of triaxial accelerometers in medical applications", *Sensors and Actuators A: Physical*, vol. 68, pp. 221–228.

Luce, R.D. & Krumhansl, C. (1988): "Measurement, scaling, and psychophysics", in Stevens' Handbook of Experimental Psychology (Atkinson R.C., Herrnstein R.J., Lindzey G., & Luce R.D.), *New York*: Wiley, pp. 1–74.

Lueth, T.C.; D'Angelo, L.T. & Czabke, A. (2010): "Chart 4: TUM–AgeTech: A New Framework for Pervasive Medical Devices", in Pervasive and Smart Technologies for Healthcare: Ubiquitous Methodologies and Tools (Coronato, A. & Pietro, G.D.). *New York*: IGI Global, pp. 295–321.

Luinge, H.J. & Veltink, P. H. (2005): "Measuring orientation of human body segments using miniature gyroscopes and accelerometers", *Med. Biol. Eng. Comput.*, vol. 43, pp. 273–282.

Louis, E.D. & Ferreira, J.J. (2010): "How common is the most common adult movement disorder? Update on the worldwide prevalence of essential tremor", *Mov. Disord.*, vol. 25, pp. 534–541.

Machado, A.; Rezai, A.R.; Kopell, B.H.; *et al.* (2006): "Deep brain stimulation for Parkinson's disease: surgical technique and perioperative management", *Movement Disorders*, vol. 21, Suppl. 14, pp. 247–258.

Madgwick, S.O.H.; Harrison, A.J.L. & Vaidyanathan, A. (2011): "Estimation of IMU and MARG orientation using a gradient descent algorithm", *IEEE ICORR Conf.*, Zurich, pp. 1–7.

Mauro, R. (1990): "Understanding L.O:V.E. (Left Out Variables Error): a method for estimating the effects of omitted variables", *Psychological Bulletin*, vol. 108, no. 2, pp. 314–329.

McClelland III, S. (2011): "A cost analysis of intraoperative microelectrode recording during subthalamic stimulation for Parkinson's disease", *Movement Disorders*, vol. 26, no. 8, pp. 1422–1427.

Mera, T.O.; Vitek, J.L.; Alberts, J.L. & Giuffrida, J.P. (2011): "Kinematic optimization of deep brain stimulation across multiple motor symptoms in Parkinson's disease", J. *Neurosci. Methods*, vol. 198, no. 2, pp. 280–286.

Mera, T.O.; Burack, M.A. & Giuffrida, J.P. (2012): "Quantitative assessment of Levodopa-induced dyskinesia using automated motion sensing technology", *IEEE EMBS Conf.*, pp. 154–157.

Moore, G.P.; Ding, L. & Bronte-Stewart, H.M. (2000): "Concurrent Parkinson tremors", *J Physiol.*, vol. 529, pp. 273–281.

Mostile, G.; Giuffrida, J.P.; Adam, O.R.; Davidson, A. & Jankovic, J. (2010): "Correlation between Kinesia system assessments and clinical tremor scores in patients with essential tremor movement", *Movement Disorders*, vol. 25, no. 12, pp. 1938–1943.

Nakagawa, S. & Cuthill, I.C. (2010): "Effect size, confidence interval and statistical significance: a practical guide for biologists", *Biological Reviews Cambridge Philosophical Society*, vol. 82, pp. 591–605.

Narcisa, V.; Aguilar, D.; Nquyen, D.V.; *et al.* (2011): "A quantitative assessment of tremor and ataxia in female FMR1 premutation carriers using CATSYS", *Curr. Gerontol. Geriatr. Res.*, vol. 2011, pp. 1–7.

National Instrument Inc. (2011): LabVIEW User Tutorials. USA.

NDI Digital Inc. (2010): Aurora V2 User Guide. Canada.

Niazmand, K.; Jehle, C.; D'Angelo, L.T. & Lueth, T.C. (2010): "A new washable low-cost garment for everyday fall detection", *IEEE EMBS Conf., Buenos Aires*, pp. 6377–6380.

Niazmand, K.; Tonn, K.; Kalaras, A.; Fietzek, U.M.; Mehrkens, J.H. & Lueth, T.C. (2011a): " Quantitative evaluation of Parkinson's disease using sensor based smart glove", *IEEE Symposium on Computer-Based Medical Systems-CBMS*, Bristol, pp. 1–8.

Niazmand, K., Kalaras, A., Dai, H., Lueth, T.C. (2011b): "Comparison of methods for tremor frequency analysis for patients with Parkinson's disease", *The 4th International Conference on BioMedical Engineering and Informatics (IEEE CBEI)*, Shanghai, pp: 1312-1316.

Norman, K.E.; Edwards, R. & Beuter, A. (1999): "The measurement of tremor using a velocity transducer: comparison to simultaneous recordings using transducers of displacement, acceleration and muscle activity", *Journal of Neuroscience Methods*, vol. 92, pp. 41–54.

Okun, M.S. & Foote, K.D. (2010): "Parkinson's disease DBS: what, when, who and why? The time has come to tailor DBS targets", *Expert Review Neurotherapeutics*, vol. 10, pp. 1847–1857.

Okuno, R.; Yokoe, M.; Akazawa, K.; Abe, K. & Sakoda, S. (2006): "Finger taps movement acceleration measurement system for quantitative diagnosis of Parkinson's disease", *IEEE EMBS Conf., Suppl*, pp. 6623–6626.

Olivares, A.; Olivares, G.; Gorriz, J.M. & Ramirez, J. (2009): "High-efficiency low-cost accelerometer-aided gyroscope calibration", *IEEE International Conference on Test and Measurement (ICTM)*, pp. 354–360.

Oluigbo, C.O.; Salma, A. & Rezai, A.R. (2012): "Deep brain stimulation for neurological disorders", *IEEE Reviews in Biomedical Engineering*, vol. 5, pp. 88–99.

Ostrem, J.L.; Galifianakis, N.B.; Markun, L.C.; Grace, J.K.; Martin, A.J.; Starr, P.A. & Larson PS. (2013): "Clinical outcomes of PD patients having bilateral STN DBS using high-field interventional MR-imaging for lead placement", *Clin. Neurol. Neurosurg.*, vol. 115, no. 6, pp. 708–712.

O'Suilleabhain, P.E. & Matsumoto, J.Y. (1998): "Time-frequency analysis of tremors", *Brain*, vol. 121, pp. 2127–2134.

Park, B.K.; Kwon, Y.; Kim, J.W.; Lee, J.H.; Eom, G.M.; Koh, S.B. *et al.* (2011): "Analysis of viscoelastic properties of wrist joint for quantification of parkinsonian rigidity", *IEEE Transactions on Neural Systems and Rehabilitation Engineering*, vol. 19, no. 2, pp. 167–176.

Patel, S.; Hughes, R.; Huggins, N.; Standaert, D.; Growdon, J.; Dy, J. & Bonato, P. (2008): "Using wearable sensors to predict the severity of symptoms and motor complications in late stage Parkinson's disease", *IEEE EMBS Conf.*, pp. 3686–3689.

Patel, S.; Lorincz, K.; Hughes, R.; Huggins, N.; Growdon, J.; Standaert, D. *et al.* (2009): "Monitoring motor fluctuations in patients with Parkinson's disease using wearable sensors", *IEEE Trans. Inf. Technol. in Biomed.*, vol. 13, no. 6, pp. 864–873.

Patrick, S.K.; Denington, A.A.; Gauthier, M.J.; Gillard, D.M. & Prochazka, A. (2001): "Quantification of the UPDRS rigidity scale", *IEEE Trans. Neural Syst. Rehabil. Eng.*, vol. 9, pp. 31–41.

Pahwa, R. & Lyons, K.E. (2007): Handbook of Parkinson's Disease (4th ed.), *New York*: Informa Healthcare (USA) Inc.

Pavel, P. & Popelka, J. (2012): "IMU aiding using two AHRS units", *IEEE/AIAA Digital Avionics System Conference (DASC)*, pp. 5B1-1–5B1-13.

Post, B.; Maruschka, M.P.; de Bie, R.M.; de Haan, R.J. & Speelman, J.D. (2005): "Unified Parkinson's disease rating scale motor examination: are ratings of nurses, residents in neurology, and movement disorders specialists interchangeable?", *European Journal of Nuclear Medicine and Molecular Imaging*, vol. 20, no. 12, pp. 1577–1584.

Powell, Jr.H.C.; Hanson, M.A. & Lach, J. (2007): "A wearable inertial sensing technology for clinical assessment of tremor", *IEEE Biomedical Circuits and Systems Conference*, BIOCAS 2007, pp. 9–12.

Popovic, L.Z., Sekara, T.B. & Popovic, M.B. (2008): "Adaptive band-pass filter (ABPF) for tremor extraction from inertial sensor data", *Computer Methods and Programs in Biomedicine*, vol. 99, pp. 298–305.

Prochazka, A.; Bennett, D.J.; Stephens, M.J.; Patrick, S.K.; Sears-Duru, R.; Roberts, T. & Jhamandas J.H. (1997): "Measurement of rigidity in Parkinson's disease", *Movement Disorders*, vol. 12, pp. 24–32.

Richard, G.B.; Sasha, C.B.; Peter, G.B.; Sarah, L.O.; Carol, J.; David, S. & Tipu, Z.A. (2005): "Deep brain stimulation for movement disorders and pain", *Journal of Clinical Neuroscience*, vol. 12, no. 4, pp. 457–463.

Rigas, G.; Tzallas, A.T.; Tsalikakis, D.G.; Konitsiotis, S. & Fotiadis, D.I. (2009) "Real-time quantification of rest tremor in the Parkinson's disease", *IEEE EMBS Conf.*, Minneapolis, pp. 1306-1309.

Rissanen, S.M.; Kankannpää, M.; Tarvainen, M.P.; Nuutinen, J.; Tarkka, I.M.; Airaksinen, O. & Karialainen, P.A. (2007): "Analysis of surface EMG signal morphology in Parkinson's disease", *Physiological Measurement*, vol. 28, pp. 1507–1521.

Rissanen, S.M.; Kankaanpaa, M.; Tarvainen, M. P.; Novak, V.; Hu, K.; Manor, B. *et al.* (2011): "Analysis of EMG and acceleration signals for quantifying the effects of Deep Brain Stimulation in Parkinson's disease", *IEEE Trans. Biomed. Eng.*, vol. 99, pp. 1–9.

Riviere, C.N.; Reich, S.G. & Thankor, N.V. (1997): "Adaptive Fourier modelling for quantification of tremor", *Journal of Neuroscience Methods*, vol. 74, pp: 77–87.

Sakoda, S.; Akazawa, K.; Okuno, R.; Yokoe, M. & Endo, T. (2011): "Muscle tonus measuring apparatus", *United States Patent Application Publication*, pub. no.: US2011/0087128 A1.

Salarian, A.; Russmann, H.; Wider, C.; Burkhard, P.R.; Vingerhoets, F.J. & Aminian, K. (2007): "Quantification of tremor and bradykinesia in Parkonson's disease using a novel ambulatory monitoring system", *IEEE Trans. Biomed Eng.*, vol. 54, pp. 313–322.

Sepehri, B.; Esteki, A.; Ebrahimi-Takamjani, E. *et al.* (2007): "Quantification of rigidity in Parkinson's disease", *Ann. Biomed. Eng.*, vol. 35, pp. 2196–2203.

Singh, A.; Kammermeier, S.; Mehrkens, J.H. & Bötzel, K. (2012): "Movement kinematic after deep brain stimulation associated microlesions", *J. Neurol. Neurosurg. Psychiatry*, vol. 82, pp. 1022–1026.

Shaeffer, D.K. (2013): "MEMS inertial sensors: A tutorial overview", *IEEE Communications Magazine*, vol. 51, no.4, pp. 100–109.

Shany, T.; Redmond, S.J.; Narayanan, M.R. & Lovell, N.H. (2012): "Sensors-based wearable systems for monitoring of human movement and falls", *IEEE Sensors Journal*, vol. 12, no. 3, pp. 658–670.

Shapiro, M.B.; Vaillancourt, D.E.; Sturman, M.M.; *et al.* (2007): "Effects of STN DBS on rigidity in Parkinson's disease", *IEEE Trans. Neural. Syst. Rehabil. Eng.*, vol. 15, pp. 173–181.

Shima, K.; Tsuji, T.; Kan, E.; Kandori, A., Yokoe, M. & Sakoda, S. (2008): "Measurement and evaluation of finger tapping movements using magnetic sensors", *IEEE EMBS Conf.*, pp. 5628–5631.

Smeja, M.; Foerster, F.; Fuchs, G.; Emman, D.; Hornig, A. & Fahrenberg, J. (1999): "24-h assessment of tremor activity and posture in Parkinson's disease by multi-channel acceelerometry", *Journal of Psychosiology*, vol. 13, pp. 245–256.

Spieker, S.; Jentgens, C.; Boose, A. & Dichgans, J. (1995): "Reliability, specificity and sensitivity of long-term tremor recordings", *Electroencephalography and Clinical Neurophysiology*, vol. 97, pp. 326–331.

Spyers-Ashby, J.M. & Stokes, M.J. (2000): "Reliability of tremor measurements using a multidimensional electromagnetic sensor system", *Clin. Rehabil.*, vol. 14, no. 4, pp. 425–432.

Sturman, M.M.; Vaillancourt, D.E.; Metman, L.V.; Bakay, R.A.E & Corcos, D.M. (2004): "Effects of subthalamic nucleus stimulation and medication on rest and postural tremor in Parkinson's disease", *Brain*, vol. 127, pp. 2131–2143.

Su, Y.; Allen, C.R.; Geng, D.; Burn, D.; Brechany, U.; Bel, G.D. & Rowland, R.(2003): "3-D motion system ("data-gloves"): application for Parkinson's", *IEEE Trans. Instr. Measur.*, vol. 52, no. 3, pp. 662–674.

Synnott, J.; Chen, L.; Nugent, C.D. & Moore, G. (2012): "WiiPD-objective home assessment of Parkinson's disease using the Nintendo Wii remote", *IEEE Trans. Inf. Technol. in Biomed.*, vol. 16, no. 6, pp. 1304–1312.

Tagliati, M.; Guten, G.N. & Horne, J. (2007): "Parkinson's Disease for Dummies", *Indianapolis*: Wiley Publishing Inc.

Takuyuki, E.; Masaru, Y.; Harutoshi, F. & Saburo, S. (2011): "Chapter 9: Novel Methods to Evaluate Symptoms in Parkinson's Disease–Rigidity and Finger Tapping", in Diagnostics and Rehabilitation of Parkinson's Disease (Dushanova, J.), *Croatia*: InTech, pp. 191–206.

Teräväinen, H. & Calne, D.B. (1980): "Action tremor in Parkinson's disease", *J. Neurol. Neurosurg. Psychiatry*, vol. 43, no. 3, pp. 257–267.

Timmer, J.; Gantert, C.; Deuschl G. & Honerkamp, J. (1993): "Characteristics of hand tremor time series", *Biol. Cybern.*, vol. 70, pp. 75–80.

Timmer, J.; Lauk, M. & Lücking, C.H. (1997): "Confidence regions for spectral peak frequencies", *Biometrical Journal*, vol. 39, no. 7, pp. 849–861.

Timmer, J.; Lauk, M.; Vach, W. & Lücking, C.H. (1999): "A test for a difference between spectral peak frequencies", *Journal Computational Statistics & Data Analysis*, vol. 30, no. 1, pp. 45–55.

Timmer, J.; Häussler, S.; Lauk, M. & Lücking, C.H. (2000a): "Pathological tremors: deterministic chaos or nonlinear stochastic oscillators?", *Chaos*, vol. 10, no. 1, pp. 278–288.

Timmer, J.; Lauk, M.; Häußler, S. & Radt, V. (2000b): "Cross-spectral analysis of tremor time series", *International Journal of Bifurcation and Chaos*, vol. 10, no. 11, pp. 2595–2610.

Thümler, R. (2002): "Morbus Parkinson: Ein Leitfaden für Klinik und Praxis", *Berlin*: Springer.

Van Dillen, L.R.; Roach, K.E. (1988): "Interrater Reliability of a Clinical Scale of Rigidity", *Physical Therapy*, vol. 68, pp. 1679–1681.

Van Someren, E.J.; Vonk, B.E.; Thijssen, W.A.; Speelman, J.D.; Schuurman, P.R.; Mirmiran, M. & Swaab, D.F. (1998): "A new actigraph for long-term registration of the duration and intensity of tremor and movement", *IEEE Trans. Biomed. Eng.*, vol. 45, no. 3, pp. 386–395.

Veluvolu K.C. & Ang, W.T. (2011): "Estimation of physiological tremor from accelerometers for real-time applications", *Sensors*, vol. 11, no. 3, pp. 3020–3036.

Winestone, J.S.; Zaidel, A.; Bergman, H. & Israel, Z. (2006): "The use of macroelectordes in recording cellular spiking activity", *Clinical Neuroscience*, vol. 206, pp. 34–39.

Winqeier, B.; Tcheng, T.; Koop, M.M.; Hill, B.C.; Heit, G. & Bronte-Stewart, H.M. (2006): "Intra-operative STN DBS attenuates the prominent beta rhythm in the STN in Parkinson's disease", *Exp. Neurol.*, vol. 197, no. 1, pp. 244–251.

Yuting, Z.; Markovic, S; Wagenaar, R.C. & Little, T.D.C. (2011): "Continuous functional activity monitoring based on wearable tri-axial accelerometer and gyroscope", *Pervasive Computing Technologies for Healthcare (PervasiveHealth)*, Dublin, vol. 99, pp. 1–9.